

# Analysis and Numerical Investigation of Dynamic Models for Liquid Chromatography

**Dissertation**

zur Erlangung des akademischen Grades

**doctor rerum naturalium**

**(Dr. rer. nat.)**

von **MS Math. Shumaila Javeed**

geb. am 29. Januar 1985 in Rawalpindi, Pakistan

genehmigt durch die Fakultät für Mathematik  
der Otto-von-Guericke-Universität Magdeburg

**Gutachter:**

Prof. Dr. Gerald Warnecke

Prof. Dr. Thomas Sonar

**Eingereicht am:** 19.11.2012

**Verteidigung am:** 25.06.2013



# Abstract

In this work models capable to describe non-reactive and reactive liquid chromatography are investigated numerically and theoretically. These models have a wide range of industrial applications e.g. to produce pharmaceuticals, food ingredients, and fine chemicals. Two established models of liquid chromatography, the equilibrium dispersive model and the lumped kinetic model, are analyzed using Dirichlet and Robin boundary conditions to solve the column balances. The models consist of systems of convection-diffusion-reaction partial differential equations with dominating convective terms coupled via differential or algebraic equations. The Laplace transformation is used to solve them analytically for the special case of single component linear adsorption. Statistical moments of step responses are calculated and compared with numerical predictions generated by using the methods studied in this thesis for both sets of boundary conditions. For nonlinear adsorption isotherms, only numerical techniques provide solutions. However, the strong nonlinearities of realistic thermodynamic functions and the stiffness of reaction terms pose major difficulties for the numerical schemes. For this reason, computational efficiency and accuracy of numerical methods are of large relevance and a focus of this work. Another goal is to analyze the influence of temperature gradients on reactive liquid chromatography, which are typically neglected in theoretical studies. By parametric calculations the influence of temperature gradients on conversion and separation processes during reactive liquid chromatography are analyzed systematically. Additionally, the complex coupling of concentration and thermal fronts is illustrated and key parameters influence the reactor performance are identified. Two numerical schemes, namely the finite volume scheme of Koren and the discontinuous Galerkin finite element method, are applied to numerically approximate the models considered. These schemes give a high order accuracy on coarse grids, resolve sharp fronts, and avoid numerical diffusion and dispersion. Several case studies to analyze non-reactive and reactive liquid chromatographic processes are carried out. The results of the suggested numerical methods are validated qualitatively and quantitatively against some finite volume schemes from the literature. The results achieved verify that the proposed methods are robust and well suited for dynamic simulations of chromatographic processes.



# Zusammenfassung

In dieser Arbeit geht es um die numerische und theoretische Untersuchung von Modellen, welche die reaktive und die nichtreaktive Flüssig-Chromatographie beschreiben. Diese Modelle finden in einem großen Rahmen industrielle Anwendungen, z.B. bei der Produktion von Arzneimitteln, Nahrungsmitteln und Feinchemikalien. Zwei gängige Modelle der Flüssig-chromatographie, das "Equilibrium Dispersive Model" und das "Lumped Kinetic Model", werden mit Hilfe der von Dirichlet- und Robin-Randbedingungen untersucht. Die Modelle bestehen aus Systemen von partiellen Differentialgleichungen, welche die Konvektions-Diffusions-Reaktion sprozesse beschreiben, bei denen der konvektive Term dominiert und die mit Differentialgleichungen oder algebraischen Gleichungen gekoppelt werden. Um diese modellgleichungen analytisch für den Spezialfall der linearen Adsorption von Einzelkomponenten zu lösen, wird die Laplace-Transformation benutzt. Dabei werden die statistischen Momente der Übergangsfunktion berechnet und mit den numerischen Voraussagen verglichen, die mit Hilfe der hier untersuchten Methoden für beide Randbedingungen gewonnen wurden. Für nichtlinearen Adsorptionsisothermen können Lösungen nur mit numerischen Methoden gewonnen werden. Die starke Nichtlinearität von realen thermodynamischen Funktionen und die Steifigkeit der Reaktionsterme stellen im Allgemeinen eine große Schwierigkeit für numerischen Methoden dar. Aus diesem Grund stehen die Effizienz bei der Berechnung sowie die Genauigkeit der numerischen Methoden im Fokus dieser Arbeit. Ein weiteres Ziel ist die Analyse des Einflusses von Temperaturgradienten auf die reaktive Flüssig-chromatographie, welcher bisher in theoretischen Arbeiten nur selten betrachtet werden. Mit Hilfe von parametrischen Berechnungen wurde der Einfluss von Temperaturgradienten auf Konversions- und Seperationsprozesse, die während der reaktiven Flüssigchromatographie stattfinden, systematisch untersucht. Zusätzlich wird die komplexe Kopplung von Konzentrations- und Wärmefronten erklärt und es die werden Parameter identifiziert, die einen wesentlichen Einfluss auf die Reaktorleistung haben. Zwei numerische Methoden, die Finite Volumenmethode von Koren und die diskontinuierliche Galerkin-Finite-Elementemethode, werden hier vorgeschlagen, um die betrachteten

Modellgleichungen numerisch zu approximieren. Diese Methoden erlauben eine hohe Genauigkeit auf groben Gittern, lösen scharfe Fronten auf und vermeiden numerische Diffusion und Dispersion. Es wurden verschiedene Fallstudien durchgeführt, um reaktive und nichtreaktive chromatographische Prozesse zu analysieren. Die mit den hier vorgeschlagenen Methoden erreichten Ergebnisse wurden qualitativ und quantitativ im Vergleich mit von Resultaten der Finiten-Volumen-Methoden aus der Literatur validiert. Die Ergebnisse zeigen, dass die hier vorgeschlagenen Methoden robust und gut geeignet sind für die dynamische Simulation von chromatographischen Prozessen.

# Acknowledgments

This thesis originated during my tenure as a Research Scholar at the Max Planck Institute for Dynamics of Complex Technical Systems in Magdeburg, Germany.

First and foremost, I am grateful to my supervisor Prof. Gerald Warnecke who always encouraged me and gave me remarkable suggestions and invaluable supervision throughout my thesis work. His advices, constructive criticism and kind behavior have always been the driving force towards the successful completion of research projects.

I am highly indebted to Prof. Andreas Seidel-Morgenstern, who gave me a chance to work at the Max Planck Institute Magdeburg and to utilize its excellent research platform. His valuable advice, kind attitude, constant encouragement, technical discussions have helped me immensely to improve my research capabilities and to finish the doctoral studies in an adequate time.

I am pleased to acknowledge my deepest gratitude to Prof. Shamsul Qamar for his guidance, constructive criticism and valuable suggestions during this thesis project.

This thesis would not have been possible without the funding from the International Max Planck Research School, Magdeburg and the state of Saxony-Anhalt. I am also grateful to Dr. Jürgen Koch and Dr. Barbara Witter for the support they provided.

I would like to express my heart-felt sense of gratitude to my grandfather Muhammad Basharat Kiyani (Late). To obtain a PhD degree was my grandfather's dream for me from my early childhood. He was the driving force behind my every endeavor throughout my life. I can never thank him rightfully for his countless love, giving me confidence and high aims regarding my studies.

I thank my parents, especially my mother, for instilling in me the qualities of integrity and willingness to always pursue more knowledge. Her endless support, care, and friendship, are something immeasurable. Thanks to her for bearing my absence, during my stay in Germany just for my desire to study abroad.

To you my loving brother Wajahat Kiyani, my source of inspiration, my light in the dark. Thanks for your support, love and extreme desire to complete this degree.





# Contents

<b>1</b>	<b>Introduction</b>	<b>1</b>
1.1	Overview . . . . .	1
1.2	Early development of chromatography . . . . .	4
1.3	Problems and motivation . . . . .	4
1.4	Outline of the thesis . . . . .	9
<b>2</b>	<b>Theory of Chromatography</b>	<b>12</b>
2.1	Overview . . . . .	12
2.2	Model parameters . . . . .	13
2.2.1	Column porosities . . . . .	13
2.2.2	Efficiency . . . . .	15
2.2.3	Adsorption isotherms . . . . .	16
2.3	Continuous chromatographic models . . . . .	17
2.3.1	The ideal model . . . . .	18
2.3.2	The equilibrium dispersive model (EDM) . . . . .	19
2.3.3	The lumped kinetic model (LKM) . . . . .	19
2.3.4	The general rate model (GRM) . . . . .	20
<b>3</b>	<b>Numerical Schemes</b>	<b>23</b>
3.1	The FVMs formulation for FBCR models . . . . .	23
3.2	The DG method formulation for FBCR models . . . . .	29

---

<b>4</b>	<b>Analytical Solution and Moment Analysis for Linear Models</b>	<b>36</b>
4.1	The lumped kinetic model (LKM) . . . . .	36
4.2	Analytical solutions of EDM and LKM for linear isotherm . . . . .	37
4.2.1	Analytical solution of EDM . . . . .	37
4.2.2	Analytical solution of LKM . . . . .	39
4.3	Reduced EDM and LKM: Moment models . . . . .	40
4.4	Numerical test problems . . . . .	43
4.5	Conclusion . . . . .	51
<b>5</b>	<b>Numerical Solutions of Linear and Non-Linear Chromatographic Models</b>	<b>55</b>
5.1	Numerical test problems . . . . .	56
5.1.1	Non-reactive single-component elution . . . . .	57
5.1.2	Non-reactive binary elution . . . . .	63
5.1.3	Three-component elution . . . . .	72
5.1.4	Four-component reactive elution . . . . .	79
5.2	Conclusion . . . . .	85
<b>6</b>	<b>Thermal Effects in Reactive Liquid Chromatography</b>	<b>86</b>
6.1	The non-isothermal chromatographic reactor model . . . . .	87
6.2	Formulation of numerical scheme . . . . .	91
6.3	Consistency tests for validation . . . . .	95
6.3.1	Identity of integrated extents of reaction . . . . .	95
6.3.2	Integrated energy balance considering the extent of reaction . . . . .	96
6.4	Demonstrations of thermal effects . . . . .	97
6.4.1	Trivial limiting cases . . . . .	97
6.4.2	Non-trivial test problems . . . . .	98
6.5	Conclusion . . . . .	112
<b>7</b>	<b>Summary and Conclusions</b>	<b>113</b>

---

A Mathematical Derivations	117
B Nomenclature	124
Bibliography	126
Curriculum Vitae	138



# List of Tables

3.1	Different flux limiters used in (3.20). . . . .	28
4.1	Analytically determined moments for EDM and LKM. . . . .	42
4.2	Parameters for Section 4.4. . . . .	45
4.3	Errors and CPU times at 50 grid points. . . . .	45
4.4	Errors and CPU times at 100 grid points. . . . .	46
5.1	Section 5.1.1 (Linear isotherm): $L^1$ -errors and CPU times of schemes. . . .	59
5.2	Section 5.1.1 (Linear isotherm): $L^1$ -errors and EOC of the DG scheme. . .	59
5.3	Section 5.1.1 (Linear isotherm): $L^1$ -errors and EOC of the Koren scheme. .	60
5.4	Section 5.1.1 (Linear isotherm): EOC of schemes for $D_{\text{app}} = 0.002 \text{ m}^2/\text{s}$ . .	60
5.5	Section 5.1.1 (Linear isotherm): EOC of schemes for $D_{\text{app}} = 2 \times 10^{-5} \text{ m}^2/\text{s}$ . 60	60
5.6	Section 5.1.1 (Nonlinear isotherm): $L^1$ -errors and CPU times of schemes. .	62
5.7	Section 5.1.2 (case 2): Inlet and initial conditions for problems. . . . .	69
5.8	Section 5.4: Temperature dependent reaction and adsorption parameters. .	83
6.1	Problem 1: Isothermal case study. . . . .	100
6.2	Problem 2: Influence of the enthalpy of reaction $\Delta H_{A,i} = 0$ , $E_A = 60 \text{ kJ/mol}$ .102	102
6.3	Problem 3: Influence of enthalpy of adsorption $\Delta H_R = 0$ , $E_A = 60 \text{ kJ/mol}$ .. 104	104
6.4	Problem 4a: Influence of both enthalpies of reaction and adsorption. . . . .	107

# List of Figures

1.1	Principle of non-reactive and reactive liquid chromatography. . . . .	3
2.1	Left: linear isotherm, right: nonlinear isotherm. . . . .	17
3.1	Cell centered finite volume grid. . . . .	24
3.2	Grids near the boundaries. . . . .	28
4.1	Comparison of different numerical schemes for LKM. . . . .	46
4.2	Dispersion and mass transfer effects. . . . .	47
4.3	Comparison of analytical and numerical solutions for Dirichlet conditions. .	48
4.4	Comparison of analytical and numerical solutions for Danckwerts conditions.	48
4.5	Effect of boundary conditions for different values of Peclet number. . . . .	49
4.6	First moments $\mu_1$ of EDM and LKM for different flow rates $u$ . . . . .	52
4.7	Second moments $\mu_2'$ for both models, analytical versus numerical results. .	52
4.8	Third moments $\mu_3'$ for both models, analytical versus numerical results. . .	53
5.1	Section 5.1.1 (linear): Comparison of schemes for single component. . . . .	61
5.2	Section 5.1.1 (nonlinear): Comparison of schemes for single component. . .	62
5.3	Section 5.1.1 (nonlinear): Errors at different number of mesh points. . . . .	63
5.4	Section 5.1.2 (case 1): Two-component elution with linear isotherm. . . . .	64
5.5	Section 5.1.2 (case 2a): Riemann problem leads to the $S_2 - C_1$ solution. . .	67
5.6	Section 5.1.2 (case 2a): A comparison of the DG and Koren schemes. . . . .	68
5.7	Section 5.1.2 (case 2b): Riemann problem leads to the $C_2 - S_1$ solution. . .	68
5.8	Section 5.1.2 (case 2c): Riemann problem leads to the $C_2 - C_1$ solution. . .	69

5.9	Section 5.1.2 (case 2d): Riemann problem leads to the $C_2 - C_1$ solution. . .	70
5.10	Section 5.1.2 (case 2e): Riemann problem leads to the $S_2 - S_1$ solution. . .	70
5.11	Section 5.1.2 (case 2f): Riemann problem leads to the delta-shocks. . . . .	71
5.12	Section 5.1.2 (case 2f): Delta-shocks for different theoretical plate numbers.	71
5.13	Section 5.1.3: 3-component isothermal reactive elution with linear isotherm.	74
5.14	Section 5.1.3: Representation of the operating line. . . . .	76
5.15	Section 5.1.3: Formation of displacement train with $c_1^{\text{in}} = c_2^{\text{in}} = c_d^{\text{in}} = 1 \text{ g/l}$ .	77
5.16	Section 5.1.3: A comparison of the DG and Koren schemes. . . . .	78
5.17	Section 5.1.3: Displacement chromatography with $c_d^{\text{in}} = 0.5 \text{ g/l}$ . . . . .	80
5.18	Section 5.1.3: Displacement chromatography with $c_d^{\text{in}} = 0.1 \text{ g/l}$ . . . . .	80
5.19	Section 5.1.3: A schematic diagram of counter-current adsorption process. .	81
5.20	Section 5.1.3: Displacement chromatography on counter-current bed. . . .	82
5.21	Section 5.1.4: 4-component linear reactive elution at different temperatures.	84
5.22	Section 5.1.4: 4-component nonlinear elution at temperature $T = 318$ . . . .	84
6.1	Trivial limiting case study with $\Delta H_{A,i} = 0$ for $i=A,B,C$ , $k_{\text{for}}(T^{\text{ref}}) = 0$ . . . .	99
6.2	Limiting case: Temperature transients for three inlet values. . . . .	99
6.3	Problem 1: Isothermal case, $\Delta H_{A,i} = 0$ , $\Delta H_R = 0$ . . . . .	101
6.4	Problem 2: Influence of the enthalpy of reaction, $\Delta H_{A,i} = 0$ , for $i=A,B,C$ . .	103
6.5	Problem 3: Influence of enthalpies of adsorption, $\Delta H_R = 0$ . . . . .	105
6.6	Problem 4a: Influence of both enthalpies of reaction and adsorption. . . . .	107
6.7	Problem 4a: Influence of activation energy on the process. . . . .	108
6.8	Problem 4b: Enthalpy of adsorption (componentwise). . . . .	110
6.9	Problem 5: Influence of dispersion terms. . . . .	111





# Chapter 1

## Introduction

This chapter presents a general overview regarding chromatographic separation processes and limitations of existing numerical techniques for chromatographic models capable to describe front propagation phenomena taking place in chromatographic columns. In addition, numerical solution techniques, such as finite-difference, finite-element and finite volume methods are briefly reviewed and basic requirements on the quality of numerical solutions are discussed. Moreover, a short summary of recent relevant results related to the topic of this work and an outline of the thesis are presented.

### 1.1 Overview

The separation and purification of components of a mixture are highly important for several industries. Examples are related to the production of pharmaceuticals, food, and fine chemicals. Chromatography is one of the most versatile separation techniques widely used for analysis and purification of multi-component mixtures that are difficult to separate by conventional separation processes, such as distillation or extraction. Chromatography is successfully applied to perform numerous complex separation processes, such as the separation of enantiomers and the isolation from fermentation broths of proteins. It has a potential to provide the required purities and offers high yield at reasonable production rates. Chromatography is in particular effective for difficult separation tasks when high purity products are demanded. The technology has gained immense industrial popularity

in the past few decades [30].

Reactive chromatography can be an attractive technique to effectively reduce the number of units and enhance the performance of processes providing pure reaction products. In reactive chromatography, chemical reactions and chromatographic separation of the products take place simultaneously in the column. This principle is comparable to reactive distillation, reactive extraction or reactive absorption [85]. The concept is particularly advantageous to perform equilibrium limited reversible reactions due to the separation based shifting of chemical equilibrium allowing to improve conversion, yield and separation efficiency. The reactive chromatography reduces capital investment, energy and operating costs, equipment sizes and waste. It improves selectivity, purity, and productivity. Despite several theoretical investigations of reactive chromatography, accurate databases and models are still lacking for broader commercialization. There are several reviews available describing the principle and a few applications of chromatographic reactors, e.g. [4, 24, 25, 80, 102]. The motivation of most current research works is to provide more profound insight into all aspects for identifying fields of application and for scaling up the process to industrial relevant sizes.

Chromatographic separation is based on different adsorptivities of the mixture components to a specific adsorbent which is fixed in a chromatographic column. The simplest process is batch chromatography involving a single packed column charged with pulses of feed solution. The injected mixtures are carried through the column by a continuously flowing desorbent. The components to be separated now move with different velocities in the column due to their specific affinities with the solid phase. A low retained component exits the column earlier than a more retained one and, hence, separation is achieved. The illustration of the chromatography principle is given in Figure 1.1.

Chromatographic reactors were patented in the early 60's, see e.g. [18, 26, 55]. A packed bed chromatographic reactor (FBCR) is defined by Langer [47] as a "chromatographic column in which a solute or several solutes are intentionally converted, either partially or totally, to products during their residence in the column. The solute reactant or reactant mixture is injected into the chromatographic reactor as a pulse. Both conversion to product

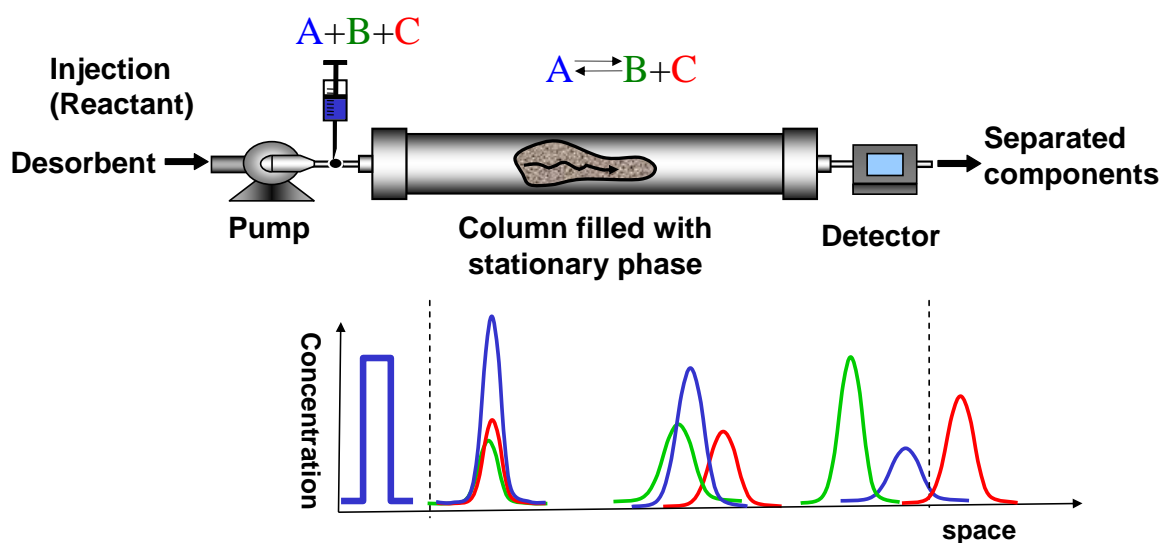


Figure 1.1: A schematic illustration of the principle of non-reactive and reactive liquid chromatography.

and separation take place in the course of passage through the column; the device is truly both a reactor and a chromatograph”.

The basic concept of fixed-bed chromatographic reactors can be easily illustrated by considering a single chromatographic column in which a reversible reaction of the type  $A \rightleftharpoons B+C$  takes place. In reactive chromatography, rectangular pulses of reactant A are periodically fed into the inert carrier stream instead of injecting mixtures in process used just for separation. Thus, reactant A is transported through the column packed and reacts to form the products B and C eventually supported by catalytic effects of the solid phase. Different affinities of components B and C produce different migration velocities of the products, which leads to their separation, suppresses the backward reaction and provides high conversion of reactant A at the column outlet, see Figure 1.1. A very favorable situation exists for this type of reaction, when A elutes between the products B and C. Complete conversion of A is possible provided the residence in the column is long enough.

## 1.2 Early development of chromatography

Techniques affiliated to chromatography have long been practiced to purify substances, for instance to purify dyes from plant extracts. The Russian chemist and botanist Michael Tswett [96, 97] first used the word chromatography to describe the separation of plant pigments. In his experiment, he used a vertical glass column packed with adsorptive materials, as alumina or silica. Afterwards, he injected a solution of plant pigments at the upper end of the column and washed the column with an organic solvent. As a result, a series of colored pigment bands appeared in the column, separated by regions free from pigments. Due to these color bands, he named this method *chromatography* which means *color writing*, deduced from the Greek for color-chroma and for write-graphein. His work was largely ignored until the work of Kuhn et al. [44] on the separation of plant pigments and the first book published by Zechmeister and Chohnoky [106] on chromatography. The modern form of chromatography came up in the 1940s and 1950s. A breakthrough in partition chromatography is due to the work of Martin [57] and related to the subsequent development of different chromatography methods such as, paper chromatography, gas-solid and gas-liquid chromatography and various techniques of column liquid chromatography. Further advances constantly improved the performance of chromatography and promoted application for the separation of many complex mixtures.

## 1.3 Problems and motivation

Mathematical modeling has gained an immense importance in chemical process engineering. Various mathematical models, defined as an abstraction of the physical world are developed, considering different levels of complexity to describe the processes. Due to the exponential increase of computing power in terms of memory size and speed, numerical simulation has increasingly become a very prominent approach to solve complex practical problems in engineering and science. Numerical simulation provides an alternative tool for scientific investigations instead of carrying out expensive, time-consuming or even dangerous experiments in laboratories. The numerical tools are often more valuable than the

conventional experimental methods in terms of providing more profound insights and complete information that cannot be directly measured or observed [30, 81].

Standard chromatographic models contain systems of convection-diffusion partial differential equations with dominating convective terms, coupled with some algebraic equations. Analytical solutions can be obtained in the Laplace domain for linear models. If no analytical inversion could be performed, the numerical inversion can be used to generate the corresponding time domain solutions. Moment analysis is an effective strategy for deducing important information about the retention equilibrium and mass transfer kinetics in the column. Such a moment analysis approach has been found frequently instructive in the literature [30, 41, 42, 43, 62, 63, 64, 65, 76, 82, 87]. The Laplace transformation can be used as a basic tool to obtain moments. The numerical inverse Laplace transformation of the equations provides complete elution profiles. The retention equilibrium-constant and parameters of the mass transfer kinetics in the column are related more simply just to the moments of these profiles available from the Laplace domain solution.

For nonlinear chromatographic models, analytical solutions cannot be derived. For that reason, numerical simulations are needed to predict the dynamic behavior of chromatographic columns. Therefore, computational efficiency and accuracy of a numerical method are of large relevance. However, accurate numerical solutions are difficult to obtain due to the strong nonlinearity introduced typically by the underlying thermodynamic algebraic functions (adsorption isotherms). Steep concentration fronts and shock layers may occur due to the convection dominated partial differential equations (PDEs) of chromatographic models and, hence, efficient numerical methods are required to obtain accurate and physically realistic solutions. Moreover, the simulation of reactive chromatography is also a challenging task for a numerical scheme because of stiffness of the reactive source terms. These stiff terms may produce rapid variations in the solution and can render numerical methods unstable, unless the time step sizes are sufficiently small. Thus, an efficient and accurate numerical technique is needed to avoid excessive dissipation, incorrect phase speeds, spurious oscillations, and to capture sharp discontinuities of the elution profiles. Thus, much effort has been invested already to develop appropriate numerical schemes for

producing efficient and accurate solutions [30, 51, 84, 89].

Generally, three well-known classes of discretization methods can be used to simulate processes, namely the finite difference methods (FDMs), the finite elements methods (FEMs) and the finite volume methods (FVMs) [30]. In the method of finite differences, the model equations are approximated by finite difference formulas and different orders of accuracies can be achieved. An efficient algorithm named as Godunov-Rouchon [75], employs backward difference for the advective term and forward differences for time evolution to solve the model equations. This algorithm gives more reliable results for single components with refined specific meshes than for multi-component systems using averaged meshes. Moreover, implementation of the Godunov-Rouchon algorithm in gradient-elution or in reactive chromatography is not very convenient. In general, classical FDMs may fail at shock discontinuities because of non-uniqueness of the solution.

Finite element methods are one of the prominent and highly effective techniques for obtaining approximate solutions to a wide variety of complex computational problems. The term finite element was first coined by Clough in 1960 [8]. The first book on the FEMs by Zienkiewicz and Chung was published in 1967 [109]. In the early 1960s, FEMs received widespread glory and have been employed to solve a large variety of transport problems arising in nearly every scientific and engineering problems e.g. solid mechanics, fluids flow, heat problems, dynamics and electrostatic problems. These methods, e.g. the orthogonal collocation finite element method (OCFEM), were already applied in the field of chromatography [6, 54]. FEMs are more accurate than the finite difference approach, but they are computationally expensive, and not necessarily conservative locally. Moreover, such methods are unable to suppress numerical oscillations in convection dominated problems. To deal with such problems, stabilization procedures e.g. Galerkin/Least-square (GLS) and Streamline-Upwind/Petrov-Galerkin (SUPG) can be used to eliminate overshoots and undershoots produced by the convective term [32, 33].

The finite volume methods are well known in the computational dynamics field [20, 46, 50, 66, 68, 94]. They refer to small volumes surrounding the nodal points in the domain and are capable of enforcing the integral form of conservation laws on each discretized cell.

The FVMs were originally developed for nonlinear hyperbolic equations and are natural candidates to numerically approximate such chromatographic models. The schemes give high order accuracy on coarse grids, resolve sharp discontinuities, and avoid numerical dispersion which may lead to incorrect solutions [50]. FVMs, which preserve such properties, were already applied to simulate different chromatographic processes [16, 51, 60, 103]. In this thesis, we applied the finite volume method of Koren to chromatographic models and validated the results with some existing finite volume schemes in the literature [34].

Discontinuous Galerkin (DG) methods belong to the class of finite element methods (FEMs) which have several advantages over finite difference methods (FDMs) and finite volume methods (FVMs). For instance, they inherit geometrical flexibility of FVMs and FEMs, retain the conservation properties of FVMs, and possess the high-order properties of FEMs. Therefore, DG-methods are locally conservative, stable, and high order accurate. These methods satisfy the total variation boundedness (TVB) property that guarantees the positivity of the schemes [9, 11, 12, 108]. Positivity is the most common and fundamental mathematical requirement in physical models. In our case, concentrations are non-negative by their nature and their approximations should be non-negative as well. However, numerical solutions of scientific models often generate negative and thus meaningless values. This may happen even when the numerical method is stable and highly accurate. In fact, the tendency to produce negative values may, paradoxically, increase with the order of accuracy of the numerical discretization. Loss of positivity may cause a computation to fail or produce meaningless results, especially conservation of mass can not be achieved. In contrast to high order FDMs and FVMs, DG-methods require a simple treatment of the boundary conditions in order to achieve high order accuracy uniformly. Moreover, DG-methods allow discontinuous approximations and produce block-diagonal mass matrices that can be easily inverted through algorithms of low computational cost. These methods incorporate the idea of numerical fluxes and slope limiters in a very natural way to avoid spurious oscillations (wiggles), which usually occur due to shocks, discontinuities or sharp changes in the solution.

The Discontinuous Galerkin finite element method was initially introduced by Reed and

Hill [71] for solving neutron transport equations. Afterwards, various DG-methods were developed and formulated by Cockburn and Shu for nonlinear hyperbolic system in a series of papers, see for example [9, 11, 12, 13]. DG-methods are being applied in the main stream of computational fluid dynamic models [1, 2, 3, 7, 14, 31]. The DG-methods are versatile, flexible, and have intrinsic stability making them suitable for convection dominated problems. The stability is an intrinsic property of the method to keep the solution bounded, i.e. numerical errors (roundoff due to finite precision of computers) which are generated during the solution of discretized equations should not be magnified. The numerical solution itself should remain uniformly bounded. The DG-methods can be efficiently applied to partial differential equations (PDEs) of all kinds, including equations whose type changes within the computational domain. They were not applied to chromatographic models up to now. In this work, the Runge-Kutta discontinuous Galerkin (RKDG) method is proposed to solve the chromatographic processes [35].

Apart from the above mentioned numerical methods a commercial software, named gPROMS (generalized Process Modeling System) based on difference or orthogonal collocation finite element methods, is quite common in the chromatography community. This software is able to solve several chemical processes, but coarse mesh points produce physically unrealistic numerical oscillations near steep adsorption fronts and refined meshes increase the computational time [50, 61, 95]. Moreover as a black box solver, it is difficult to make changes according to the problems requirement in the software. Therefore, search for an efficient and accurate numerical method is imperative for the correct prediction of chromatographic fronts with reliable accuracy and low computational time.

In this thesis, different numerical schemes are implemented and analyzed for reactive chromatographic models. Another focus is theoretical modeling and simulation of non-isothermal reactive liquid chromatography. Thermal effects are widely discussed in the case of gas phase reactions in solid packings [21, 27, 40, 104, 105]. In reactive liquid chromatography, thermal effects are typically not considered and modeling of the process assumes that effects of heats of sorption and reaction are negligible. Only very few contributions considering thermal effects can be found in the literature [77, 78, 79, 90]. The



purpose of this work is to quantify how temperature gradients can influence conversion and separation in reactive liquid chromatography. Additionally, the coupling of concentration and thermal fronts should be illustrated and key parameters influencing the reactor performance should be identified.

Non-isothermal reactive chromatography can be described by a convection dominated system of nonlinear convection-diffusion-reaction type partial differential equations and algebraic equations describing thermodynamic and kinetic phenomena. The corresponding systems have to be solved numerically because analytical solutions cannot be obtained in such situations. The simulation of non-isothermal reactive chromatography is a challenging task for a numerical scheme due to the nonlinearity of the convection-dominated mass and energy balance equations and because of stiffness of the reactive source terms. Finite volume schemes were already applied in the chromatographic field [16, 34, 51, 60, 103], but were never implemented to the complex non-isothermal reactive chromatographic model considered in this work. This study is an effort to provide more profound insights into various aspects of non-isothermal reactive chromatography and to contribute to improve the performance of the process, so that it can be further developed and scaled up.

## 1.4 Outline of the thesis

The contents of the thesis are arranged in the following manner:

In Chapter 2, the theoretical basis related to chromatography is presented. Moreover, different chromatographic models with model parameters and adsorption isotherms are briefly described.

In Chapter 3, a high resolution finite volume scheme is applied for solving chromatographic models. The third order accuracy of the finite volume scheme is verified by using Taylor expansion of the solution. To suppress the numerical oscillations and preserve the monotonicity of the scheme a minmod limiter is used. Moreover, the total variation bounded Runge-Kutta DG-scheme is implemented for the numerical approximation of chromatographic models. The scheme employs a DG-method in the axial-coordinate that converts

the given PDE to a system of ordinary differential equations (ODEs). The resulting ODE-system is then solved by using explicit and nonlinearly stable high order Runge-Kutta method.

In Chapter 4, the equilibrium dispersive and a non-equilibrium adsorption lumped kinetic model are solved analytically for linear isotherm. For this purpose, the Laplace transformation is utilized as a basic tool to transform the PDEs of the models for linear isotherms to ODEs. The corresponding analytical solutions of EDM and LKM are obtained along with Dirichlet and Robin boundary conditions (BCs). If no analytical inversion could be performed, the numerical inversion is used to generate the time domain solution for different types of boundary conditions. To analyze the considered linear models, the moment method is employed to get expressions for retention times, band broadenings and front asymmetries. In this thesis, a method for describing chromatographic peaks by means of statistical moments is used and the central moments up to third order are calculated and compared with numerically obtained moments.

Chapter 5 presents several test problems of isothermal non-reactive and reactive chromatographic processes under linear and nonlinear conditions. For linear models, analytical solutions are obtained in Chapter 4, while for nonlinear models, only numerical techniques provide solutions. Test Problems are numerically approximated by using the proposed numerical schemes. The performance of the suggested methods is validated against available analytical solutions and some other flux-limiting schemes given in the literature. The case studies include single-component elution, two-component elution, and displacement chromatography on non-movable (fixed) and movable (counter-current) beds. Moreover, practical examples of reactive chromatography are also discussed.

Chapter 6 is focused on modeling and simulation of non-isothermal reactive liquid chromatography [36]. The model is formed by a system of convection-diffusion-reaction partial differential equations. To solve this problem, a flux-limiting semi-discrete high resolution finite volume scheme of Koren [39] is proposed for the numerical approximation of non-isothermal reactive chromatographic models. The scheme discretizes the model in axial-coordinate only, while keeps the time variable continuous. The suggested scheme

is found to be second to third order accurate analytically and numerically in our earlier work of this dissertation on dispersive chromatographic models [34]. Several challenging case studies are carried out which elucidate the effect of several sources for non-isothermal behavior. The numerical results were evaluated critically by performing consistency tests evaluating both mass and energy balances including considerations of limiting cases, which can be theoretically predicted.

Finally, Chapter 7 is dedicated to the conclusion, remarks and future prospectives of our research work.

At the end of the thesis we put an appendix. Appendix A presents the derivation of first three moments for equilibrium dispersive and lumped kinetic models using Dirichlet and Robin boundary conditions. Appendix B provides a notation for this work.

Most of the content of this thesis is already published in several research journals.

Chapter 3 and 4 consist of

1. Javeed, S., Qamar, S., Ashraf, W., Warnecke, G., Seidel-Morgenstern, A., 2013. Analysis and numerical investigation of two dynamic models of liquid chromatography. *Chemical Engineering Science* 90, 17-31.

Chapter 5 summarizes the manuscripts

2. Javeed, S., Qamar, S., Seidel-Morgenstern, A., Warnecke, G., 2011. Efficient and accurate numerical simulation of nonlinear chromatographic processes. *Computer & chemical Engineering* 35, 2294-2305.

3. Javeed, S., Qamar, S., Seidel-Morgenstern, A., Warnecke, G., 2011. A discontinuous Galerkin method to solve chromatographic models. *Journal of Chromatography A* 1218, 7137-7146.

The results presented in Chapter 6 appeared already in

4. Javeed, S., Qamar, S., Seidel-Morgenstern, A., Warnecke, G., 2012. Parametric study of thermal effects in reactive liquid chromatography. *Chemical Engineering Journal* 191, 426-440.

Note that the material for this thesis has been taken from the above mentioned publications without putting the corresponding text passages in quotation marks.

# Chapter 2

## Theory of Chromatography

Mathematical models of chromatographic processes are required to predict the migration behavior of the components in the columns filled with the stationary phases. This chapter briefly introduces chromatographic standard models describing the process on different levels of complexity. Moreover, model parameters and adsorption isotherms are introduced.

### 2.1 Overview

The chromatographic standard models can be mainly divided into three categories, such as the discrete plate models, continuous models using differential equations and statistical variants [28].

The plate models equally divide the column length  $L$  into a finite number of well mixed equilibrium stages or theoretical plates, in which the mobile phase is passing through each of these stages after equilibrium is accomplished. The important examples of plate models are the continuous plate model proposed by Martin and Synge [57] and the discontinuous plate model by Craig [15]. In these models, axial dispersion is described by using the number of theoretical plates and mass transfer effects are typically ignored. The chromatographic solution profiles of both models are the same for a sufficiently high number of theoretical plates.

Another prominent modeling approach is the use of continuous models. This approach is based on differential mass balances of each solute in slices of the column, that leads to a

set of partial differential equations. Afterwards, there is a need to find the mathematical solution of the set of partial differential equations to describe the chromatographic behavior in a column. Continuous models are further classified into many categories depending on different levels of complexity of describing the mass transfer and partition processes. Various mathematical models are available in the literature for understanding and analyzing dynamic composition fronts in chromatographic columns. The most important of these models are the general rate model, the lumped kinetic model, the equilibrium-dispersive model, and the ideal model of chromatography.

The third approach to modeling is a microscopic statistical method for chromatography. The corresponding models deal with the probability density function for solute molecules in time and space. An entire discussion on this topic is beyond the scope of this work. For more details, the readers are referred to consult [19, 81].

## 2.2 Model parameters

This section focuses on the parameters entering into the chromatographic model equations presented in the next section. Firstly, the porosity and the efficiency of a column related to the apparent dispersion coefficient are explained. Afterwards, the adsorption isotherms are discussed.

### 2.2.1 Column porosities

The chromatographic column is packed with porous particles. The volume of a column  $v_{col}$  can be divided into an interstitial volume of mobile phase  $v_m$  and a stationary phase volume  $v_{st}$ . The stationary phase volume  $v_{st}$  can be further divided into two sub-volumes, such as the solid volume  $v_s$  and the intraparticle volume of the pores  $v_{pore}$ . Thus, the total volume of the column becomes

$$v_{col} = v_m + v_s + v_{pore}. \quad (2.1)$$

On the basis of these volumes two types of porosities, the interstitial porosity  $\epsilon_{int}$  and the total porosity  $\epsilon$  can be formulated as

$$\text{Interstitial porosity: } \epsilon_{int} = \frac{v_m}{v_{col}}, \quad (2.2)$$

$$\text{Total porosity: } \epsilon = \frac{v_m + v_{pore}}{v_{col}}. \quad (2.3)$$

The volume of a column is given as

$$v_{col} = \frac{\pi d^2}{4} L, \quad (2.4)$$

where,  $d$  is diameter of a column, while  $L$  represents the length of a column. The interstitial porosity  $\epsilon_{int}$  is relevant for large molecules, while for small molecules the total porosity  $\epsilon$  can be considered. The total porosity can be estimated from the formula given below

$$\epsilon = \frac{t_0 \dot{V}}{v_{col}}, \quad (2.5)$$

where  $\dot{V}$  is the actual volumetric flow rate of the mobile phase. The  $t_0$  denotes the dead time of the column and can be calculated from the ratio of first and zeroth moments of an elution profile of a non retained component after a pulse injection is

$$t_0 = \frac{\int_0^\infty c t dt}{\int_0^\infty c dt}. \quad (2.6)$$

In this work, the total porosity, c.f. Eq. (2.5), was taken into account.

**The Phase ratio (F):** The ratio between the volume fractions of the columns which are occupied by the stationary  $v_{st}$  and the mobile phases  $v_m$ . Using the total porosity  $\epsilon$ , it is defined as

$$F = \frac{1 - \epsilon}{\epsilon}. \quad (2.7)$$

**Linear velocity ( $u$ ):** The linear (or interstitial) velocity  $u$  can be calculated from the subsequent formula, provided the volumetric flow rate  $\dot{V}$  and the total porosity  $\epsilon$  are constant.

$$u = \frac{\dot{V}}{\epsilon \frac{\pi d^2}{4}}. \quad (2.8)$$

### 2.2.2 Efficiency

The efficiency of a column is related to the number of theoretical plates  $N_t$ . This number is related to the height equivalent to a theoretical plate (HETP) as

$$HETP = \frac{L}{N_t}. \quad (2.9)$$

The number of theoretical plates or HETP can be measured by the statistical moment method from measured elution profiles. The  $n$ -th moment of the chromatographic band profile denoted by  $C(x, t)$  at the exit of column bed of length  $x = L$  is

$$M_n = \int_0^\infty C(x = L, t) t^n dt. \quad (2.10)$$

The  $n$ -th initial normalized moment is

$$\mu_n = \frac{\int_0^\infty C(x = L, t) t^n dt}{\int_0^\infty C(x = L, t) dt}. \quad (2.11)$$

The second central moment or the variance can be defined as

$$\sigma^2 = \mu'_2 = \frac{\int_0^\infty C(x = L, t) (t - \mu_1)^2 dt}{\int_0^\infty C(x = L, t) dt}. \quad (2.12)$$

The number  $N_t$  can be obtained by considering the first normalized moment  $\mu_1$  (c.f. Eq. (2.11)), and the second central moment  $\mu'_2$  or variance ( $\sigma^2$ ) (c.f. Eq. (2.12)), as

$$N_t = \frac{\mu_1^2}{\sigma^2}. \quad (2.13)$$

For uniformly packed columns with incompressible fluid flow and for an analytical peak with near Gaussian shape,  $N_t$  can be estimated easily as

$$N_t = 5.54 \left( \frac{t_R}{w_{1/2}} \right)^2, \quad (2.14)$$

where  $t_R$  is the first initial moment of the component peak or the retention time of the elution profile. Further,  $w_{1/2}$  is the peak width at half height. A dispersion coefficient  $D_{\text{app}}$  is related for efficient columns to the number of theoretical plates  $N_t$  by

$$D_{\text{app}} = \frac{Lu}{2N_t}. \quad (2.15)$$

The HETP is a function of linear velocity  $u$  and can be correlated by the Van Deemter equation which can be expressed as (e.g. in [98])

$$HETP = A + \frac{B}{u} + Cu. \quad (2.16)$$

In the above equation,  $A$  is the eddy diffusion term,  $B$  is the axial diffusion term and  $C$  is the mass transfer resistance term. The first term  $A$  is influenced by packing imperfections and by the particle size distributions. The second term  $B$  represents the axial diffusion of the molecules, which can be usually ignored provided the velocity is high enough. The last term represents a linear dependence with interstitial velocity, where  $C$  takes into account mass transfer resistances, which are unavoidable at very high velocities.

### 2.2.3 Adsorption isotherms

Isotherms provide thermodynamic information for designing a chromatographic separation processes and are important to accurately predict the development of concentration profiles in the column. The adsorption isotherm is the equilibrium relationship between the solute molecules in the mobile phase and the molecules adsorbed on the surface of the stationary phase at a constant temperature. This functional relationship is essential to describe the interactions between the components in the mixture to be separated. By evaluating the shape of the *isotherm*, one can distinguish between linear chromatography and nonlinear chromatography.

In linear chromatography, the equilibrium isotherm is defined by a linear equation given as

$$q_i^* = a_i c_i, \quad i = 1, 2, \dots, N_c, \quad (2.17)$$

where the  $a_i$  are Henry's coefficients and  $N_c$  represent the number of components in the sample.

In nonlinear chromatography, the equilibrium relationship between the liquid phase and solid phase concentrations is nonlinear. A nonlinear effect occurs in most applications of preparative chromatography. Many nonlinear adsorption isotherm models are available in the literature, namely Langmuir, Bilangmuir, Freudlich, and Flower models [30]. Nonlinear



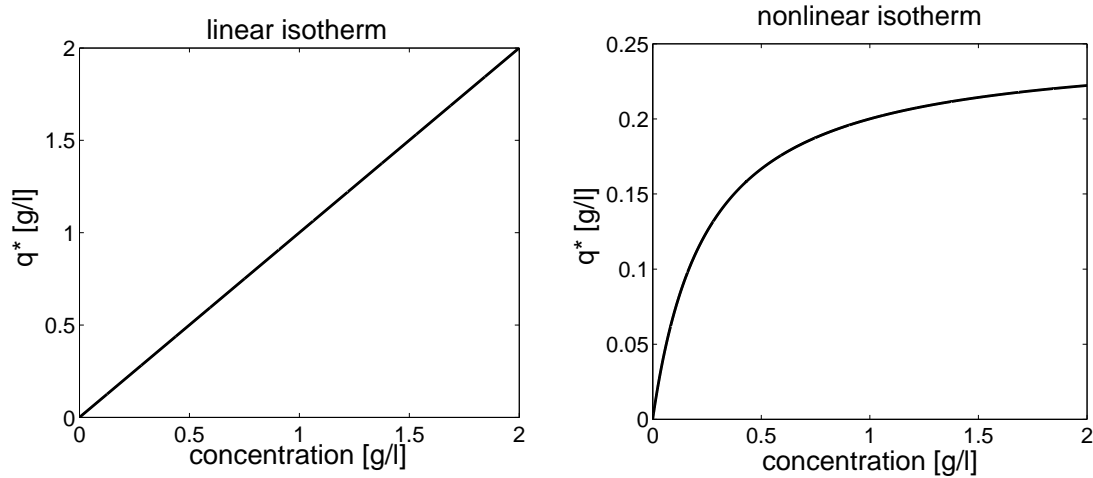


Figure 2.1: Left: linear isotherm, right: nonlinear isotherm.

isotherm can have various complex forms. A special case of convex isotherm is the Langmuir adsorption isotherm, defined for multiple component mixtures as

$$q_i^* = \frac{a_i c_i}{1 + \sum_{j=1}^{N_c} b_j c_j}, \quad i = 1, 2, \dots, N_c, \quad (2.18)$$

where, the  $a_i$  represent again the Henry's coefficients and the  $b_j$  quantify the nonlinearity of the single component isotherms. For demonstration, plots of linear and nonlinear isotherms for a single component with  $a = 1$  and  $b = 4$  are displayed in Figure 2.1. At very low concentrations, the isotherm behaves linearly due to the vanishing influence of the second term in the denominator of Eq. (2.18), while in case of higher concentrations, the influence of this denominator becomes significant causing the nonlinearity.

## 2.3 Continuous chromatographic models

This part explains four well established models of chromatographic columns, namely the ideal model, the equilibrium-dispersive model, the lumped kinetic model, and the general rate model of chromatography. These models can be used for both linear and nonlinear chromatography. All considered models were derived exploiting several basic assumptions which are listed as follows

1. The chromatographic process is isothermal.
2. The bed is homogeneous and the packing material used in the stationary phase is made of porous spherical particles of uniform size.
3. Radial concentration gradients in the column can be neglected.
4. Axial dispersion occurs, and causes band broadening.
5. The mobile phase is considered to be incompressible. This holds for liquid chromatography.
6. There is no interaction between the solvent (mobile) and the solid (stationary) phase.

### 2.3.1 The ideal model

The ideal model assumes that the column has an infinite efficiency. It means that the axial dispersion is negligible i.e.,  $D_{\text{app}} = 0$ , and the thermodynamic equilibrium is achieved instantaneously. The one dimensional mass balance equation for incompressible fluid and the isotherm are given as

$$\frac{\partial c_i}{\partial t} + F \frac{\partial q_i^*}{\partial t} + u \frac{\partial c_i}{\partial z} = 0, \quad i = 1, 2, \dots, N_c, \quad (2.19)$$

$$q_i^* = f(c_i). \quad (2.20)$$

In the above equations,  $N_c$  represents the number of mixture components in the sample,  $c_i$  denotes the  $i$ -th liquid phase concentration,  $q_i^*$  is the  $i$ -th solid concentration, c.f. Eq. (2.18),  $u$  is the interstitial velocity,  $F = (1 - \epsilon)/\epsilon$  is the phase ratio based on the porosity  $\epsilon \in ]0, 1[$ ,  $t$  is time, and  $z$  stands for the axial-coordinate. This model provides a first estimation of the concentration profiles but cannot predict accurately the elution profiles for low-efficiency columns. In such situations, the contributions of the mass transfer kinetics and axial dispersion become eminent.

### 2.3.2 The equilibrium dispersive model (EDM)

The equilibrium dispersive model still assumes that the mass transfer is of infinite rate. Moreover, all contributions due to non-equilibrium and axial dispersion are aggregated into the corresponding apparent (lumped) dispersion coefficient  $D_{\text{app}}$ . The mass balance equation of the multi-component equilibrium dispersive model for a fixed bed chromatography column is written as

$$\frac{\partial c_i}{\partial t} + F \frac{\partial q_i^*}{\partial t} + u \frac{\partial c_i}{\partial z} = D_{\text{app},i} \frac{\partial^2 c_i}{\partial z^2}, \quad i = 1, 2, \dots, N_c. \quad (2.21)$$

Here,  $D_{\text{app},i}$  represents the  $i$ -th apparent axial dispersion coefficient. The EDM predicts the chromatographic profiles accurately when the column efficiency is high and small particles are used as the stationary phase in the column. The mass balance equation of the multi-component fixed-bed chromatographic reactor (FBCR) model adds a reaction term and is given as

$$\frac{\partial c_i}{\partial t} + F \frac{\partial q_i^*}{\partial t} + u \frac{\partial c_i}{\partial z} = D_{\text{app},i} \frac{\partial^2 c_i}{\partial z^2} + F \nu_i r, \quad i = 1, 2, \dots, N_c, \quad (2.22)$$

where,  $r$  is the rate of the reaction, and the  $\nu_i$  are the corresponding stoichiometric coefficients of the components. Note that, the stoichiometric coefficients  $\nu_i$  are negative for reactants and positive for products.

For convenience, the source term in Eq. (2.22) can be re-written as

$$\frac{\partial c_i}{\partial t} + F \frac{\partial q_i^*}{\partial t} + u \frac{\partial c_i}{\partial z} = D_{\text{app},i} \frac{\partial^2 c_i}{\partial z^2} + Q_i(t, z, c), \quad i = 1, 2, \dots, N_c. \quad (2.23)$$

The source term  $Q_i(t, z, c)$  will be explicitly defined in the test problems discussed in Chapter 5.

### 2.3.3 The lumped kinetic model (LKM)

The lumped kinetic model incorporates with the rate of variation of the local concentration of solute in the stationary phase and local deviation from equilibrium concentrations. The model lumps the contribution of internal and external mass transport resistances into a

mass transfer coefficient  $k$ . The one-dimensional mass balance laws of a multi-component LKM are expressed as

$$\frac{\partial c_i}{\partial t} + u \frac{\partial c_i}{\partial z} = D_i \frac{\partial^2 c_i}{\partial z^2} - \frac{k_i}{\epsilon} (q_i^* - q_i), \quad (2.24)$$

$$\frac{\partial q_i}{\partial t} = \frac{k_i}{1 - \epsilon} (q_i^* - q_i), \quad (2.25)$$

$$q_i^* = f(c_i), \quad i = 1, 2, \dots, N_c. \quad (2.26)$$

This simple model accounts for the mass transfer kinetics and is more exact than the equilibrium dispersive model.

### 2.3.4 The general rate model (GRM)

The GRM considers several contributions of mass transfer kinetics occurring in chromatography. As there are several ways to describe these effects, there are many versions of this model. Usually, axial dispersion, the mass transfer between mobile and stationary phase and intraparticle the pore diffusion are included in the equations. Also possible limited rates of adsorption-desorption are often still ignored. The GRM contains two mass balance equations for the solute, one for inside the particles, and the other for outside the particles. The mass balance for a fluid percolating through a bed of spherical particles of radius  $R_P$  is given as

$$\epsilon \frac{\partial c_i}{\partial t} + u \frac{\partial c_i}{\partial z} = \epsilon D_i \frac{\partial^2 c_i}{\partial z^2} - (1 - \epsilon) k_{\text{exp},i} a_P \times (c_i - c_{P,i}(r = R_P)), \quad (2.27)$$

where,  $c_{P,i}$  is the concentration in the particle pores,  $k_{\text{exp}}$  is the external mass transfer coefficient, and  $a_P$  represents the external surface area of the adsorbent particles. The mass balance inside the particles can be given by

$$\epsilon_P \frac{\partial c_{P,i}}{\partial t} + (1 - \epsilon_P) \frac{\partial q_i^*}{\partial t} = D_{\text{eff},i} \frac{1}{r^2} \frac{\partial}{\partial r} \left( r^2 \frac{\partial c_{P,i}}{\partial r} \right), \quad (2.28)$$

where,  $\epsilon_P$  is the internal porosity of the particles and the  $D_{\text{eff},i}$  are the effective pore diffusion coefficients. In principle the GRM has the potential to achieve an accurate description of chromatographic profiles. However, the implementation and the computation of the GRM

is rather expensive and requires many input parameters. Therefore, simplified versions of the GRM, namely the LKM and the EDM are usually applied to simulate chromatographic separation processes. For this reason, in this dissertation, the lumped kinetic and the equilibrium dispersive models are our main concern.

To solve the related mass balance equations given above, appropriate initial and boundary conditions have to be specified to close the model formulations.

### **The Initial conditions:**

The initial conditions for the liquid phase concentrations typically assume not preloaded columns as

$$c_i(0, z) = c_i^{\text{init}} = c_{i,0}(z), \quad i = 1, 2, \dots, N_c. \quad (2.29)$$

The corresponding initial conditions used in LKM for fully regenerated columns are given as

$$c_i(0, z) = 0, \quad q_i(0, z) = 0, \quad i = 1, 2, \dots, N_c. \quad (2.30)$$

Two types of boundary conditions are applied to solve the above second order PDE models.

### **Boundary conditions of type I: Dirichlet boundary conditions**

The Dirichlet boundary conditions at the column inlet is

$$c_i|_{z=0} = c_i^{\text{in}}(t, 0) = c_{i,0}, \quad i = 1, 2, \dots, N_c. \quad (2.31a)$$

One useful and realistic outlet condition is

$$c_i(\infty, t) = 0, \quad i = 1, 2, \dots, N_c. \quad (2.31b)$$

### **Boundary conditions of type II: Robin type boundary conditions**

The following more accurate inlet boundary conditions is typically used for models containing dispersion terms [17, 83]. This Robin type of boundary conditions are known in chemical engineering as Danckwerts conditions

$$c_i|_{z=0} = c_{i,0} + \frac{D_i}{u} \frac{\partial c}{\partial z} \Big|_{z=0} \quad i = 1, 2, 3, \dots, N_c. \quad (2.32a)$$

These inlet conditions are usually applied together with the following outlet conditions

$$\frac{\partial c_i(L, t)}{\partial z} = 0. \quad (2.32b)$$

Other boundary conditions can also be used to solve the model equations introduced above. In this thesis, the lumped kinetic model and the equilibrium dispersive model are used due to their relative simplicity and their demonstrated strength [37]. The finite volume method of Koren and the discontinuous Galerkin method, presented in the next chapter, are proposed to numerically approximate these chromatographic models.

# Chapter 3

## Numerical Schemes

Several numerical schemes have been used in the literature for the approximation of chromatographic models [30, 75]. This chapter presents the derivation of two numerical methods for solving fixed-bed chromatographic reactive (FBCR) models. In section 1, a high resolution finite volume scheme introduced by Koren [39] is applied for the numerical approximation of the reactive chromatographic model. In section 2, a discontinuous Galerkin method is derived for the numerical simulation of reactive chromatographic model.

### 3.1 The FVMs formulation for FBCR models

This section contains the derivation of the finite volume method of Koren to solve equilibrium dispersive model with reaction. The scheme is second to third order accurate in the axial-coordinate. The order of the scheme is verified analytically during the derivation of the scheme. For simplicity, a single component equilibrium dispersive model equation with reaction term, c.f. Eq. (2.23), is taken into account

$$\frac{\partial c}{\partial t} + F \frac{\partial q^*}{\partial t} + u \frac{\partial c}{\partial z} = D_{\text{app}} \frac{\partial^2 c}{\partial z^2} + Q(t, z, c). \quad (3.1)$$

In the Eq. (3.1),  $Q(t, z, c)$  denotes the reaction or source term which will be explicitly defined in the test problems. If the source or reaction term set equal to zero, i.e.  $Q(t, z, c) = 0$ , then Eq. (3.1) leads to the equilibrium dispersive model (c.f. Eq. (2.21)).

Let us define  $w := w(c) = c + Fq^*(c)$  and  $f(c) = uc$ , the above equation becomes

$$\frac{\partial w}{\partial t} + \frac{\partial f(c)}{\partial z} = D_{\text{app}} \frac{\partial^2 c}{\partial z^2} + Q(t, z, c). \quad (3.2)$$

Before applying the proposed numerical scheme to Eq. (3.2), it is required to discretize the computational domain. Let  $N$  represents the number of discretization points and  $(z_{j-\frac{1}{2}})_{j \in \{1, \dots, N+1\}}$  are partitions of the given interval  $[0, L]$ . For each  $j = 1, 2, \dots, N$ ,  $\Delta z$  is a constant width of each mesh interval,  $z_j$  denote the cell centers, and  $z_{j \pm \frac{1}{2}}$  refer to the cell boundaries, (c.f. Figure 3.1). We assign,

$$z_{1/2} = 0, \quad z_{N+1/2} = L, \quad z_{j+1/2} = j \cdot \Delta z, \quad \text{for } j = 1, 2, \dots, N. \quad (3.3)$$

Moreover,

$$z_j = (z_{j-1/2} + z_{j+1/2})/2 \quad \text{and} \quad \Delta z = z_{j+1/2} - z_{j-1/2} = \frac{L}{N+1}. \quad (3.4)$$

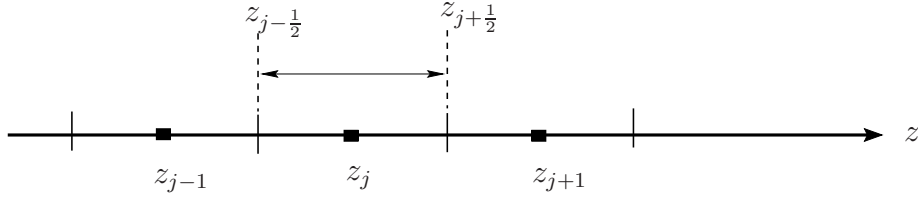


Figure 3.1: Cell centered finite volume grid.

Let  $I_j := [z_{j-1/2}, z_{j+1/2}]$  for  $i \geq 1$ . The cell averaged initial data  $w_0(z)$  in each cell is given as

$$w_j(0) = \frac{1}{\Delta z} \int_{I_j} w_0(z) dz, \quad \text{for } j = 1, 2, \dots, N. \quad (3.5)$$

By integrating Eq. (3.2) over the interval  $I_j = [z_{j-1/2}, z_{j+1/2}]$ , we obtain

$$\int_{I_j} \frac{\partial w}{\partial t} dz = - \left( f_{j+1/2} - f_{j-1/2} \right) + D_{\text{app}} \left( \left( \frac{\partial c}{\partial z} \right)_{j+1/2} - \left( \frac{\partial c}{\partial z} \right)_{j-1/2} \right) + \int_{I_j} Q(t, z, c) dz. \quad (3.6)$$



In each  $I_j$ , the averaged values of the conservative variable  $w(t)$  are given as

$$w_j := w_j(t) = \frac{1}{\Delta z} \int_{I_j} w(t, z) dz. \quad (3.7)$$

Therefore, by using Eq. (3.7) in Eq. (3.6), the following semi-discrete scheme is obtained

$$\frac{dw_j}{dt} = -\frac{f_{j+\frac{1}{2}} - f_{j-\frac{1}{2}}}{\Delta z} + \frac{D_{\text{app}}}{\Delta z} \left( \left( \frac{\partial c}{\partial z} \right)_{j+\frac{1}{2}} - \left( \frac{\partial c}{\partial z} \right)_{j-\frac{1}{2}} \right) + Q_j \quad j = 1, 2, \dots, N. \quad (3.8)$$

Here,  $N$  represents the number of mesh points in the domain of computations and differential terms in the diffusion part can be approximated as

$$\left( \frac{\partial c}{\partial z} \right)_{j\pm\frac{1}{2}} = \pm \left( \frac{c_{j\pm 1} - c_j}{\Delta z} \right). \quad (3.9)$$

The next step is to approximate the convective fluxes,  $f_{j\pm\frac{1}{2}}$ , in Eq. (3.8) and different approximations give different numerical schemes. Let us exploit the following inequalities  $u > 0$  and  $f > 0$ .

**First order scheme:** In this case, the fluxes are approximated as

$$f_{j+\frac{1}{2}} = f_j = (uc)_j, \quad f_{j-\frac{1}{2}} = f_{j-1} = (uc)_{j-1}. \quad (3.10)$$

This approximation gives a first order accurate scheme in the axial-direction.

**High resolution schemes:** To achieve higher order accuracy, a piecewise interpolation polynomial can be used, such as

$$f_{j+\frac{1}{2}} = f_j + \frac{1+\kappa}{4}(f_{j+1} - f_j) + \frac{1-\kappa}{4}(f_j - f_{j-1}), \quad \kappa \in [-1, 1]. \quad (3.11)$$

Similarly,  $f_{j-\frac{1}{2}}$  can be written as

$$f_{j-\frac{1}{2}} = f_{j-1} + \frac{1+\kappa}{4}(f_j - f_{j-1}) + \frac{1-\kappa}{4}(f_{j-1} - f_{j-2}), \quad \kappa \in [-1, 1], \quad (3.12)$$

where, the parameter  $\kappa$  is selected from the interval  $[-1, 1]$ . Here,  $\kappa = -1$  and  $\kappa = 1$  give second order central schemes, while other values of  $\kappa \in (-1, 1)$  give one sided upwind schemes. Basically, van Leer [100] is the pioneer of  $\kappa$  interpolation schemes.

**Truncation error:** The following definition is utilized for evaluating the truncation error.

**Definition:** The *truncation error* in the interval  $\Omega_j$  is a residual that remains after substituting the exact solution  $w_j$  into Eq. (3.8) as

$$\tau_j(t) := \frac{dw_j}{dt} + \frac{f_{j+\frac{1}{2}} - f_{j-\frac{1}{2}}}{\Delta z} - \frac{D_{\text{app}}}{\Delta z} \left( \left( \frac{\partial c}{\partial z} \right)_{j+\frac{1}{2}} - \left( \frac{\partial c}{\partial z} \right)_{j-\frac{1}{2}} \right) - Q_j. \quad (3.13)$$

Let  $\boldsymbol{\tau}(t) := [\tau_1(t), \tau_2(t), \dots, \tau_N(t)]^T$ . The scheme (3.8) is called consistent of order  $p^*$  if, for  $\Delta z \rightarrow 0$ ,

$$\|\boldsymbol{\tau}(t)\| := \mathcal{O}(\Delta z^{p^*}) \quad (3.14)$$

uniformly for all  $t$ . Here,  $\|\cdot\|$  denotes a vector norm in  $\mathbb{R}^N$ .

Let  $c_t := \frac{\partial c}{\partial t}$ ,  $f_z := \frac{\partial f}{\partial z}$  and similarly the higher order derivatives. The Taylor expansions of Eqs. (3.11) and (3.12) at point  $z_j$  give after some manipulations,

$$\begin{aligned} f(t, z_{j+\frac{1}{2}}) &= f(t, z_j) + \frac{\Delta z}{2}(f_z)(t, z_j) + \frac{\kappa \Delta z^2}{2 \cdot 2!}(f_{zz})(t, z_j) \\ &\quad + \frac{\Delta z^3}{2 \cdot 3!}(f_{zzz})(t, z_j) + \frac{\kappa \Delta z^4}{2 \cdot 4!}(f_{zzzz})(t, z_j) + \mathcal{O}(\Delta z^5), \\ f(t, z_{j-\frac{1}{2}}) &= f(t, z_j) - \frac{\Delta z}{2}(f_z)(t, z_j) + \frac{\kappa \Delta z^2}{2 \cdot 2!}(f_{zz})(t, z_j) \\ &\quad + \left(1 - \frac{3}{2}\kappa\right) \frac{\Delta z^3}{3!}(f_{zzz})(t, z_j) + \left(-3 - \frac{7}{2}\kappa\right) \frac{\Delta z^4}{4!}(f_{zzzz})(t, z_j) + \mathcal{O}(\Delta z^5). \end{aligned}$$

By putting the above expressions in Eq. (3.13), we get after using Eq. (3.2)

$$\begin{aligned} \tau_j(t) &:= \frac{dw(t, z_j)}{dt} + \frac{f(t, z_{j+\frac{1}{2}}) - f(t, z_{j-\frac{1}{2}})}{\Delta z} - \frac{D_{\text{app}}}{\Delta z} \left( \left( \frac{\partial c}{\partial z} \right)_{j+\frac{1}{2}} - \left( \frac{\partial c}{\partial z} \right)_{j-\frac{1}{2}} \right) - Q_j \\ &= \underbrace{w_t(t, z_j) + f_z(t, z_j) - D_{\text{app}} c_{zz}(t, z_j) - Q_j}_{=0} + \left( \frac{3}{2}\kappa - \frac{1}{2} \right) \frac{\Delta z^2}{3!} f_{zzz}(t, z_j) \\ &\quad + D_{\text{app}} \frac{\Delta z^2}{12} c_{zzzz}(t, z_j) + \mathcal{O}(\Delta z^3) \\ &= \left( \frac{3}{2}\kappa - \frac{1}{2} \right) \frac{\Delta z^2}{3!} f_{zzz}(t, z_j) - D_{\text{app}} \frac{\Delta z^2}{12} c_{zzzz}(t, z_j) + \mathcal{O}(\Delta z^3). \end{aligned} \quad (3.15)$$

For  $\kappa = \frac{1}{3} \left( 1 + D_{\text{app}} \frac{c_{zzzz}(t, z_i)}{f_{zzz}(t, z_i)} \right)$ , one gets a third order accurate scheme, i.e.  $\|\boldsymbol{\tau}(t)\| = \mathcal{O}(\Delta z^3)$ . The disadvantage of this  $\kappa$  value is its comparative computational difficulty in calculating the term  $\frac{c_{zzzz}(t, z_j)}{f_{zzz}(t, z_j)}$ , especially in the case of difficult flux functions. One can

avoid this problem by considering a higher influence of the advection term as compared to the dispersion term and can choose  $\kappa = \frac{1}{3}$ . This selection of  $\kappa$  is also suitable for the approximation of current advection dominated dispersive model. However, this assumption will affect the accuracy of the scheme when the model is diffusion dominated.

**Koren scheme:** Here,  $\kappa = \frac{1}{3}$  is chosen which is third order accurate when there is no flux-limiting as shown above. For this choice of  $\kappa$ , Eq. (3.11) becomes

$$f_{j+\frac{1}{2}} = f_j + \frac{1}{2} \left( \frac{1}{3} + \frac{2}{3} \frac{f_{j+1} - f_j}{f_j - f_{j-1}} \right) (f_j - f_{j-1}). \quad (3.16)$$

However, such approximations of flux terms may give negative solutions due to oscillations in regions of strong variations. To deal with such problems, Koren [39] has used the following Sweby-type flux-limiter [88],

$$f_{j+\frac{1}{2}} = f_j + \frac{1}{2} \phi \left( r_{j+\frac{1}{2}} \right) (f_j - f_{j-1}), \quad (3.17)$$

where,  $r_{j+\frac{1}{2}}$  is the ratio of consecutive flux gradients

$$r_{j+\frac{1}{2}} = \frac{f_{j+1} - f_j + \eta}{f_j - f_{j-1} + \eta}. \quad (3.18)$$

Here,  $\eta \approx 10^{-10}$  is used to avoid division by zero and the limiting function  $\phi$  is given as

$$\phi(r_{j+\frac{1}{2}}) = \max \left( 0, \min \left( 2r_{j+\frac{1}{2}}, \min \left( \frac{1}{3} + \frac{2}{3}r_{j+\frac{1}{2}}, 2 \right) \right) \right). \quad (3.19)$$

Due to flux-limiting, the above scheme is second to third order accurate [39]. The scheme gives third order accuracy for a convection dominated equilibrium dispersive model and gives second order accuracy for a model with very small dispersion coefficient, i.e. when the model tends to equilibrium case. The same behavior of the scheme is numerically verified in a test problem.

**Other flux-limiting schemes:** Several other flux-limiting schemes are available in the literature. These schemes are different because they involve different flux-limiting functions [74, 100]. In these schemes,  $\kappa = -1$  is used in Eqs. (3.11) and (3.12) to obtain fluxes at the cell boundaries. For example, a limited flux at the right boundary of cell  $I_j$  is given as

$$f_{j+\frac{1}{2}} = f_j + \frac{1}{2} \varphi \left( \theta_{j+\frac{1}{2}} \right) (f_{j+1} - f_j). \quad (3.20)$$

Table 3.1: Different flux limiters used in (3.20).

Flux limiter	Formula
van Leer ([100])	$\varphi(r) = \frac{ r +r}{1+ r }$
Superbee ([74])	$\varphi(r) = \max(0, \min(2r, 1), \min(r, 2))$
Minmod ([74])	$\varphi(r) = \max(0, \min(1, r))$
MC ([100])	$\varphi(r) = \max(0, \min(2r, \frac{1}{2}(1+r), 2))$

In similar manner, the left cell-boundary flux can be approximated. Here,  $\theta_{j+\frac{1}{2}}$  is the ratio of consecutive flux gradients

$$\theta_{j+\frac{1}{2}} = \frac{f_j - f_{j-1} + \eta}{f_{j+1} - f_j + \eta}. \quad (3.21)$$

A few well known flux limiters are selected in this study which are listed in Table 3.1. The efficiency and accuracy of the Koren scheme will be analyzed against these schemes for selected test problems.

**Scheme strategy at the boundaries:** The approximations (3.17) and (3.20) are not applicable to the boundary intervals. Let us consider the left boundary with inflow boundary condition. The position of the interval face  $z_{\frac{1}{2}}$  and inflow boundary are identical. However,  $z_0$  is not known, therefore Eqs. (3.17) and (3.20) are not applicable at  $z_{\frac{3}{2}}$ . To overcome this problem, the first order approximation (3.10) can be practiced at the cell interfaces  $z_{\frac{3}{2}}$  and  $z_{N+\frac{1}{2}}$ . Let  $f^{\text{in}}$  indicates the injected flux, then

$$f_{\frac{1}{2}} = f^{\text{in}}, \quad f_{\frac{3}{2}} = f_1, \quad f_{N+\frac{1}{2}} = f_N. \quad (3.22)$$

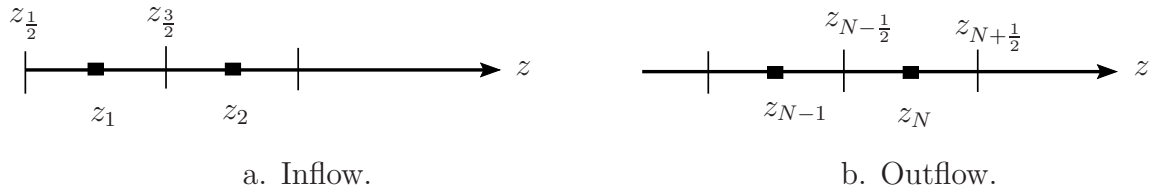


Figure 3.2: Grids near the boundaries.

The fluxes at other cell interfaces can be computed by using Eqs. (3.17) or (3.20). However, the use of a first order scheme in the boundary intervals would not effect the global accuracy of the method.

At each time step, the liquid concentration  $c$  is needed for updating the values of isotherm  $q^*(c)$  and flux  $f(c) = uc$ . However, Eq. (3.8) gives the updated values of  $w_j(t) = c_j(t) + Fq_j^*(c)$  in each mesh interval  $\Omega_j$ . Therefore, the chain rule can be used in Eq. (3.8) which gives for  $j = 1, 2, \dots, N$

$$\frac{dc_j}{dt} = - \left( 1 + F \left( \frac{dq^*}{dc} \right)_j \right)^{-1} \left[ \frac{f_{j+\frac{1}{2}} - f_{j-\frac{1}{2}}}{\Delta z} - \frac{D_{\text{app}}}{\Delta z} \left( \left( \frac{\partial c}{\partial z} \right)_{j+\frac{1}{2}} - \left( \frac{\partial c}{\partial z} \right)_{j-\frac{1}{2}} \right) - Q_j \right]. \quad (3.23)$$

The resulting system of ODEs can be solved by using any standard ODE-solver. In this dissertation, the Runge-Kutta 45 method was used to solve the ODE-system, c.f. Eq. (3.23).

## 3.2 The DG method formulation for FBCR models

In this section, the TVB Runge-Kutta DG-scheme of Cockburn [9] and Qiu et al. [70] is implemented for solving the FBCR model given in Eq. (3.1). Firstly, we suitably rewrite the original system as a degenerate (transformed) first-order system to obtain the weak formulation for deriving the numerical scheme. Then, the TVB Runge-Kutta DG-scheme is applied in axial-coordinate that converts the given PDE to an ODE-system. The resulting ODE-system is approximated by using the TVB Runge-Kutta method. For convenience, one-component FBCR model is considered and is given as

$$\frac{\partial c}{\partial t} + F \frac{\partial q^*}{\partial t} + u \frac{\partial c}{\partial z} = D_{\text{app}} \frac{\partial^2 c}{\partial z^2} + Q(t, z, c). \quad (3.24)$$

Let us re-write the above equation as

$$\frac{\partial}{\partial t} (c + Fq^*(c)) + \frac{\partial}{\partial z} \left( uc - D_{\text{app}} \frac{\partial c}{\partial z} \right) = Q(t, z, c) \quad (3.25)$$

and define

$$w(c) := c + Fq^*(c), \quad g(c) := \sqrt{D_{\text{app}}} \frac{\partial c}{\partial z}, \quad f(c, g) := uc - \sqrt{D_{\text{app}}} g(c). \quad (3.26)$$

Then, Eq. (3.25) changes to the following system of PDEs

$$\frac{\partial w}{\partial t} = -\frac{\partial f}{\partial z} + Q(t, z, c), \quad (3.27)$$

$$g = \sqrt{D_{\text{app}}} \frac{\partial c}{\partial z}. \quad (3.28)$$

The axial-length variable  $z$  is discretized as follows. For  $j = 1, 2, 3, \dots, N$ , let  $z_{j+\frac{1}{2}}$  be the cell partitions,  $I_j = ]z_{j-\frac{1}{2}}, z_{j+\frac{1}{2}}[$  be the domain of cell  $j$ ,  $\Delta z_j = z_{j+\frac{1}{2}} - z_{j-\frac{1}{2}}$  be the width of cell  $j$ , and  $I = \cup I_j$  be the partition of the whole domain. We seek an approximate solution  $w_h(t, z)$  to  $w(t, z)$  such that for each time  $t \in [0, T]$ ,  $w_h(t, z)$  belongs to the finite dimensional space

$$V_h = \{v \in L^1(I) : v|_{I_j} \in P^p(I_j), j = 1, 2, 3, \dots, N\}, \quad (3.29)$$

where  $P^p(I_j)$  denotes the set of polynomials of degree up to  $p$  defined on the cell  $I_j$ . Note that in  $V_h$ , the functions are allowed to have jumps at the cell interface  $z_{j+\frac{1}{2}}$ . In order to determine the approximate solution  $w_h(t, z)$ , a weak formulation is needed. To obtain weak formulation, Eqs. (3.27) and (3.28) are multiplied by an arbitrary smooth function  $v(z)$  followed by integration by parts over the interval  $I_j$ , we get

$$\begin{aligned} \int_{I_j} \frac{\partial w(t, z)}{\partial t} v(z) dz &= - \left( f(c_{j+\frac{1}{2}}, g_{j+\frac{1}{2}}) v(z_{j+\frac{1}{2}}) - f(c_{j-\frac{1}{2}}, g_{j-\frac{1}{2}}) v(z_{j-\frac{1}{2}}) \right) \\ &\quad + \int_{I_j} \left( f(c, g) \frac{\partial v(z)}{\partial z} + Q(t, z, c) v(z) \right) dz, \end{aligned} \quad (3.30)$$

$$\int_{I_j} g(c) v(z) dz = \sqrt{D_{\text{app}}} \left( c_{j+\frac{1}{2}} v(z_{j+\frac{1}{2}}) - c_{j-\frac{1}{2}} v(z_{j-\frac{1}{2}}) \right) - \sqrt{D_{\text{app}}} \int_{I_j} c(z) \frac{\partial v(z)}{\partial z} dz. \quad (3.31)$$

One way to implement (3.29) is to choose Legendre polynomials,  $P_l(z)$ , of order  $l$  as local basis functions. In this case, the  $L^2$ -orthogonality property of Legendre polynomials can be exploited, namely

$$\int_{-1}^1 P_l(s) P_{l'}(s) ds = \left( \frac{2}{2l+1} \right) \delta_{ll'}. \quad (3.32)$$

For each  $z \in I_j$ , the solution  $w_h$  and  $g_h$  can be expressed as

$$w_h(t, z) = \sum_{l=0}^p w_j^{(l)} \varphi_l(z), \quad g_h(c_h(t, z)) = \sum_{l=0}^p g_j^{(l)} \varphi_l(z), \quad (3.33)$$

where

$$\varphi_l(z) = P_l(2(z - z_j)/\Delta z_j), \quad l = 0, 1, \dots, p. \quad (3.34)$$

If  $p = 0$  the approximate solution  $w_h$  uses the piecewise constant basis functions, if  $p = 1$  the linear basis functions are used, and so on. In this thesis the linear basis functions were taken into account, therefore  $l = 0, 1$ .

By using Eqs. (3.32)-(3.34), it is easy to verify that

$$w_j^{(l)}(t) = \frac{2l+1}{\Delta z_j} \int_{I_j} w_h(t, z) \varphi_l(z) dz, \quad g_j^{(l)}(t) = \frac{2l+1}{\Delta z_j} \int_{I_j} g_h(c_h) \varphi_l(z) dz. \quad (3.35)$$

Then, the smooth function  $v(z)$  can be replaced by the test function  $\varphi_l \in V_h$  and the exact solutions  $w$  and  $g$  by the approximate solutions  $w_h$  and  $g_h$ . Moreover, the function  $f(c_{j+\frac{1}{2}}, g_{j+\frac{1}{2}}) = f(c(t, z_{j+\frac{1}{2}}), g(c_{j+\frac{1}{2}}))$  is not defined at the cell interface  $z_{j+\frac{1}{2}}$ . Therefore, it has to be replaced by a numerical flux that depends on two values of  $c_h(t, z)$ , at the discontinuity, i.e.,

$$f(c_{j+\frac{1}{2}}, g_{j+\frac{1}{2}}) \approx h_{j+\frac{1}{2}} = h(c_{j+\frac{1}{2}}^-, c_{j-\frac{1}{2}}^+). \quad (3.36)$$

As  $g := g(c)$ , it can be dropped from the arguments of  $h$  for simplicity. Here,

$$c_{j+\frac{1}{2}}^- := c_h(t, z_{j+\frac{1}{2}}^-) = \sum_{l=0}^p c_j^{(l)} \varphi_l(z_{j+\frac{1}{2}}), \quad c_{j-\frac{1}{2}}^+ := c_h(t, z_{j-\frac{1}{2}}^+) = \sum_{l=0}^p c_j^{(l)} \varphi_l(z_{j-\frac{1}{2}}). \quad (3.37)$$

Using the above definitions, the weak formulations (3.30) and (3.31) simplify to

$$\begin{aligned} \frac{dw_j^{(l)}(t)}{dt} &= -\frac{2l+1}{\Delta z_j} \left( h_{j+\frac{1}{2}} \varphi_l(z_{j+\frac{1}{2}}) - h_{j-\frac{1}{2}} \varphi_l(z_{j-\frac{1}{2}}) \right) \\ &\quad + \frac{2l+1}{\Delta z_j} \int_{I_j} \left( f(c_h, g_h) \frac{d\varphi_l(z)}{dz} + Q(t, z, c) \varphi_l(z) \right) dz, \end{aligned} \quad (3.38)$$

$$g_j^{(l)}(t) = \frac{2l+1}{\Delta z_j} \sqrt{D_{\text{app}}} \left( c_{j+\frac{1}{2}} \varphi_l(z_{j+\frac{1}{2}}) - c_{j-\frac{1}{2}} \varphi_l(z_{j-\frac{1}{2}}) - \int_{I_j} c_h(t, z) \frac{d\varphi_l(z)}{dz} dz \right). \quad (3.39)$$

At each time step, the liquid concentration  $c$  is needed for updating the values of the isotherm  $q^*(c)$  and flux  $f(c, g(c))$ . However, Eq. (3.38) gives the updated values of  $w_j = c_j(t) + Fq_j^*(c)$  in each mesh interval  $I_j$ . Therefore, the chain rule can be used in Eq. (3.38) and the system of ordinary differential equations in terms of  $c_j$  can be obtained. Thus, the scheme in Eqs. (3.38) and (3.39) takes the following form

$$\begin{aligned} \frac{dc_j^{(l)}(t)}{dt} = & - \left( 1 + F \left( \frac{dq^*}{dc} \right)_j^{(l)} \right)^{-1} \frac{2l+1}{\Delta z_j} \left[ h_{j+\frac{1}{2}} \varphi_l(z_{j+\frac{1}{2}}) - h_{j-\frac{1}{2}} \varphi_l(z_{j-\frac{1}{2}}) \right] \\ & + \left( 1 + F \left( \frac{dq^*}{dc} \right)_j^{(l)} \right)^{-1} \frac{2l+1}{\Delta z_j} \int_{I_j} \left( f(c_h, g_h) \frac{d\varphi_l(z)}{dz} + Q(t, z, c) \varphi_l(z) \right) dz, \end{aligned} \quad (3.40)$$

$$g_j^{(l)}(t) = \frac{2l+1}{\Delta z_j} \sqrt{D_{\text{app}}} \left( c_{j+\frac{1}{2}} \varphi_l(z_{j+\frac{1}{2}}) - c_{j-\frac{1}{2}} \varphi_l(z_{j-\frac{1}{2}}) - \int_{I_j} c_h(t, z) \frac{d\varphi_l(z)}{dz} dz \right). \quad (3.41)$$

The initial data for the above system are given as, c.f. Eq. (3.35),

$$c_j^{(l)}(0) = \frac{2l+1}{\Delta z_j} \int_{I_j} c(0, z) \varphi_l(z) dz, \quad g_j^{(l)}(0) = g(c_j^{(l)}(0)). \quad (3.42)$$

It remains to choose the appropriate numerical flux function  $h$ . The above equation defines a monotone scheme if the numerical flux function  $h(a, b)$  is consistent,  $h(c, c) = f(c, g(c))$ , and satisfies the Lipschitz continuity condition, i.e.  $h(a, b)$  is a non-decreasing function of its first argument and non-increasing function of its second argument. In other words, a scheme is called monotone if it preserves the monotonicity of the numerical one-dimensional solution when passing from one time step to another. The following numerical fluxes are available in the literature, that satisfy the above mentioned properties [46, 50, 107].

(i) The Godunov flux:

$$h^G(a, b) = \begin{cases} \min_{a \leq n \leq b} f(n, g(n)) & \text{if } a \leq b, \\ \max_{a \geq n \geq b} f(n, g(n)) & \text{if } a > b. \end{cases} \quad (3.43)$$

(ii) The Lax-Friedrichs flux:

$$h^{LF}(a, b) = \frac{1}{2} [f(a, g(a)) + f(b, g(b)) - C(b-a)], \quad C = \max_{\inf n^0(x) \leq s \leq \sup n^0(x)} |f'(s, g(s))|. \quad (3.44)$$



(iii) The Local Lax-Friedrichs flux:

$$h^{LLF}(a, b) = \frac{1}{2}[f(a, g(a)) + f(b, g(b)) - C(b - a)], \quad (3.45)$$

$$C = \max_{\min(a,b) \leq s \leq \max(a,b)} |f'(s, g(s))|. \quad (3.46)$$

(iv) The Roe flux with ‘entropy fix’:

$$h^R(a, b) = \begin{cases} f(a, g(a)), & \text{if } f'(n, g(n)) \geq 0 \\ f(b, g(b)), & \text{if } f'(n, g(n)) \leq 0 \\ h^{LLF}(a, b), & \text{otherwise.} \end{cases} \quad \text{for } n \in [\min(a, b), \max(a, b)], \quad (3.47)$$

In this thesis, we used the Local Lax-Friedrich flux for the investigated models. The Gauss-Lobatto quadrature rule of order 10 was used to approximate the integral terms appearing on the right-hand-side of (3.40) and (3.41).

In order to achieve the total variation stability, some limiting procedure has to be introduced. For that purpose, it is needed to modify  $c_{j+\frac{1}{2}}^\pm$  in (3.36) by some local projection. For more details, readers are referred to see e.g. [9]. To this end, we write (3.37) as

$$c_{j+\frac{1}{2}}^- = c_j^{(0)} + \tilde{c}_j, \quad c_{j-\frac{1}{2}}^+ = c_j^{(0)} - \hat{c}_j, \quad (3.48)$$

where

$$\tilde{c}_j = \sum_{l=1}^p c_j^{(l)} \varphi_l(z_{j+\frac{1}{2}}) \quad \hat{c}_j = - \sum_{l=1}^p c_j^{(l)} \varphi_l(z_{j-\frac{1}{2}}). \quad (3.49)$$

In this study, we consider the linear basis functions, therefore  $l=0,1$ . In above equation, when  $p = 0$ ,  $\tilde{c}_j = \hat{c}_j = 0$  and when  $p = 1$ ,  $\tilde{c}_j = \hat{c}_j = 6c_j^{(1)}$  etc.

Next,  $\tilde{c}_j$  and  $\hat{c}_j$  can be modified as

$$\tilde{c}_j^{(\text{mod})} = \text{mm}(\tilde{c}_j, \Delta_+ c_j^{(0)}, \Delta_- c_j^{(0)}), \quad \hat{c}_j^{(\text{mod})} = \text{mm}(\hat{c}_j, \Delta_+ c_j^{(0)}, \Delta_- c_j^{(0)}), \quad (3.50)$$

where,  $\Delta_\pm := \pm(c_{j\pm 1} - c_j)$  and mm is the usual minmod function defined as

$$\text{mm}(a_1, a_2, a_3) = \begin{cases} s \cdot \min_{1 \leq i \leq 3} |a_i| & \text{if } \text{sign}(a_1) = \text{sign}(a_2) = \text{sign}(a_3) = s, \\ 0 & \text{otherwise.} \end{cases} \quad (3.51)$$

Then, Eq. (3.48) modifies to

$$c_{j+\frac{1}{2}}^{-(\text{mod})} = c_j^{(0)} + \tilde{c}_j^{(\text{mod})}, \quad c_{j-\frac{1}{2}}^{+(\text{mod})} = c_j^{(0)} - \hat{c}_j^{(\text{mod})} \quad (3.52)$$

and replace (3.36) by

$$h_{j+\frac{1}{2}} = h(c_{j+\frac{1}{2}}^{-(\text{mod})}, c_{j-\frac{1}{2}}^{+(\text{mod})}). \quad (3.53)$$

This local projection limiter does not affect the accuracy in the smooth regions and convergence can be achieved without oscillations near shocks, see e.g. [9]. Finally, a Runge-Kutta method that maintains the TVB property of the scheme is needed to solve the resulting ODE-system. Let us rewrite Eqs. (3.40) and (3.41) in a concise form as

$$\frac{dc_h}{dt} = L_h(c_h, t). \quad (3.54)$$

Then, the  $r$ -order TVB Runge-Kutta method can be used to approximate Eq. (3.54)

$$(c_h)^p = \sum_{l=0}^{p-1} [\alpha_{pl}(c_h)^{(l)} + \beta_{pl}\Delta t L_h((c_h)^{(l)}, t^s + d_l\Delta t)], \quad p = 1, 2, \dots, r, \quad (3.55)$$

where based on Eq. (3.42)

$$(c_h)^{(0)} = (c_h)^s, \quad (c_h)^{(r)} = (c_h)^{s+1}. \quad (3.56)$$

where,  $s$  is the  $s$ -th time step. For second order TVB Runge-Kutta method the coefficient are given as (e.g. [9])

$$\alpha_{10} = \beta_{10} = 1, \quad \alpha_{20} = \alpha_{21} = \beta_{21} = \frac{1}{2}, \quad \beta_{20} = 0; \quad d_0 = 0, \quad d_1 = 1. \quad (3.57)$$

While, for the third order TVB Runge-Kutta method the coefficient are given as

$$\begin{aligned} \alpha_{10} = \beta_{10} = 1, \quad \alpha_{20} = \frac{3}{4}, \quad \beta_{20} = 0, \quad \alpha_{21} = \beta_{21} = \frac{1}{4}, \quad \alpha_{30} = \frac{1}{3} \\ \beta_{30} = \alpha_{31} = \beta_{31} = 0, \quad \alpha_{32} = \beta_{32} = \frac{2}{3}; \quad d_0 = 0, \quad d_1 = 1, \quad d_2 = \frac{1}{2}. \end{aligned} \quad (3.58)$$

The CFL condition is given as, [9],

$$\Delta t \leq \left( \frac{1}{2p+1} \right) \min \left( 1 + F \left( \frac{dq}{dc} \right)_j^{(0)} \right) \min \left( \frac{\Delta z_j}{u}, \frac{\Delta z_j^2}{2D_{\text{app}}} \right), \quad (3.59)$$

where,  $p = 1, 2$  for second and third order schemes, respectively.

**Boundary conditions:** Let us put the boundary at  $z_{-\frac{1}{2}} = 0$ . The left boundary condition given by Eqs. (2.32a) and (2.32b) can be implemented as

$$c_{-\frac{1}{2}}^-(t) = c_0^{(0)} + \frac{D}{u} \frac{c_1^{(0)} - c_0^{(0)}}{\Delta z}, \quad (3.60)$$

$$\tilde{c}_0^{(\text{mod})} = \text{mm} \left( \tilde{c}_0, \Delta_+ c_0^{(0)}, 2 \left( c_0^{(0)} - c^{\text{in}} \right) \right), \quad \hat{c}_0^{(\text{mod})} = \text{mm} \left( \hat{c}_0, \Delta_+ c_0^{(0)} \right). \quad (3.61)$$

Outflow boundary condition is used on the right end of the column,  $c_{N+1}^{(l)} = c_N^{(l)}$ .

In the following chapters, the above models and corresponding numerical schemes will be used for the simulation of selected chromatographic processes and operation regimes. Returning to the main chromatographic models considered in this work, namely the EDM and the LKM, can be further classified into two sub-models, i.e., the isotherm function  $q_i^* = f(c_i)$ , depending on the thermodynamic properties. The first simpler case is related to linear isotherm, Eq. (2.17). In such situations, there exist the possibility to solve the equation of the EDM and LKM analytically. This will be demonstrated in Chapter 4. In this chapter, also reduced models based on the statistical moments will be introduced and provided analytically. The analytical solution give the opportunity for critical validation of the numerical predictions using the schemes discussed in the current chapter. The second, more difficult sub-model corresponds to nonlinear isotherm Eq. (2.18). In case of nonlinear isotherm, no analytical solution can be acquired. Therefore, a validation of numerical schemes can be done only by comparing with predictions of the schemes. In Chapter 5, schemes are applied to numerically approximate multi-component nonlinear chromatographic model equations. The numerical schemes once validated for single component linear adsorption in Chapter 4, are seen as powerful tools to simulate a wide range of processes, c.f. Chapter 5.

# Chapter 4

## Analytical Solution and Moment Analysis for Linear Models

This chapter is concerned with the analytical solution of two established models for simulating liquid chromatographic processes namely, the equilibrium dispersive and lumped kinetic models. The models are analyzed using Dirichlet and Robin boundary conditions for linear isotherms. The Laplace transformation is applied to solve these models analytically for single component adsorption under linear conditions. Statistical moments of step responses are calculated and compared with the numerical predictions for both types of boundary conditions.

### 4.1 The lumped kinetic model (LKM)

The mass balance law of a single component LKM is expressed as

$$\frac{\partial c}{\partial t} + u \frac{\partial c}{\partial z} = D \frac{\partial^2 c}{\partial z^2} - \frac{k}{\epsilon} (q^* - q), \quad (4.1)$$

$$\frac{\partial q}{\partial t} = \frac{k}{1 - \epsilon} (q^* - q). \quad (4.2)$$

The three characteristic times in the model Eqs. (4.1)-(4.2) are defined as

$$\tau_C = \frac{L}{u}, \quad \tau_D = \frac{D}{u^2}, \quad \tau_{MT} = \frac{1}{k}. \quad (4.3)$$

The ratios of these characteristic times provide dimensionless quantities as

$$\tilde{\tau}_1 = \frac{\tau_C}{\tau_D} = \frac{Lu}{D}, \quad \tilde{\tau}_2 = \frac{\tau_C}{\tau_{MT}} = \frac{Lk}{u}. \quad (4.4a)$$

Here,  $\tilde{\tau}_1$  typically is frequently called the Peclet number  $Pe$

$$Pe = \tilde{\tau}_1 = \frac{Lu}{D}, \quad (4.4b)$$

where  $L$  denotes the length of the column.

For diluted systems or small concentrations, linear isotherms is used and is defined as

$$q^* = ac. \quad (4.5)$$

### The equilibrium dispersive model (EDM)-a limiting case of LKM

The basic assumption of EDM is that the kinetics of mass transfer in the chromatographic column and the kinetics of adsorption-desorption are faster. In Eqs. (4.1) and (4.2),  $k$  is the mass transport coefficient. As the value of  $k$  becomes larger, i.e.  $k \rightarrow \infty$ , the model Eqs. (4.1)-(4.2) change to the equilibrium dispersive model ( $\frac{\partial q}{\partial t} = \frac{\partial q^*}{\partial t}$ ) as given below

$$\frac{\partial c}{\partial t} + F \frac{\partial q^*}{\partial t} + u \frac{\partial c}{\partial z} = D_{\text{app}} \frac{\partial^2 c}{\partial z^2}. \quad (4.6)$$

Here,  $F$  is the phase ratio related to porosity, i.e.  $F = \frac{1-\epsilon}{\epsilon}$ ,  $D_{\text{app}}$  is the apparent dispersion coefficient related to the Peclet number by  $Pe = Lu/D_{\text{app}}$ .

## 4.2 Analytical solutions of EDM and LKM for linear isotherm

In this section, single component ( $N_c = 1$ ) linear chromatographic models are considered. Analytical solutions are derived in a Laplace domain for linear isotherms (Eq. (4.5)) with Dirichlet (Eq. (2.31a)) and Danckwerts (Eq. (2.32a)) inlet boundary conditions. To simplify the notations, we consider  $c(x, t) = c_1(x, t)$ .

### 4.2.1 Analytical solution of EDM

The Laplace transformation is defined as

$$C(x, s) = \int_0^{\infty} e^{-st} c(x, t) dt, \quad s > 0. \quad (4.7)$$

After normalizing Eq. (4.6) by defining

$$x = z/L \quad Pe = Lu/D_{\text{app}} \quad (4.8)$$

and by applying the Laplace transformation Eq. (4.7) to Eq. (4.6) with  $N_c = 1$  and  $c^{\text{init}}(t = 0, z) = 0$ , we obtain

$$\frac{d^2C}{dx^2} - Pe \frac{dC}{dx} - sPe \frac{L}{u} (1 + aF)C = 0. \quad (4.9)$$

The solution of this equation is given as

$$C(x, s) = A \exp(\lambda_1 x) + B \exp(\lambda_2 x), \quad (4.10)$$

$$\lambda_{1,2} = \frac{Pe}{2} \mp \frac{1}{2} \sqrt{Pe^2 + 4Pe \frac{L}{u} (1 + aF)s}. \quad (4.11)$$

After applying the Dirichlet boundary conditions in Eqs. (2.31a) and (2.31b), the values of A and B are given as

$$A = \frac{c_0}{s}, \quad B = 0. \quad (4.12)$$

Then, Eq. (4.10) takes the following simple form

$$C(x, s) = \frac{c_0}{s} \exp\left(\left(\frac{Pe}{2} - \frac{1}{2} \sqrt{Pe^2 + 4Pe \frac{L}{u} (1 + aF)s}\right)x\right). \quad (4.13)$$

The solution in the time domain  $c(x, t)$ , can be obtained by using the exact formula for the back transformation as

$$c(x, t) = \frac{1}{2\pi i} \int_{\gamma-i\infty}^{\gamma+i\infty} e^{ts} C(x, s) ds, \quad (4.14)$$

where,  $\gamma$  is a real constant that exceeds the real part of all singularities of  $C(x, s)$ . On applying Eq. (4.14) to Eq. (4.13), we obtain

$$c(x, t) = \frac{c_0}{2} \operatorname{erfc}\left(\frac{\sqrt{\frac{Pe}{2}} \frac{L}{u} (1 + aF)x - t}{\sqrt{\frac{L}{u} t} (1 + aF)}\right) + \frac{c_0}{2} \exp(xPe) \operatorname{erfc}\left(\frac{\sqrt{\frac{Pe}{2}} \frac{L}{u} (1 + aF)x + t}{\sqrt{\frac{L}{u} t} (1 + aF)}\right), \quad (4.15)$$

where,  $\operatorname{erfc}$  denotes the complementary error function.

If we consider the second set of boundary conditions given by Eqs. (2.32a) and (2.32b), the values of  $A$  and  $B$  take the following forms

$$A = \frac{c_0}{s} \frac{\lambda_2 \exp(\lambda_2)}{\left(1 - \frac{\lambda_1}{Pe}\right) \lambda_2 \exp(\lambda_2) - \left(1 - \frac{\lambda_2}{Pe}\right) \lambda_1 \exp(\lambda_1)}, \quad (4.16)$$

$$B = \frac{-c_0}{s} \frac{\lambda_1 \exp(\lambda_1)}{\left(1 - \frac{\lambda_1}{Pe}\right) \lambda_2 \exp(\lambda_2) - \left(1 - \frac{\lambda_2}{Pe}\right) \lambda_1 \exp(\lambda_1)}. \quad (4.17)$$

With these values  $A$  and  $B$ , the back transformation of Eq. (4.10) is not doable analytically. However, well established numerical inverse Laplace transformation could be used to get  $c(x, t)$ . In this work, the Fourier series approximation of Eq. (4.14) is used [73].

### 4.2.2 Analytical solution of LKM

After applying the Laplace transformation to the single component LKM with Dirichlet boundary conditions, The Eqs. (4.1) and (4.2) take the forms

$$\frac{d^2 C}{\partial x^2} - Pe \frac{dC}{dx} - \frac{PeL}{u} Cs - \frac{L^2}{\epsilon D} akC + \frac{L^2}{\epsilon D} k\tilde{Q} = 0, \quad (4.18)$$

$$s\tilde{Q} = \frac{k}{1-\epsilon}(aC - \tilde{Q}) \Rightarrow \tilde{Q} = \frac{\frac{ka}{(1-\epsilon)}}{s + \frac{k}{(1-\epsilon)}} C. \quad (4.19)$$

On putting the value of  $\tilde{Q}$  in Eq. (4.18), we obtain

$$\frac{d^2 C}{\partial x^2} - Pe \frac{dC}{dx} - Pe \frac{L}{u} Cs - \frac{L^2}{\epsilon D} akC + \frac{L^2}{\epsilon D} \frac{\frac{k^2 a}{(1-\epsilon)}}{s + \frac{k}{(1-\epsilon)}} C = 0, \quad (4.20)$$

or

$$\frac{d^2 C}{\partial x^2} - Pe \frac{dC}{dx} - \left( Pe \frac{L}{u} s - \frac{L^2}{\epsilon D} \frac{\frac{k^2 a}{(1-\epsilon)}}{s + \frac{k}{(1-\epsilon)}} + \frac{L^2}{\epsilon D} ak \right) C = 0. \quad (4.21)$$

Thus, the Laplace domain solution is given as

$$C(x, s) = A \exp(\lambda_1 x) + B \exp(\lambda_2 x), \quad (4.22)$$

where

$$\lambda_{1,2} = \frac{Pe}{2} \mp \sqrt{\left(\frac{Pe}{2}\right)^2 + \left( Pe \frac{L}{u} s - \frac{L^2}{\epsilon D} \frac{\frac{k^2 a}{(1-\epsilon)}}{s + \frac{k}{(1-\epsilon)}} + \frac{L^2}{\epsilon D} ak \right)}. \quad (4.23)$$

For the simplified boundary conditions, Eqs. (2.31a) and (2.31b), we have again

$$A = \frac{c_o}{s}, \quad B = 0. \quad (4.24)$$

Using these values of  $A$  and  $B$  in Eq. (4.22), we obtain

$$C(x, s) = \frac{c_o}{s} \exp \left( \frac{Pe}{2} - \sqrt{\left(\frac{Pe}{2}\right)^2 + \left( Pe \frac{L}{u} s - \frac{L^2}{\epsilon D} \frac{k^2 a}{(1-\epsilon)} + \frac{L^2}{\epsilon D} ak \right)} \right) x, \quad (4.25)$$

or

$$C(x, s) = \frac{c_o}{s} \exp \left( \frac{Pe}{2} - \frac{1}{2} \sqrt{Pe^2 + 4Pe \frac{L}{u} s \left( 1 + \frac{aF}{1 + \frac{s(1-\epsilon)}{k}} \right)} \right) x. \quad (4.26)$$

For sufficiently large values of  $k$  in Eq. (4.26), i.e. when  $k \rightarrow \infty$ , the transformed solution  $C(x, s)$  for LKM becomes the solution of EDM given by Eq. (4.13). Once again, the numerical inverse Laplace transformation is employed to find the original solution  $c(x, t)$  of Eq. (4.26).

For Danckwerts boundary conditions in Eqs. (2.32a) and (2.32b), the solution in the Laplace domain takes the same form as given by Eq. (4.22). The values of  $A$  and  $B$  are provided by Eqs. (4.16) and (4.17), whereas,  $\lambda_{1,2}$  can be found in Eq. (4.23). The numerical inverse Laplace transformation was employed to find the original solution  $c(x, t)$ .

### 4.3 Reduced EDM and LKM: Moment models

Moment analysis is an effective strategy for deducing important information about the retention equilibrium and mass transfer kinetics in the column [30, 43, 64, 65, 76, 82, 86]. The Laplace transformation can be used as a basic tool to obtain moments. The numerical inverse Laplace transformation of the equations provides the optimum solution, but this solution is not helpful to study the behavior of chromatographic band in the column. The retention equilibrium-constant and parameters of the mass transfer kinetics in the column are related to the moments in the Laplace domain. In this section, a method for describing chromatographic peaks by means of statistical moments is used and the central moments up to third order are calculated for two sets of boundary conditions. The moment of an



elution profile response to pulse inputs at the exit of chromatographic bed of length  $x = L$  is

$$\mu_n = \int_0^{\infty} C(x = L, t) t^n dt. \quad (4.27)$$

The  $n$ -th initial normalized moment is

$$\mu_n = \frac{\int_0^{\infty} C(x = L, t) t^n dt}{\int_0^{\infty} C(x = L, t) dt}. \quad (4.28)$$

The  $n$ -th central moment is

$$\mu'_n = \frac{\int_0^{\infty} C(x = L, t) (t - \mu_1)^n dt}{\int_0^{\infty} C(x = L, t) dt}. \quad (4.29)$$

In this study, the first three moments are calculated for the equilibrium dispersive and lumped kinetic models. The formulas for the finite moments  $\mu_0, \mu_1, \mu'_2, \mu'_3$  corresponding to the EDM and LKM with both sets of boundary conditions are given in Table 4.1. Complete derivations of these moments for EDM and LKM are presented in Appendix A. It is well known that the first moment  $\mu_1$  corresponds to the retention time  $t_R$ . The value of the equilibrium constant  $a$  can be estimated from the slopes of a straight lines,  $\mu_1 = t_R$  over  $1/u$  for constant column length and porosity. It is shown (c.f. Table 4.1) that effects of longitudinal diffusion are not significant with respect to retention time or first moment. The second central moment  $\mu_2$  or the variance of the elution breakthrough curves or peaks provides significant information related to mass transfer processes in the column. The quantitative value of  $\mu_2$  or variance indicates the band broadening or width of breakthrough curves or peaks and helps to calculate the HETP (height equivalent to theoretical plates). A zeroth value of third statistical moment  $\mu'_3$  designates symmetric curves. Finally, the third central moment  $\mu'_3$  was analyzed which evaluates front asymmetries. The second and the third central moment for the more general Danckwerts BCs reduce to the moments for the Dirichlet BCs in case  $D_{app}$  approaches to zero. A comparison of analytical moments and numerical moments obtained by the proposed numerical scheme is given in the next section.

Table 4.1: Analytically determined moments for EDM and LKM for  $x = 1$  and  $c_0 = 1$ ,  $\mu_0 = 1$  and  $\mu_1 = \frac{L}{u}(1 + aF)$ .

models and BC's	$\mu_2$	$\mu_3$
EDM (Dirichlet)	$\frac{2LD_{\text{app}}(1+aF)^2}{u^3}$	$\frac{12LD_{\text{app}}^2}{u^5}(1+aF)^3$
EDM (Danckwerts)	$\frac{2LD_{\text{app}}}{u^3}(1+aF)^2 \left[ 1 + \frac{D_{\text{app}}}{Lu} (e^{-Lu/D_{\text{app}}} - 1) \right]$	$\frac{12LD_{\text{app}}^2}{u^5}(1+aF)^3 \left[ \left( 1 + \frac{2D_{\text{app}}}{Lu} \right) e^{-Lu/D_{\text{app}}} + \left( 1 - \frac{2D_{\text{app}}}{Lu} \right) \right]$
LKM (Dirichlet)	$\frac{2LD(1+aF)^2}{u^3} + \frac{1}{k} \left( \frac{2LaF(1-\epsilon)}{u} \right)$	$\frac{12LD^2}{u^5}(1+aF)^3 + \frac{1}{k} \left( \frac{12LD(1+aF)aF(1-\epsilon)}{u^3} \right) + \frac{1}{k^2} \left( \frac{6LaF(1-\epsilon)^2}{u} \right)$
LKM (Danckwerts)	$\frac{2LD}{u^3}(1+aF)^2 \left[ 1 + \frac{D}{Lu} (e^{-Lu/D} - 1) \right] + \frac{1}{k} \left( \frac{2LaF\epsilon}{u} \right)$	$\frac{12LD^2(1+aF)^3}{u^5} \left[ \left( 1 + \frac{2D}{Lu} \right) e^{-Lu/D} + \left( 1 - \frac{2D}{Lu} \right) \right] + \frac{1}{k} \left[ \frac{12LDaF^2\epsilon(1+aF)}{u^3} \left( \frac{D}{Lu} e^{-Lu/D} + 1 - \frac{D}{Lu} \right) \right] + \frac{1}{k^2} \left( \frac{6LaF^3\epsilon^2}{u} \right)$

## 4.4 Numerical test problems

### Single component breakthrough curves for linear isotherms

In this chapter, only single component breakthrough curves with linear isotherms are considered. To validate the results, several numerical test problems are taken into account. The DG-method and the finite volume scheme of Koren already discussed in Chapter 3 for EDM is employed to solve the test problems. The Koren scheme is flux-limiting second to third order accurate in space coordinate and guarantees the positivity of the solution. In this study, the suggested DG-scheme uses linear basis functions in each cell, giving a second order accurate scheme in axial-coordinate. The ODE-system is solved by a third-order Runge-Kutta method given in Eq. (3.57). The program is written in the C-language under a Linux operating system and was compiled on a computer with an Intel(R) Core 2 Duo processor of speed 2 GHz and memory (RAM) 3.83 GB.

### Error analysis for LKM

The purpose of this part is to quantitatively analyze the performance of different numerical schemes for single component linear chromatographic models. Here, a comparison of different numerical schemes is presented for lumped kinetic model. The parameters of the problem are given in Table 4.2. The numerical schemes are already presented in Chapter 3 for the EDM and the remaining flux limiters can be found in Table 3.1. The numerical results at the column outlet are shown in Figure 4.1. In that figure, the concentration profiles generated by using different numerical schemes on 100 grid points are compared with the analytical solution obtained from the Laplace transformation. It can be observed that DG and Koren methods have better accuracy as compared to other flux limiting finite volume schemes. Further, the zoomed plot of Figure 4.1 shows that the solution of DG-scheme is closest to the analytical solution. The  $L^1$ -error in time at the column outlet was calculated using the formula

$$L^1 - \text{error} = \sum_{\hat{n}=1}^{N_T} |c_R^{\hat{n}} - c_N^{\hat{n}}| \Delta t. \quad (4.30)$$

The relative error can be defined as

$$\text{relative error} = \frac{\sum_{\hat{n}=1}^{N_T} |c_R^{\hat{n}} - c_N^{\hat{n}}|}{\sum_{\hat{n}=1}^{N_T} |c_R^{\hat{n}}|} \Delta t, \quad (4.31)$$

where  $c_R^{\hat{n}}$  denotes the Laplace solution at the column outlet for time  $t^{\hat{n}}$  and  $c_N^{\hat{n}}$  represents the corresponding numerical solution. Moreover,  $N_T$  denotes the total number of time steps and  $\Delta t$  represents the time step size. Comparisons of  $L^1$ -errors, relative errors and computational times of schemes are given in Tables 4.3 and 4.4 for 50 and 100 grid points, respectively. It can be observed that the DG-scheme produces small errors compared to the other schemes for both 50 and 100 grid cells, but efficiency (or CPU time) of the Koren scheme is better than the other schemes for both numbers of grid points. It can be noticed that relative errors of the DG and Koren schemes are very low for 100 grid points. For that reason, to achieve acceptable accuracy, 100 mesh points are chosen for further numerical simulations discussed in this chapter. On the basis of these results, one can conclude that the DG and Koren methods are optimal choices to approximate chromatographic models. Therefore, we are relying on the results of the DG scheme for the remaining problems of this chapter.

### Dispersion and mass transfer effects

In this problem, both the single component EDM and LKM models are considered and compared. The parameters used to solve the model equations are taken from [53] and are given in Table 4.2. Figure 4.2 (top: left) depicts the dispersion effects of EDM by considering different values of  $D_{\text{app}}$  or characteristic times  $\tau_D$ . It demonstrates that smaller values of  $D_{\text{app}}$  produce steeper fronts. Figure 4.2 (top: right), shows similar dispersion effects by varying  $D$  as described by the LKM keeping  $\tau_C = 10$  s and  $\tau_{MT} = 0.01$  s ( $k = 100$  1/s,  $\tilde{\tau}_2 = 10^3$ ) fixed. The similarity with the corresponding figure for the EDM is due to the relative large value for  $k$ . In Figure 4.2 (bottom: left), different values of the mass transfer coefficients  $k$  for fixed  $D = 10^{-5}$  m<sup>2</sup>/s ( $Pe = 10^4$ ) and  $\tau_C = 10$  s are used for the LKM. This figure shows that increasing values of  $k$  has a similar effects as produced by decreasing  $D$ . In Figure 4.2 (bottom: right), dispersion coefficient  $D = 10^{-3}$  m<sup>2</sup>/s ( $Pe =$

Table 4.2: Parameters for Section 4.4.

Parameters	values
Column length	$L = 1.0 \text{ m}$
Porosity	$\epsilon = 0.4$
Interstitial velocity	$u = 0.1 \text{ m/s}$
Characteristic time	$\tau_C = 10 \text{ s}$
Dispersion coefficient for EDM	$D_{app} = 10^{-4} \text{ m}^2/\text{s}$
Peclet no for EDM	$\tilde{\tau}_1 = Pe = 10^3$
Characteristic time for EDM	$\tau_D = 0.01 \text{ s}$
Dispersion coefficient for LKM	$D = 10^{-5} \text{ m}^2/\text{s}$
Peclet no for LKM	$\tilde{\tau}_1 = Pe = 10^4$
Characteristic time for LKM	$\tau_D = 0.001 \text{ s}$
Mass transfer coefficient	$k = 100 \text{ 1/s}$
Characteristic time	$\tau_{MT} = 0.01 \text{ s}$
Dimensionless number	$\tilde{\tau}_2 = 10^3$
Concentration at inlet	$c_{1,0} = 1.0 \text{ g/l}$
Adsorption equilibrium constant	$a = 0.85$

Table 4.3: Errors and CPU times at 50 grid points.

Limiter	$L^1$ -error	Relative error	CPU (s)
DG Scheme	0.4011	0.0100	5.86
Koren	0.5155	0.0137	4.90
Van Leer	0.9324	0.0248	8.26
Superbee	1.0732	0.0286	9.34
MC	0.9762	0.0260	8.82

$10^2$ ) is taken into consideration for different values of  $k$ . It is evident that even for a large magnitude of the mass transfer coefficient  $k$ , sharp fronts are not possible due to significant dispersion effects. All trends generated numerically are well-known and realistic for the adsorption community.

### Comparison of analytical and numerical solutions

This part focuses on the comparison of analytical and numerical results from the EDM and the LKM for both Dirichlet and Danckwerts boundary conditions. In Figure 4.3 (left), the exact solution obtained for the EDM with Dirichlet boundary conditions is compared with the numerical Laplace inversion and DG-scheme results. Good agreement of these profiles

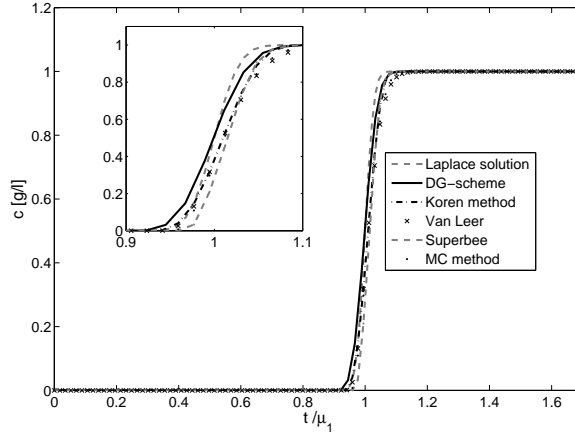


Figure 4.1: Breakthrough curves (BTC) at  $x = 1$ . Comparison of different numerical schemes for LKM (c.f. Eq. (4.14) & Eq. (4.25)) with  $\tau_C = 10$  s,  $\tau_D = 0.01$  s ( $D = 10^{-5}$  m<sup>2</sup>/s or  $\tilde{\tau}_1 = Pe = 1000$ ) and  $\tau_{MT} = 0.01$  s ( $k = 100$  1/s or  $\tilde{\tau}_2 = 10^3$ ).

Table 4.4: Errors and CPU times at 100 grid points.

Limiter	$L^1$ -error	Relative error	CPU (s)
DG Scheme	0.0139	$3.71 \times 10^{-4}$	8.46
Koren	0.0153	$4.08 \times 10^{-4}$	7.82
Van Leer	0.2255	0.0060	14.90
Superbee	0.2966	0.0079	17.73
MC	0.2477	0.0066	14.96

verify the accuracy of numerical Laplace inversion and the proposed numerical scheme. Moreover, the numerical Laplace inversion technique is found to be a reliable method to solve such model problems and will be used below in the subsequent case studies. In Figure 4.3 (right), the results of the DG method for the LKM and Dirichlet boundary conditions are compared with the numerical Laplace inversion solution. No analytical back transform solution was available for the LKM using Dirichlet boundary conditions. Figures 4.4 (left) and (right) validate the results of numerical Laplace inversion and the DG-scheme for the EDM and LKM with Danckwerts boundary conditions, respectively. These profiles show the high precision of the numerical Laplace inversion technique and the suggested numerical scheme. Thus, it can also be concluded that the considered numerical Laplace inversion technique is an effective tool for solving these linear models.

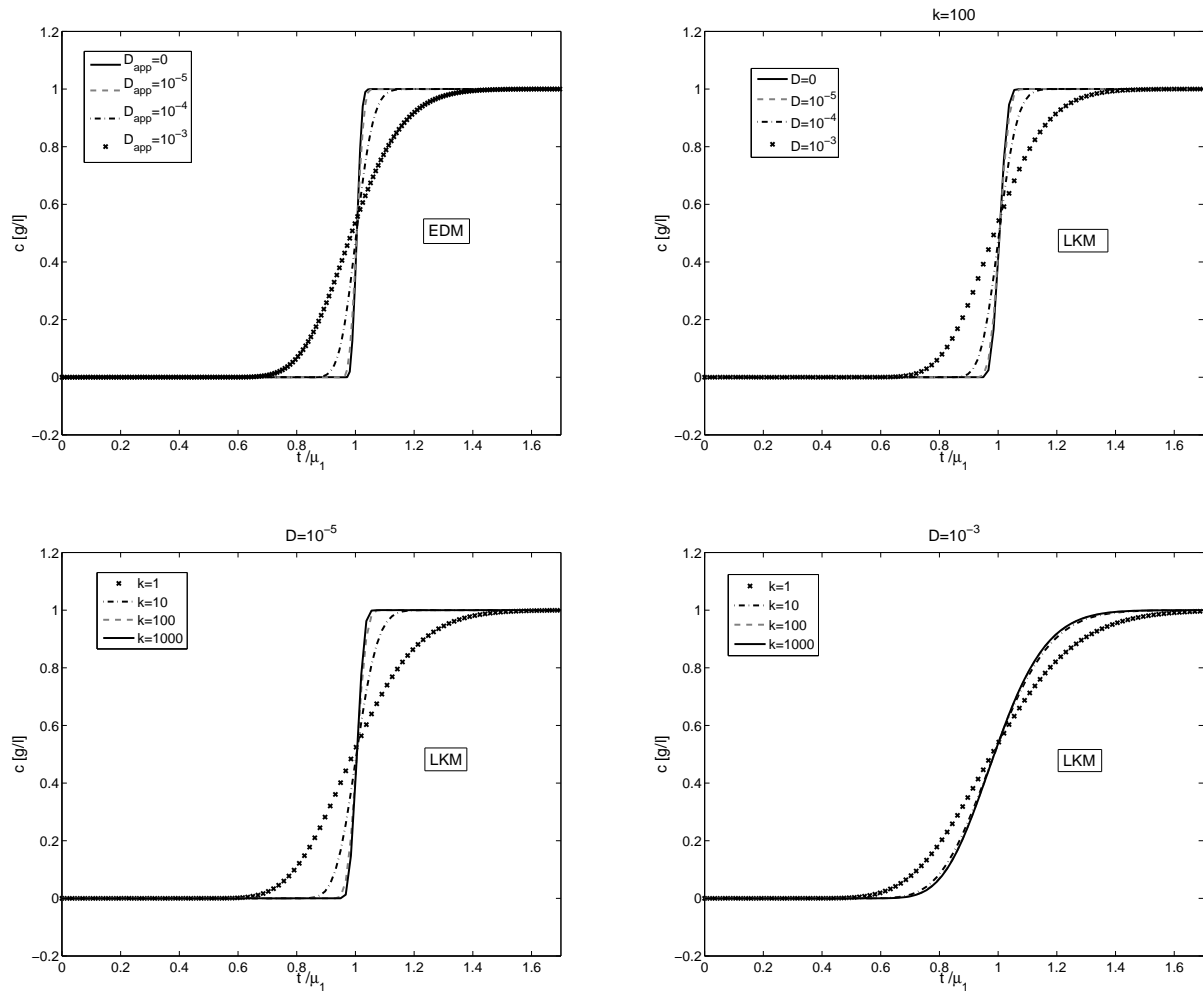


Figure 4.2: BTC at  $x = 1$ . Top (left): Dispersion effects as described by EDM keeping  $\tau_C = 10$  s constant and varying  $\tau_D$  (or  $D_{app}$ ), top(right): dispersion effects for LKM keeping  $\tau_C = 10$  s and  $\tau_{MT} = 0.01$  s ( $k = 100$  1/s or  $\tilde{\tau}_2 = 10^3$ ) constant, and varying  $\tau_D$  (or  $D$ ), bottom (left): mass transfer effects for LKM taking  $\tau_C = 10$  s,  $\tau_D = 0.001$  s ( $D = 10^{-5}$  m<sup>2</sup>/s or  $\tilde{\tau}_1 = Pe = 10^4$ ) and varying  $\tau_{MT}$  (or  $k$ ), bottom (right): mass transfer effects taking  $\tau_C = 10$  s,  $\tau_D = 0.1$  s ( $D = 10^{-3}$  m<sup>2</sup>/s or  $Pe = 10^2$ ) and varying  $\tau_{MT}$  (or  $k$ ).

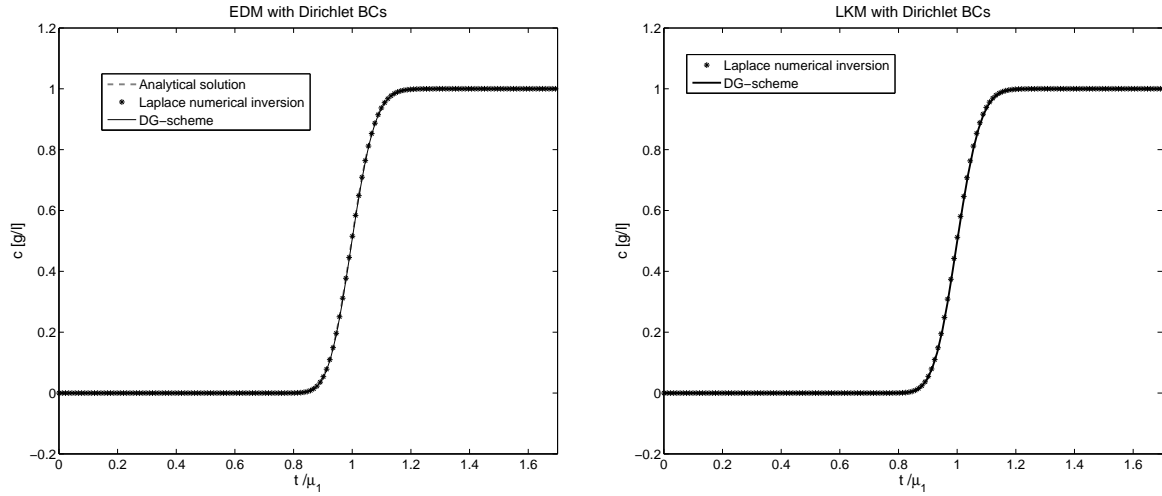


Figure 4.3: BTC at  $x = 1$ . EDM predictions using Dirichlet boundary conditions (2.31a), left: comparison of analytical solution (c.f. Eq. (4.15)), Laplace numerical inversion and DG-method solutions with  $\tau_C = 10$  s,  $\tau_D = 0.02$  s ( $D_{\text{app}} = 2 \times 10^{-4}$  m<sup>2</sup>/s or  $Pe = 500$ ). LKM predictions using Dirichlet boundary conditions (2.31a), right: comparison of Laplace numerical inversion and DG-scheme solutions with  $\tau_C = 10$  s,  $\tau_D = 0.01$  s ( $D = 10^{-4}$  m<sup>2</sup>/s or  $Pe = 1000$ ) and  $\tau_{MT} = 0.0667$  s ( $k = 15$  1/s or  $\tilde{\tau}_2 = 150$ ).

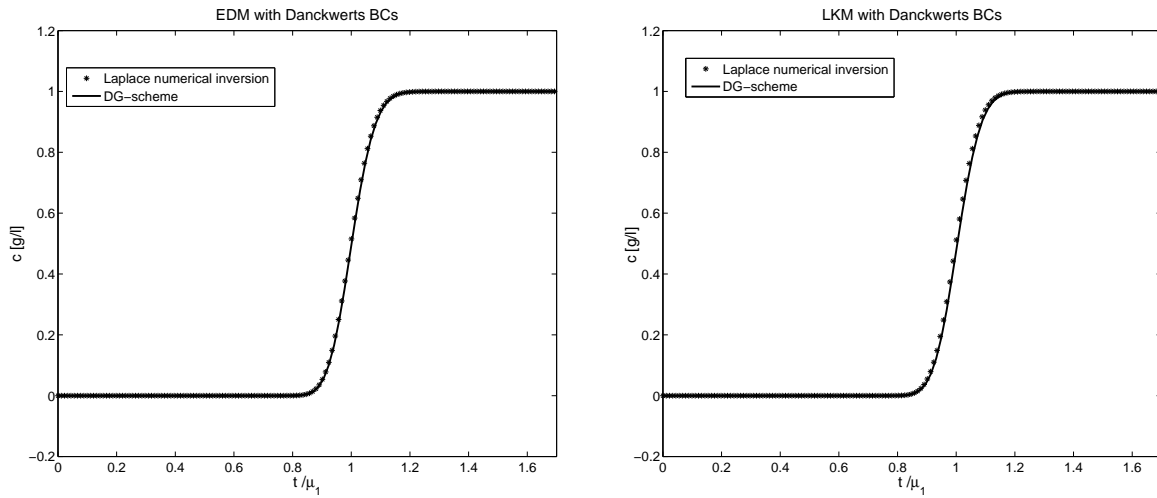


Figure 4.4: BTC at  $x = 1$ . EDM predictions using Danckwerts boundary conditions (2.32a), left: comparison of Laplace numerical inversion and DG-method solutions with  $\tau_C = 10$  s,  $\tau_D = 0.02$  s ( $D_{\text{app}} = 2 \times 10^{-4}$  m<sup>2</sup>/s or  $Pe = 500$ ). LKM predictions using Danckwerts boundary conditions (2.32a), right: comparison of Laplace numerical inversion and DG-scheme solutions with  $\tau_C = 10$  s,  $\tau_D = 0.01$  s ( $D = 10^{-4}$  m<sup>2</sup>/s or  $Pe = 1000$ ) and  $\tau_{MT} = 0.0667$  s ( $k = 15$  1/s or  $\tilde{\tau}_2 = 150$ ).



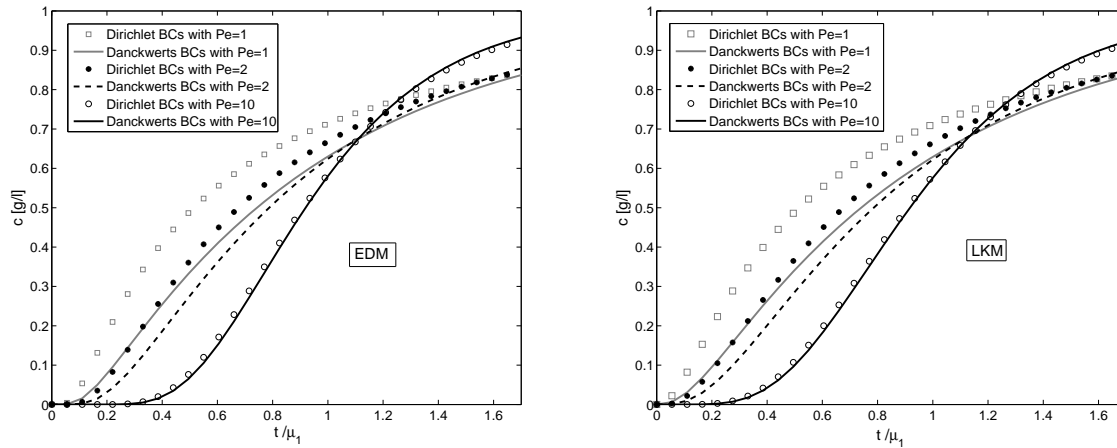


Figure 4.5: BTC at  $x = 1$ . Effect of boundary conditions for different values of Peclet number. Symbols are used for Dirichlet BCs (2.31a) and solid lines for Danckwerts BCs (2.32a), left: EDM with  $\tau_C = 10$  s, and  $Pe$  or  $\tau_D$  varies, right: LKM with  $\tau_C = 10$  s,  $\tau_{MT} = 0.01$  s ( $k = 100$  1/s or  $\tilde{\tau}_2 = 10^3$ ) and  $Pe$  or  $\tau_D$  varies.

### Effect of boundary conditions

This part is concerned with analyzing effects of boundary conditions. For the sake of generality, the Peclet number, c.f. Eq. (4.8), is taken as parameter, while  $\tilde{\tau}_2 = 10^3$  ( $\tau_{MT} = 0.01$  s) and  $\tau_C = 10$  s are assumed to be constant for this problem. The results shown in Figure 4.5 illustrate the importance of using more accurate Danckwerts boundary conditions for chromatographic model equations, in the case of relatively small Peclet numbers, e.g.  $Pe < 10$ . For such values, there are visible differences between the results obtained by using Dirichlet and Danckwerts boundary conditions. On the basis of these results, one can conclude that the implementation of Dirichlet boundary conditions is not adequate for large dispersion coefficients. For large values of Peclet number ( $Pe \gg 10$ ) or small axial dispersion coefficients as typically encountered in chromatographic columns well packed with small particles, there is no difference between Dirichlet and Danckwerts boundary conditions. The described behavior was observed in the solutions of both EDM and LKM.

### Discussion on analytically and numerically determined moments

In this part, the results regarding the theoretical (analytical) and numerical moments are discussed. The analytical moments are calculated by the formulas presented in Table 4.1

and in Appendix A. In this work, only step inputs are taken into account. In contrast to Eq. (4.29), the formulas given below use derivatives to approximate the moments and transform the step response to a pulse response which is the requirement for finite results of numerical integration. The simulated moments are obtained from our proposed numerical methods by using the following formulas for the first normalized, second central and third central moments, respectively:

$$\mu_1 = \frac{\int_0^\infty \frac{dC(x=1,t)}{dt} t dt}{\int_0^\infty \frac{dC(x=1,t)}{dt} dt}, \quad \mu_2' = \frac{\int_0^\infty \frac{dC(x=1,t)}{dt} (t - \mu_1)^2 dt}{\int_0^\infty \frac{dC(x=1,t)}{dt} dt}, \quad \mu_3' = \frac{\int_0^\infty \frac{dC(x=1,t)}{dt} (t - \mu_1)^3 dt}{\int_0^\infty \frac{dC(x=1,t)}{dt} dt}. \quad (4.32)$$

The trapezoidal rule is applied to approximate the integrals in Eq. (4.32) using  $C(x = 1, t)$  which are obtained by using the proposed numerical scheme. The quantitative comparison of first moment or (retention time) over the flow rate  $u$  for the EDM, LKM and the analytical formula (c.f. Table 4.1) can be seen in Figure 4.6 (left). The results are in good agreement with each other, verify the high precision of our numerical results and reveal the expected linear trends.

For calculations of second moments  $\mu_2'$  and third moments  $\mu_3'$ , the analytical formulas of Table 4.1 are used.

Matching  $\mu_{2EDM}'$  and  $\mu_{2LKM}'$  for the Dirichlet boundary conditions generates the following relationship between  $D_{app}$ ,  $D$  and  $k$ .

$$D_{app} = D + \frac{1}{k} \left( \frac{aF(1 - \epsilon)u^2}{(1 + aF)^2} \right). \quad (4.33)$$

For a given  $u$ ,  $a$ ,  $F$ , the above equation can be used to find possible connections between the kinetic parameters of two models which should provide very similar elution profiles. For given values of  $a$ ,  $F$  and  $\epsilon$  (c.f. Table 4.1), along with provided reference values of  $u^* = 0.35 \text{ m/s}$  and  $D_{app} = 10^{-4} \text{ m}^2/\text{s}$  for EDM,  $D = 5 \times 10^{-5} \text{ m}^2/\text{s}$  for LKM, we obtain  $k = 362 \text{ 1/s}$  from the formula (4.33). Based on these reference parameters, there is an infinite number of combinations for  $k$  and  $D$ . The crossing point mentioned in Figure 4.7 (left) indicates that for this particular value of flow rate  $u^*$ , both models produce almost the same concentration profiles as seen in Figure 4.7 (right). For other than this specific

value of flow rate keeping  $D_{\text{app}}$ ,  $D$  and  $k$  fixed, the results of equilibrium dispersive and lumped kinetic models deviate from each other because the values of  $D_{\text{app}}$ ,  $D$  and  $k$  are calculated by using this specific velocity  $u^* = 0.35 \text{ m/s}$ . This is clearly depicted in Figure 4.7 (right).

The third moment still do not match for both models, even when the second moments are equalized via Eq. (4.33). This is illustrated in the plot given in Figure 4.8 (left) showing the third moments  $\mu'_3$  for different flow rates. In Figure 4.8, the parameters  $D_{\text{app}} = 10^{-3} \text{ m}^2/\text{s}$  for the EDM and  $D = 5 \times 10^{-4} \text{ m}^2/\text{s}$  for the LKM are considered. The value of  $k$  in the LKM was always determined for the specific value of  $u$  using Eq. (4.33). A good agreement between analytical and numerical moments of our proposed numerical scheme guarantees the high precision of simulation results one more time. It can be observed that EDM gives large values of  $\mu'_3$  as compared to LKM. Thus, EDM produces more asymmetry in the concentration profiles which is illustrated in Figure 4.8 (right). The fronting edge is steeper and the tailing edge is more disperse for the EDM predictions as a clear indication of larger asymmetry compared to the LKM predictions (c.f. Figure 4.8 (right)). However, it is evident that the difference in the profiles of both models are still very small. This justifies the use of the simpler EDM for linear isotherm involving just one parameter  $D_{\text{app}}$  as compared to the more complicated LKM which involves two parameters  $D$  and  $k$ .

## 4.5 Conclusion

This chapter described analytical and numerical investigations of single component linear equilibrium dispersive and lumped kinetic models. Two sets of boundary conditions, namely Dirichlet and Danckwerts conditions were considered. The Laplace transformation was used as a basic tool to transform the single-component linear sub-model to a linear ordinary differential equation which is then solved analytically in the Laplace domain. The inverse numerical Laplace formula was employed to get back the time domain solution due to the unavailability of an exact solution. A moment analysis of both models was carried out analytically and numerically for linear isotherms. Good agreement up to third mo-

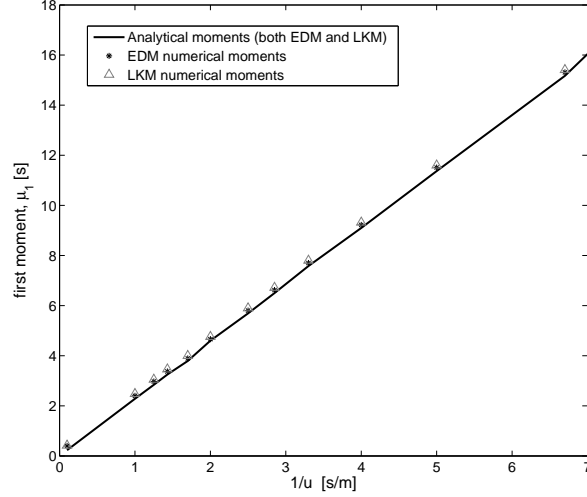


Figure 4.6: First moments  $\mu_1$  of EDM and LKM for different flow rates  $u$ . For EDM, Eq. (A.6) for analytical & Eq. (4.32) for numerical moments are used, considering  $D_{\text{app}} = 10^{-4} \text{ m}^2/\text{s}$ . For LKM, Eq. (A.26) for analytical & Eq. (4.32) for numerical moments are used, considering  $D = 5 \times 10^{-5} \text{ m}^2/\text{s}$  and  $k = 30 \text{ 1/s}$ .

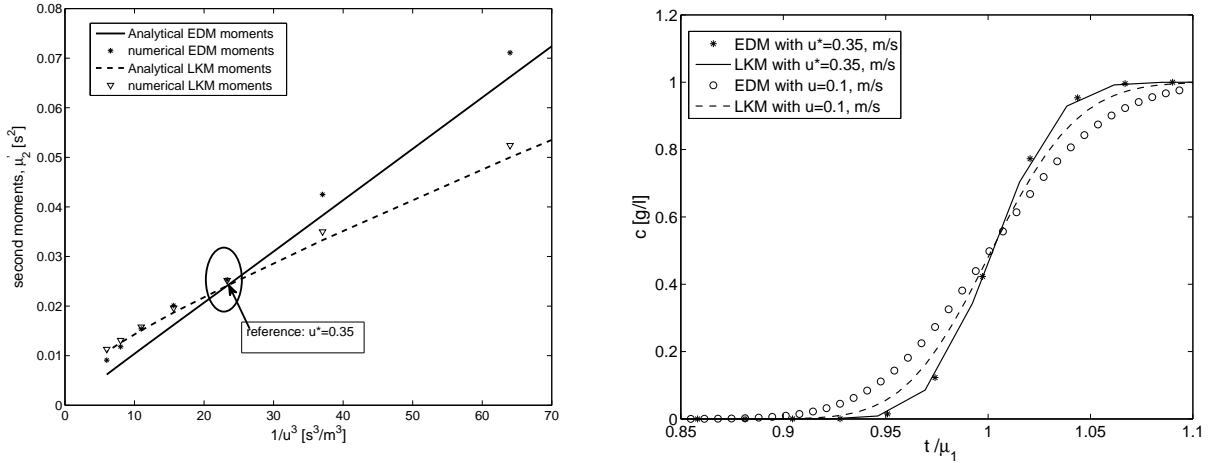


Figure 4.7: Left: Second moments  $\mu_2'$  for both models, analytical versus numerical with  $D_{\text{app}} = 10^{-4} \text{ m}^2/\text{s}$  for EDM,  $D = 5 \times 10^{-5} \text{ m}^2/\text{s}$  and  $k = 362 \text{ 1/s}$  for LKM. Crossing at  $u^* = 0.35 \text{ m/s}$ . Right: Two predicted breakthrough curves for  $u^* = 0.35 \text{ m/s}$  and  $u = 0.1 \text{ m/s}$ , respectively.

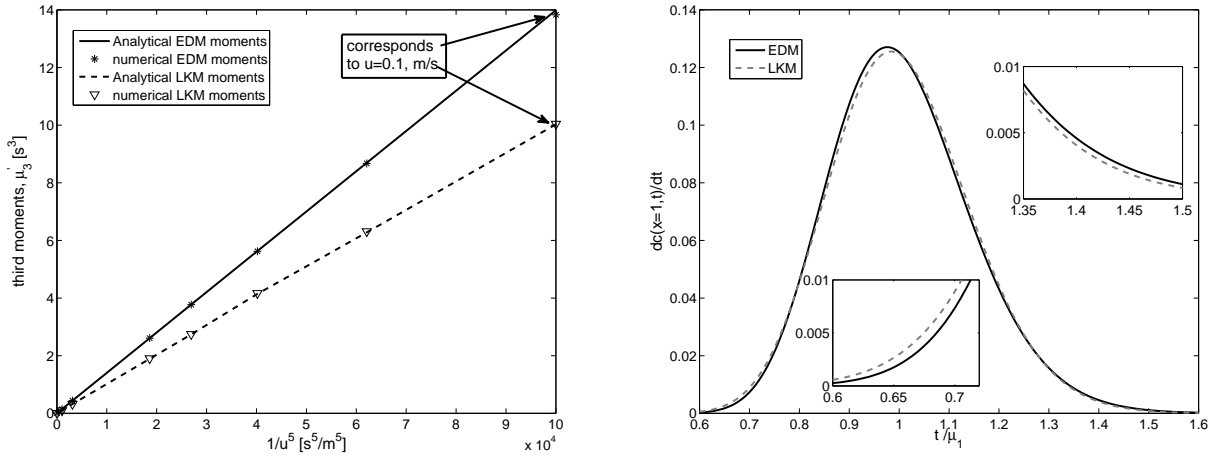


Figure 4.8: Left: Third moments  $\mu_3'$ . For EDM  $D_{\text{app}} = 10^{-3} \text{ m}^2/\text{s}$ , and for LKM,  $D = 5 \times 10^{-4} \text{ m}^2/\text{s}$  are used. Moreover,  $k$  is adjusted for each  $u$  via Eq. (4.33) to match  $\mu_3'$ . Dankwerts BCs are taken into account. Right: Illustration of effects of differences in third moments generated by EDM and LKM for  $u = 0.1 \text{ m/s}$  (corresponding to  $1/u^5 = 10^5 \text{ s}^5/\text{m}^5$ ).

ments assures the better accuracy of numerical solutions. The close connection between EDM and LKM was analyzed for linear isotherms. A concordance formula was derived and the strength of the simpler EDM was illustrated. On the basis of this result, the EDM is used to predict the chromatographic profiles in the next chapters of this thesis. For the numerical solution of the models considered, the DG and the Koren schemes were applied. The Koren scheme is a flux-limiting scheme in which fluxes are limited by using a nonlinear minmod limiter. This limiting procedure guarantees the positivity of the scheme and suppresses the numerical oscillations. The proposed DG-scheme satisfies the TVB property and gives second order accuracy. The method incorporates the ideas of numerical fluxes and slope limiters in a very natural way to capture the physically relevant discontinuities without producing spurious oscillations in their vicinity. The accuracy of proposed schemes were validated against some flux-limiting finite volume schemes and analytical solutions for linear isotherms. The DG-scheme and the Koren method were found to be suitable methods for the simulation of linear chromatographic processes in terms of accuracy and efficiency. Moreover, it seems that the DG-scheme resolves the shocks better

than the Koren scheme. In the subsequent chapter, numerical schemes are analyzed for more complicated nonlinear and reactive chromatographic models.

## Chapter 5

# Numerical Solutions of Linear and Non-Linear Chromatographic Models

In this chapter isothermal non-reactive and reactive liquid chromatographic processes are numerically investigated. Several test problems are carried out concerning both non-reactive and reactive liquid chromatographic models under linear and non-linear conditions. For linear models, analytical solution can be derived (c.f. Chapter 4), while for nonlinear models, only numerical techniques provide solutions. Test Problems are numerically approximated by using the proposed numerical schemes. The results of the suggested numerical methods are compared with available analytical solutions and some flux-limiting finite volume schemes given in the literature. Moreover, the quantitative analysis of selected problems is also presented. The case studies of non-reactive chromatography include single-component elution, two-component elution, and displacement chromatography on non-movable (fixed) and movable (counter-current) beds. Afterwards, practical examples of reactive chromatography are taken into consideration and are compared with the available analytical as well as experimental results.

The finite volume scheme of Koren [39] and the Runge-Kutta discontinuous Galerkin method, presented in Chapter 3 for FBCR model, are proposed to numerically approximate the current models. The Koren scheme is a flux-limiting scheme in which fluxes are limited by using a nonlinear minmod limiter. This limiting procedure guarantees the positivity of the scheme and hence suppresses the numerical oscillations, usually encoun-

tered in the numerical schemes of second and higher orders. In Chapter 3, the scheme was shown to be second to third order accurate in space analytically. Therefore, a third order accurate ordinary differential equation (ODE) solver is needed to make the scheme third order accurate in space and time.

The Runge-Kutta discontinuous Galerkin method [9, 10, 35] is locally conservative, stable, and high order accurate. The scheme is second order accurate in the axial coordinate and satisfy the total variation boundedness (TVB) property. In contrast to high order FDMs and FVMs, the DG-methods require a simple treatment of the boundary conditions to achieve high order accuracy uniformly. These methods incorporate the idea of numerical fluxes and slope limiters in a very natural way to avoid spurious oscillations in the region of strong variations. The DG-methods can be efficiently applied to partial differential equations (PDEs) of all kinds, including equations whose type changes within the computational domain. For the first time, these schemes are applied to chromatographic models in this dissertation.

Several numerical test problems are carried out. For quantitative analysis and validation, the results of DG-scheme are compared with some flux-limiting finite volume schemes. In all numerical test problems, linear basis functions are used in each cell, giving a second order accurate DG-scheme in the axial-coordinate. The ODEs-system was solved by a third-order Runge-Kutta method given by Eq. (3.57). Once again, the program is written in the C-language under a Linux operating system and was compiled on a computer with an Intel(R) Core 2 Duo processor of speed 2 GHz and memory (RAM) 3.83 GB.

## 5.1 Numerical test problems

In this section the proposed numerical schemes are applied to simulate different chromatographic elution, such as non-reactive single component elution, non-reactive binary elution, three component elution and four component reactive elution.



### 5.1.1 Non-reactive single-component elution

Here, we give two case studies with linear and nonlinear isotherms, respectively.

#### Case 1: Linear isotherm: quantitative analysis of the numerical schemes

The purpose of this case study is to quantitatively analyze the performance of the DG-scheme and different flux-limiting schemes discussed in Chapter 3. For the numerical simulation, the FBCR model Eq. (3.1) is considered with a linear isotherm  $q^* = ac$  and the source term  $Q(t, z, c)$  is set equal to zero. It is assumed that the column is partially pre-loaded in the region  $z = [0.2, 0.4]$  by a sinusoidal profile. Thus, we assume the following initial and boundary conditions

$$c(0, z) = \begin{cases} \sin(\pi(z - 0.2)/0.2), & 0.2 \leq z \leq 0.4, \\ 0, & \text{otherwise} \end{cases} \quad (5.1)$$

with left boundary condition  $c(0, t) = 0$ . The analytical solution for this problem is given as, e.g. [39],

$$c(t, z) = 0.5 \operatorname{real} (ie^p [\operatorname{erf}(\alpha) - \operatorname{erf}(\beta)]) , \quad (5.2)$$

where, erf represents the error function and

$$p = -0.5D_{\text{app}}t \left( \frac{\pi}{0.2} \right)^2 + i \frac{\pi}{0.2} (0.2 - z - 0.5t) , \quad (5.3)$$

$$\alpha = \frac{-0.2 + z - 0.5t}{2\sqrt{0.5D_{\text{app}}t}} - i\pi \frac{\sqrt{0.5D_{\text{app}}t}}{0.2} , \quad (5.4)$$

$$\beta = \frac{-0.4 + z - 0.5t}{2\sqrt{0.5D_{\text{app}}t}} - i\pi \frac{\sqrt{0.5D_{\text{app}}t}}{0.2} . \quad (5.5)$$

The column length  $L = 1 \text{ cm}$ ,  $a = 1$ ,  $u = 1 \text{ cm/min}$ ,  $\epsilon = 0.5$ , and the simulation time is  $0.6 \text{ min}$ . The  $L^1$ -errors in the axial-coordinate at the last simulation time is calculated by using the following formula.

$$L^1\text{-error} = \sum_{j=1}^N |c_{\text{exact}}^j - c_{\text{numeric}}^j| \Delta z , \quad (5.6)$$

where  $c_{\text{exact}}^j$  denotes the exact solution at the midpoint of each discrete cell and  $c_{\text{numeric}}^j$  represents the corresponding numerical solution at the final simulation time. Moreover,  $N$  denotes the number of discretization points and  $\Delta z$  represents the axial step size.

Table 5.1 gives a comparison of the  $L^1$ -errors of different numerical schemes using 100 grid points and for different values of the dispersion coefficients  $D_{\text{app}}$ . It can be observed that the DG-scheme gives less errors as compared to the flux-limiting finite volume schemes. Moreover, the errors produced by the Koren scheme are also less at low computational cost. Note that the DG-scheme used in this work has second order accuracy, while the Koren scheme is second to third order accurate. Table 5.2 displays the  $L^1$ -errors and the experimental order of convergence (EOC) of the DG-scheme at different grid points and for different values of  $D_{\text{app}}$ . The EOC of the DG-method is approximately second order, see Table 5.2. The DG-scheme is more effective for the convection dominated problems where the dispersion coefficient is very small, for example  $D_{\text{app}} = 2 \times 10^{-5} \text{ m}^2/\text{s}$ . Table 5.3 presents the  $L^1$ -errors and the EOC of the Koren scheme at different mesh points for different values of  $D_{\text{app}}$ . The table shows that this flux-limiting scheme is second to third order accurate. The scheme is third order accurate for the convection dominated equilibrium dispersive models with influential dispersion coefficient, for example  $D_{\text{app}} = 2 \times 10^{-3} \text{ m}^2/\text{s}$ , while the scheme is second order accurate when the dispersion coefficient tends to zero. In other words, by varying the number of grid points, the transition rate from second to third order slows down as the dispersion coefficient tends to zero, see Table 5.3. The same trends were also observed by Koren [39]. Finally, Tables 5.4 and 5.5 show the EOC of different numerical schemes for  $D_{\text{app}} = 0.002 \text{ m}^2/\text{s}$  and  $D_{\text{app}} = 2 \times 10^{-5} \text{ m}^2/\text{s}$ , respectively. It can be observed that the Koren scheme gives a better EOC as compared to other schemes for  $D_{\text{app}} = 0.002 \text{ m}^2/\text{s}$ . The DG-scheme provides a comparatively better EOC for  $D_{\text{app}} = 2 \times 10^{-5} \text{ m}^2/\text{s}$ . In addition, the EOC of other schemes for  $D_{\text{app}} = 0.002 \text{ m}^2/\text{s}$  is larger than the DG-method, but the results of the DG-scheme seems to be slightly closer to the exact solution.

The left plot in Figure 5.1 shows a comparison of different schemes using 50 grid points. For 50 grid points or less, the Superbee limiter gives the most resolved solution. However, over-predictions were observed in the solution for grid point numbers above 50. This limiter applies minimum limiting and maximum steepening. Therefore, it suffers from excessive sharpening of slopes which results in over-predictions in the solution as depicted

Table 5.1: Section 5.1.1 (Linear isotherm):  $L^1$ -errors and CPU times of schemes at 100 mesh points considering different dispersion coefficients  $D_{\text{app}}$  [ $m^2/s$ ]. Parameters are given in text.

Limiter	$L^1$ -errors				CPU (s)
	$D_{\text{app}}$	0.002	0.0002	$2 \times 10^{-5}$	
First order	0.04021	0.05303	0.06547	0.05486	0.43
DG	0.0009	0.0018	0.0028	0.0030	0.64
Koren	0.00083	0.00278	0.00405	0.00416	0.56
van Leer	0.00271	0.00574	0.00675	0.00680	0.56
Superbee	0.00336	0.00379	0.00460	0.00475	0.88
Minmod	0.00619	0.01079	0.01175	0.01180	1.45
MC	0.00227	0.00419	0.00499	0.00503	0.62

Table 5.2: Section 5.1.1 (Linear isotherm):  $L^1$ -errors and EOC of the DG scheme considering different mesh points  $N$ .

N	$D_{\text{app}} = 0.002 m^2/s$		$D_{\text{app}} = 0.0002 m^2/s$		$D_{\text{app}} = 0.00002 m^2/s$	
	$L^1$ -errors	EOC	$L^1$ -errors	EOC	$L^1$ -errors	EOC
50	0.0028		0.0062		0.0090	
100	$9.31 \times 10^{-4}$	1.60	0.0018	1.78	0.0028	1.68
200	$3.38 \times 10^{-4}$	1.46	$2.69 \times 10^{-4}$	2.73	$6.40 \times 10^{-4}$	2.13
400	$1.07 \times 10^{-4}$	1.66	$6.94 \times 10^{-5}$	1.96	$1.34 \times 10^{-4}$	2.26
800	$3.05 \times 10^{-5}$	1.81	$2.24 \times 10^{-5}$	1.63	$2.43 \times 10^{-5}$	2.47

in the right zoomed plot of Figure 5.1. For that reason, more errors were produced by the Superbee limiter and the convergence rate is very low in Tables 5.1 and 5.5, respectively. Moreover, the computational cost for the Superbee limiter is higher than the other schemes. The backward difference method takes the minimum computational time but gives a very diffusive solution which is far away from the analytical solution. The computational cost of the van Leer limiter is comparable to the DG and Koren schemes, however its solution is less resolved. The remaining two limiters have a higher computational cost and lower accuracy. From the above observations, one can conclude that the DG and Koren schemes are better choices for solving linear chromatographic models.

Table 5.3: Section 5.1.1 (Linear isotherm):  $L^1$ -errors and EOC of the Koren scheme.

N	$D_{\text{app}} = 0.002 \text{ m}^2/\text{s}$		$D_{\text{app}} = 0.0002 \text{ m}^2/\text{s}$		$D_{\text{app}} = 0.00002 \text{ m}^2/\text{s}$	
	$L^1$ -error	EOC	$L^1$ -error	EOC	$L^1$ -error	EOC
50	0.0065		0.0107		0.0114	
100	$8.31 \times 10^{-4}$	2.97	0.0028	1.93	0.004	1.51
200	$1.02 \times 10^{-4}$	3.03	$5.64 \times 10^{-4}$	2.30	0.0011	1.86
400	$1.15 \times 10^{-5}$	3.15	$9.76 \times 10^{-5}$	2.53	$2.90 \times 10^{-4}$	1.93
800	$1.98 \times 10^{-6}$	2.53	$1.32 \times 10^{-5}$	2.89	$6.21 \times 10^{-5}$	2.20

Table 5.4: Section 5.1.1 (Linear isotherm): EOC of schemes for  $D_{\text{app}} = 0.002 \text{ m}^2/\text{s}$ .

Mesh points $N$	Koren	DG	van Leer	Superbee	Minmood	MC
50						
100	2.97	1.60	2.08	0.67	1.81	1.92
200	3.03	1.46	2.06	1.34	1.99	1.93
400	3.15	1.66	2.04	1.86	2.03	1.98
800	2.53	1.81	2.02	1.97	2.02	1.99

Table 5.5: Section 5.1.1 (Linear isotherm): EOC of schemes for  $D_{\text{app}} = 2 \times 10^{-5} \text{ m}^2/\text{s}$ .

Mesh points $N$	Koren	DG	van Leer	Superbee	Minmood	MC
50						
100	1.51	1.68	1.52	0.69	1.52	1.45
200	1.86	2.13	1.54	1.54	1.14	1.65
400	1.93	2.26	1.67	1.67	1.43	1.49
800	2.20	2.47	1.70	1.13	1.52	1.52

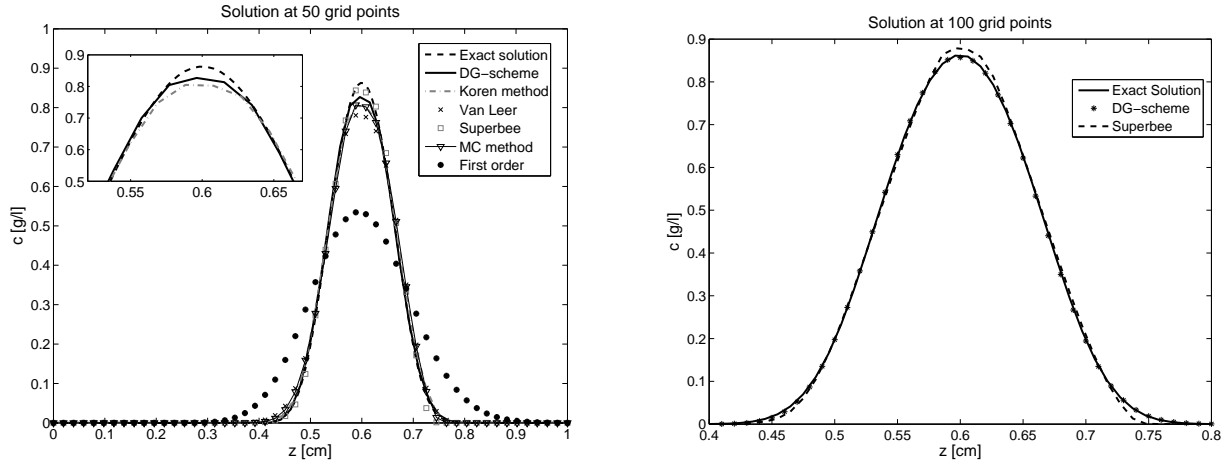


Figure 5.1: Section 5.1.1 (case 1): A comparison of different schemes for single component elution with linear isotherm.

### Case 2: Single-component model with nonlinear isotherm

The purpose of this case study is to analyze the performance of the DG-method against other flux-limiting finite volume schemes for nonlinear models. The FBCR model (3.1) is considered with the single component variant of nonlinear isotherm (c.f. Eq. (2.18)) with  $b = 1$  is  $q^*(c) = c/(1+c)$  and the source term  $Q(t, z, c) = 0$ . A pulse of height  $c^{\text{in}} = 1 \text{ g/l}$  is injected into the column initially equilibrated with the solvent, i.e.  $c^{\text{init}} = 0$  for an injection time of  $t^{\text{in}} = 0.2 \text{ min}$ . The column length  $L$  is  $1 \text{ cm}$ . Further,  $\epsilon = 0.5$ ,  $u = 1 \text{ cm/min}$ ,  $N_t = 250$ , and the simulation time is  $3 \text{ min}$ . Moreover, a grid of 100 mesh cells was used.

The reference solution was obtained from the same DG-scheme by using 2000 mesh cells. The numerical results at the column outlet are depicted in Figure 5.2, while a comparison of  $L^1$ -errors and computational times of schemes is given in Table 5.6. Figure 5.3 shows the logarithmic errors of different schemes for different numbers of grid points. It can be observed that the DG-scheme produces less error in the solution. The  $L^1$ -error in time at the column outlet was calculated by using the formula given in Eq. (4.30). It can be observed that DG and Koren methods give the most resolved solutions with small errors. The computational time of the DG-scheme is comparable to the Koren scheme and the finite volume scheme with van-Leer or minmod limiters but it is much lower than with the

Table 5.6: Section 5.1.1 (Nonlinear isotherm):  $L^1$ -errors and CPU times of schemes.

Limiter	$L^1$ -errors			CPU (s)		
	$N = 50$	$N = 100$	$N = 200$	$N = 50$	$N = 100$	$N = 200$
DG Scheme	0.0186	0.0063	0.0040	0.23	0.50	1.93
Koren	0.0497	0.0225	0.0102	0.22	0.42	1.62
van Leer	0.0586	0.0271	0.0124	0.21	0.41	1.54
Superbee	0.0582	0.0281	0.0131	0.34	0.61	2.01
MC	0.0589	0.0276	0.0126	0.26	0.32	1.76
Minmod	0.0645	0.0287	0.0125	0.22	0.48	1.57
First order	0.1146	0.0724	0.0415	0.12	0.14	0.70

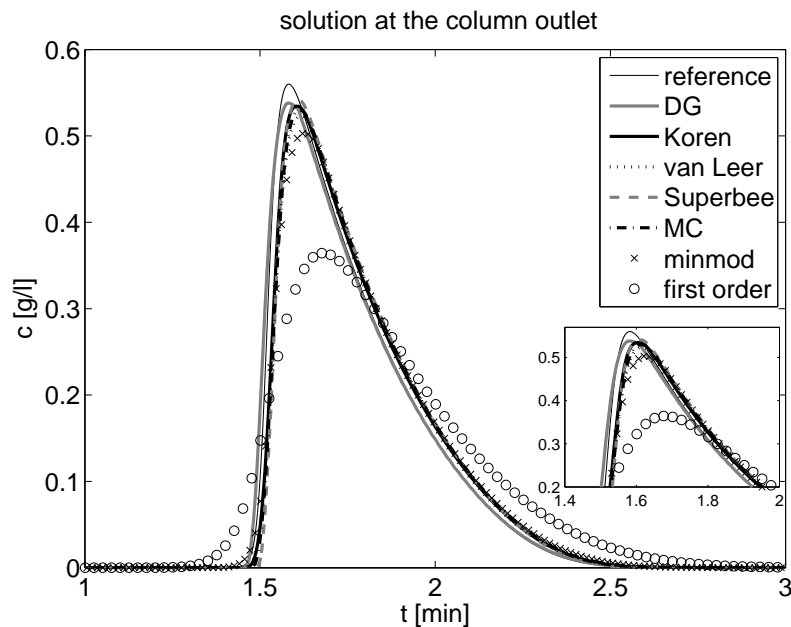


Figure 5.2: Section 5.1.1 (case 2): A comparison of different schemes for single component with nonlinear isotherm.

MC and Superbee limiters. The backward difference scheme has minimal computational time but gives a very diffusive solution which is far away from the reference solution. The above observations lead us to the conclusion that DG and Koren schemes are better choices for solving such nonlinear models.

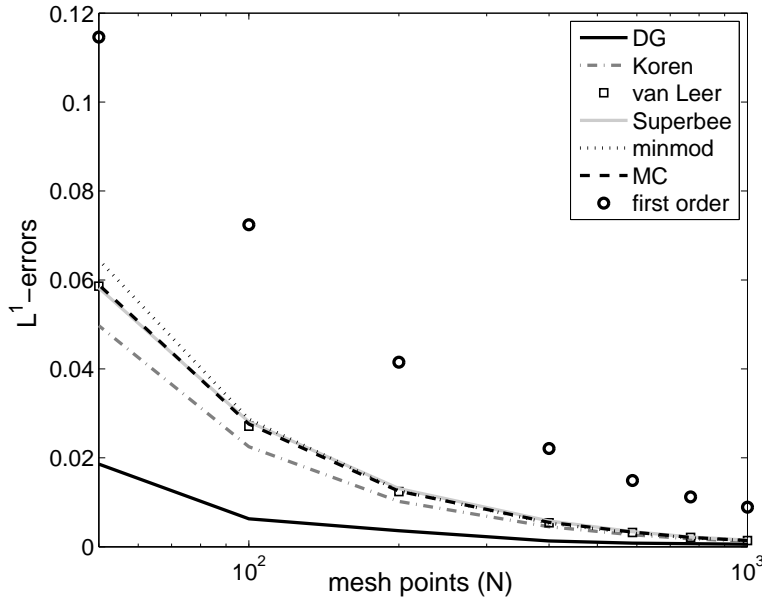


Figure 5.3: Section 5.1.1 (case 2): Logarithmic errors at different number of mesh points.

## 5.1.2 Non-reactive binary elution

This part focuses on two-component non-reactive problems with linear and nonlinear isotherms, respectively.

### Case 1: Linear isotherm

This case corresponds to the separation of a non-reactive binary mixture of components A and B. In the simulation the following parameters were considered: column length  $L = 0.25 \text{ m}$ , porosity  $\epsilon = 0.24$ ,  $N_t = 10^4$  (identical for both components),  $a_A := a_1 = 5$ , and  $a_B := a_2 = 1$ . Moreover, a mixture of concentrations  $c_1^{\text{in}} = c_A^{\text{in}} = 0.5 \text{ mol/l}$  and  $c_2^{\text{in}} = c_B^{\text{in}} = 0.5 \text{ mol/l}$  is injected for time  $t^{\text{in}} = 10 \text{ min}$  at a velocity  $u = 1 \text{ m/min}$ . For the numerical simulation, the FBCR model (2.23) is considered with linear isotherms  $q_i^* = a_i c_i$  and the source terms  $Q_i(t, z, c)$  are taken to be zero. For this particular setup, the eluted concentration profiles on 100 mesh points are shown in Figure 5.4 and the final simulation time is taken to be  $15 \text{ min}$ . The solution of the DG-scheme is compared with the analytical solution of Kumar [45] valid only for linear isotherms and the numerical solution of the

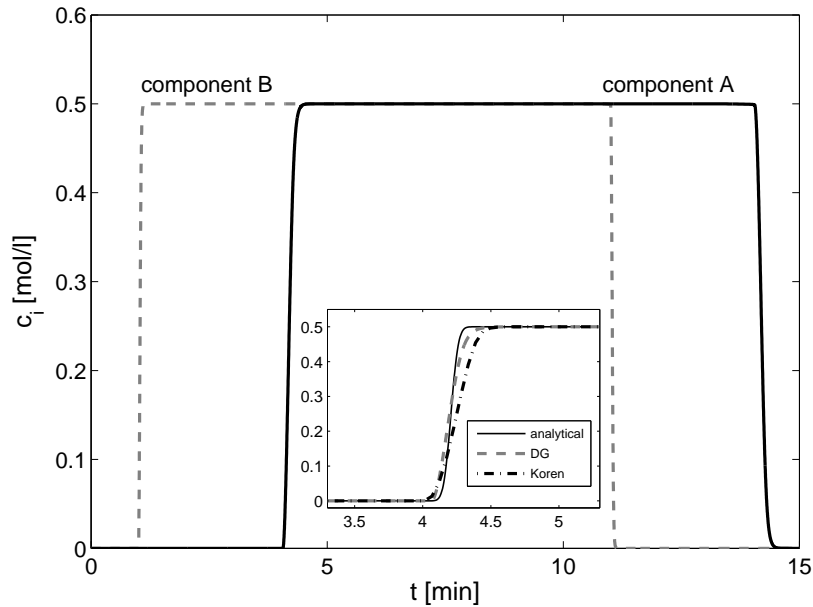


Figure 5.4: Section 5.1.2 (case 1): Two-component elution with linear isotherm.

Koren scheme.

In Figure 5.4, it can be observed that the DG-scheme solution is bit closer to the analytical solution and gives the position of the discontinuity more correctly compared to the Koren scheme.

### Case 2: Nonlinear isotherm

The propagation of a two component mixture through a column is simulated without considering reaction or source terms. In the example process considered, the column is at a constant initial state corresponding to a specific initial composition. A new state corresponding to a specific feed composition is generated by injecting a new composition into the column inlet starting at time  $t = 0$ . This setup corresponds to a Riemann problem. Three different fronts usually appear, such as a rarefaction (continuous), a shock wave and a semi-shock wave. Shocks are discontinuities in the concentration profile due to experimental conditions. Across the shock wave the concentration increases, therefore the shock is a compression wave. A rarefaction wave is an expansion wave in time and refers to the reduction of concentration or opposite to the compression. The EDM, c.f. Eq. (2.21),



with generalized Langmuir adsorption isotherm given in Eq. (2.18) is used for modeling this process as (e.g. in [58])

$$q_i^* = a_i c_i / (1 + p_1 b_1 c_1 + p_2 b_2 c_2), \quad i = 1, 2. \quad (5.7)$$

For the less retained component the value of  $a_i$  is smaller as compared to the more retained component. In the denominator, the values of  $p_1$  and  $p_2$  can be  $\pm 1$ . The case of  $p_1 = p_2 = 1$  represents the standard Langmuir isotherm defined in Eq. (5.7) and the case of  $p_1 = p_2 = -1$  refers to be anti-Langmuir isotherm. The other two situations are termed as mixed-Langmuir isotherms. In this study, exclusively a mixed-Langmuir isotherm with  $p_1 = -1$  and  $p_2 = 1$ , is considered.

Mazzotti [58] has analyzed the equilibrium model where  $D_{\text{app},i} = 0$  by using the method of characteristics. Apart from classical composition fronts, such as rarefaction, shock, and semi-shock waves, non-classical composition fronts and delta-shocks were observed in the study. Moreover, the analytical (characteristic) solutions of the equilibrium model were compared with the numerical solutions of the equilibrium-dispersive model for small values of the axial dispersion coefficient.

In this work, the results of Mazzotti [58] are numerically verified by solving the equilibrium-dispersive model with our suggested DG and Koren methods. The test problems show that these schemes preserve narrow peaks in the concentration profiles and give correct locations of discontinuities. The proposed schemes are efficient, accurate, and produce low numerical dissipation and dispersion.

A two-component mixture is considered in which component  $c_1$  is less retained as compared to component  $c_2$ . Here,  $c_1$  illustrates an anti-Langmuir and  $c_2$  depicts a Langmuir isotherm. To non-dimensionalize, Eq. (2.21) can be re-written as

$$\frac{\partial(c_i + \frac{1-\epsilon}{\epsilon} q_i^*)}{\partial t} + u \frac{\partial c_i}{\partial z} = D_{\text{app},i} \frac{\partial^2 c_i}{\partial z^2}, \quad i = 1, 2. \quad (5.8)$$

By multiplying the above equation with equilibrium constant  $b_i$ , we obtain

$$\frac{\partial(c_i b_i + \frac{1-\epsilon}{\epsilon} b_i q_i^*)}{\partial t} + u \frac{\partial(b_i c_i)}{\partial z} = D_{\text{app},i} \frac{\partial^2(b_i c_i)}{\partial z^2}, \quad i = 1, 2. \quad (5.9)$$

Let  $\mu_i := c_i b_i$  represents the  $i$ th dimensionless component of liquid phase and  $\nu_i := \frac{1-\epsilon}{\epsilon} b_i q_i^*$  denotes the  $i$ th dimensionless component of solid phase. The dimensionless time and axial coordinates are given as  $\tau = tu/L$  and  $x = z/L$ , where  $L$  is the length of the column. Moreover,  $\tau$  and  $x$  represents the dimensionless time and axial coordinates, respectively. Finally, the dimensionless diffusion term is given as  $\chi_i = D_{\text{app},i}/Lu$ . By using the above definitions, Eq. (5.9) changes to the following dimensionless form, e.g. [58],

$$\frac{\partial(\mu_i + \nu_i)}{\partial\tau} + \frac{\partial\mu_i}{\partial x} = \chi_i \frac{\partial^2 \mu_i}{\partial x^2}, \quad i = 1, 2. \quad (5.10)$$

Here,  $\nu_i = a_i \mu_i / (1 - \mu_1 + \mu_2)$  and the small parameter  $\chi_i$  are the reciprocal of already defined Peclet numbers (c.f. Eq. (4.4b)).

To apply the numerical schemes, Eq. (5.10) can be written as

$$\left( \mathbf{I} + \frac{\partial \mathbf{v}}{\partial \boldsymbol{\mu}} \right) \frac{\partial \boldsymbol{\mu}}{\partial \tau} + \frac{\partial \boldsymbol{\mu}}{\partial x} = \boldsymbol{\chi} \frac{\partial^2 \boldsymbol{\mu}}{\partial x^2}, \quad (5.11)$$

where,  $\mathbf{I}$  represents the identity matrix,  $\boldsymbol{\mu} = (\mu_1, \mu_2)^T$ ,  $\mathbf{v} = (v_1, v_2)^T$ ,  $\partial \mathbf{v} / \partial \boldsymbol{\mu}$  and  $\boldsymbol{\chi}$  is the Jacobian and diagonal matrices, respectively. The above equation is solved by using current numerical schemes presented in Chapter 3.

To validate the proposed numerical schemes, several numerical test cases are considered. A typical Riemann problem for Eq. (5.11) consists of an initial state  $(\mu_1^F, \mu_2^F)$  assigned to  $x \geq 0$  and  $\tau = 0$  and an inlet state  $(\mu_1^E, \mu_2^E)$  assigned to  $x = 0$  and  $\tau \geq 0$ , both separated by a jump discontinuity. In all test cases of this part,  $a_1 = 1.5$ ,  $a_2 = 3.0$ , and the mesh of 200 cells is selected in the axial direction. The number of theoretical plates is chosen as  $N_t = 5000$ , identical for both components, a typical number provided by commercially available analytical high performance liquid chromatography (HPLC) columns.

**Classical solutions:** In this case, we have  $\mu_1^F < \mu_2^E$  and  $\mu_1^E < \mu_2^F$ . Such solutions consist of three states, i.e the inlet state  $E$  on the left, the intermediate state  $I$  in the middle defined by the characteristic parameters, and the initial state  $F$  on the right, separated by two transition waves that can be simple waves or shocks. Four test cases, initially considered in [58], are reproduced with the suggested numerical schemes. Figures 5.7-5.9 show the results. The initial data for these test problems are given in Table 5.7. Figure

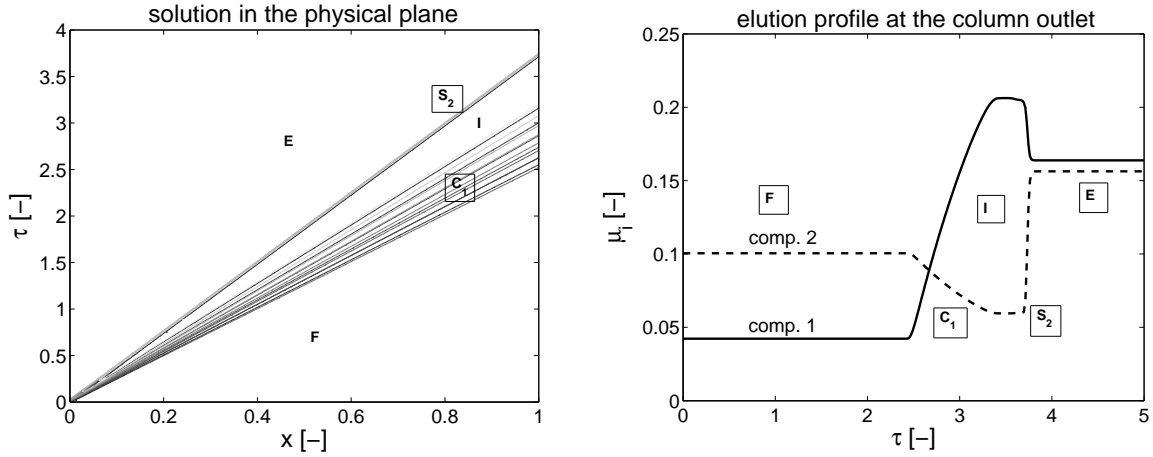


Figure 5.5: Section 5.1.2 (case 2a): Riemann problem leads to the  $S_2 - C_1$  solution,  $a_1 = 1.5, a_2 = 3.0$ , inlet state  $(\mu_1^E, \mu_2^E) = (0.1638, 0.1563)$ , initial state  $(\mu_1^F, \mu_2^F) = (0.0423, 0.1005)$ , and  $N_t = 5000$  (c.f. Eq. (4.4b)).

5.5 gives a  $S_2 - C_1$  solution, where  $S_2$  and  $C_1$  represent the left shock wave and the right simple wave. For validation, the numerical results of the DG-scheme are compared with the Koren scheme. The Figure 5.6 depicts that the DG-scheme captures sharp discontinuities better than the Koren scheme. The reference solution was obtained from the DG-scheme by considering 2000 mesh cells.

In Figure 5.7, the solution has the form  $C_2 - S_1$ , where  $C_2$  and  $S_1$  represent the left simple wave and right shock wave, respectively. In Figure 5.8, a  $C_2 - C_1$  solution is given. Finally, Figure 5.9 gives an  $S_2 - S_1$  solution. It was found that the numerical results of the DG and Koren schemes agree well with the results published by Mazzoti [58].

**Non classical solutions:** In this case, the parameter  $\mu_2$  associated with one state may be smaller than the parameter  $\mu_1$  of the other state, and vice versa, see e.g. [58]. The initial and inlet conditions are given in Table 5.7. Figure 5.10 shows a continuous non-simple wave transition. This Riemann solution has the form  $C_2 - C_e - C_1$ , where  $C_2, C_e$  and  $C_1$  correspond to a simple left wave, a non-simple wave transition and a right simple wave, respectively. The results are similar to those presented by [58]. The Riemann problem in Figure 5.11 leads to the unusual form of a delta shock solution. The existence of a delta shock has already been realized experimentally [59]. In this case, the concentration shoots

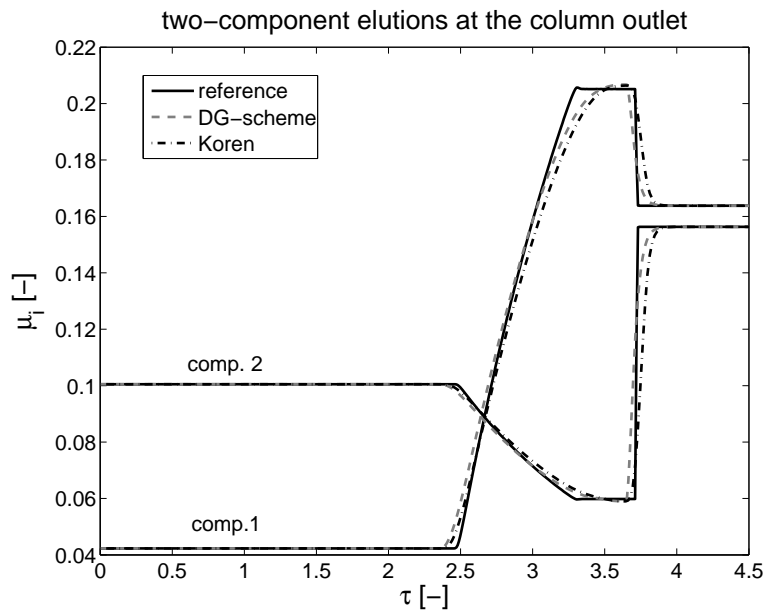


Figure 5.6: Section 5.1.2 (case 2a): A comparison of the DG and Koren schemes with  $a_1 = 1.5, a_2 = 3.0$ , inlet state  $(\mu_1^E, \mu_2^E) = (0.1638, 0.1563)$ , initial state  $(\mu_1^F, \mu_2^F) = (0.0423, 0.1005)$ , and  $N_t = 5000$  (c.f. Eq. (4.4b)).

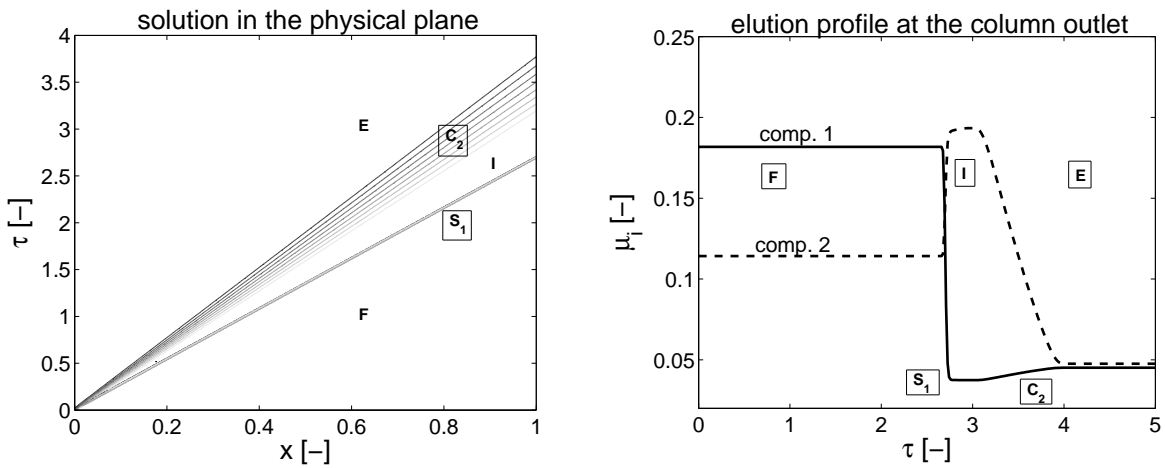


Figure 5.7: Section 5.1.2 (case 2b): Riemann problem leads to the  $C_2 - S_1$  solution,  $a_1 = 1.5, a_2 = 3.0$ , inlet state  $(\mu_1^E, \mu_2^E) = (0.0451, 0.0476)$ , initial state  $(\mu_1^F, \mu_2^F) = (0.1818, 0.1142)$ , and  $N_t = 5000$  (c.f. Eq. (4.4b)).

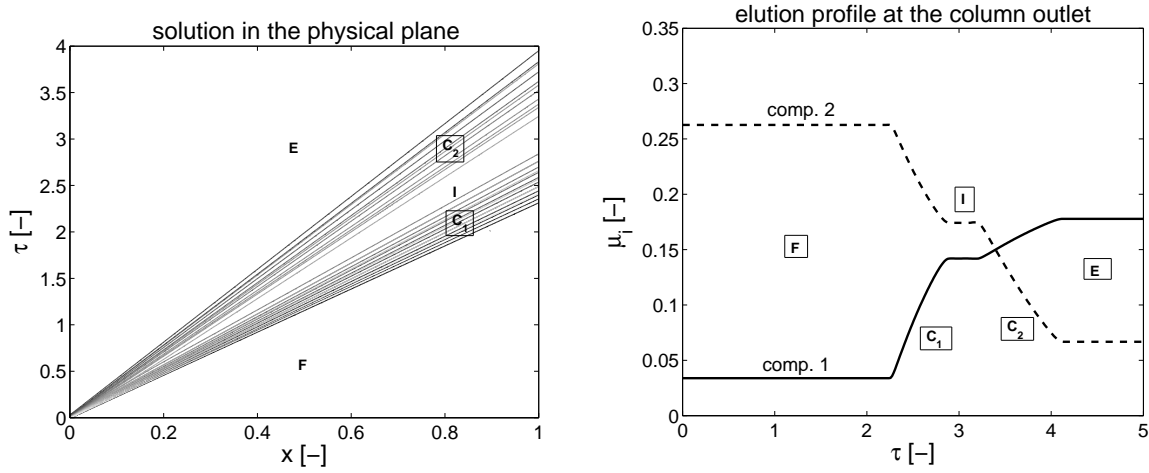


Figure 5.8: Section 5.1.2 (case 2c): Riemann problem leads to the  $C_2 - C_1$  solution,  $a_1 = 1.5, a_2 = 3.0$ , inlet state  $(\mu_1^E, \mu_2^E) = (0.1778, 0.0667)$ , initial state  $(\mu_1^F, \mu_2^F) = (0.0338, 0.2627)$ , and  $N_t = 5000$  (c.f. Eq. (4.4b)).

Table 5.7: Section 5.1.2 (case 2): Inlet and initial conditions for classical and non-classical solutions.

Case	Inlet state $(\mu_1^E, \mu_2^E)$	Initial state $(\mu_1^F, \mu_2^F)$
a	(0.1638, 0.1563)	(0.0423, 0.1005)
b	(0.0451, 0.0476)	(0.1818, 0.1142)
c	(0.20551, 0.05598)	(0.0423, 0.1005)
d	(0.1778, 0.0667)	(0.0338, 0.2627)
e	(0.0317, 0.3016)	(0.2051, 0.0598)
f	(0, 0.2)	(0.45, 0.0)

up at the jump discontinuity and behaves like a  $\delta$ -distribution. The concentration  $\mu_i = b_i c_i$  and  $1 - \mu_1 + \mu_2$  profiles are presented along the column at different simulation times. It can be observed that spikes are growing as they travel with a constant speed. Figure 5.12 gives the concentration profiles at the column outlet for different number of theoretical plates  $N_t$ . It can be seen that delta-shock gains height with the increase in  $N_t$ , i.e., with the decrease in dispersion coefficient  $\chi$  or  $D_{app}$ .

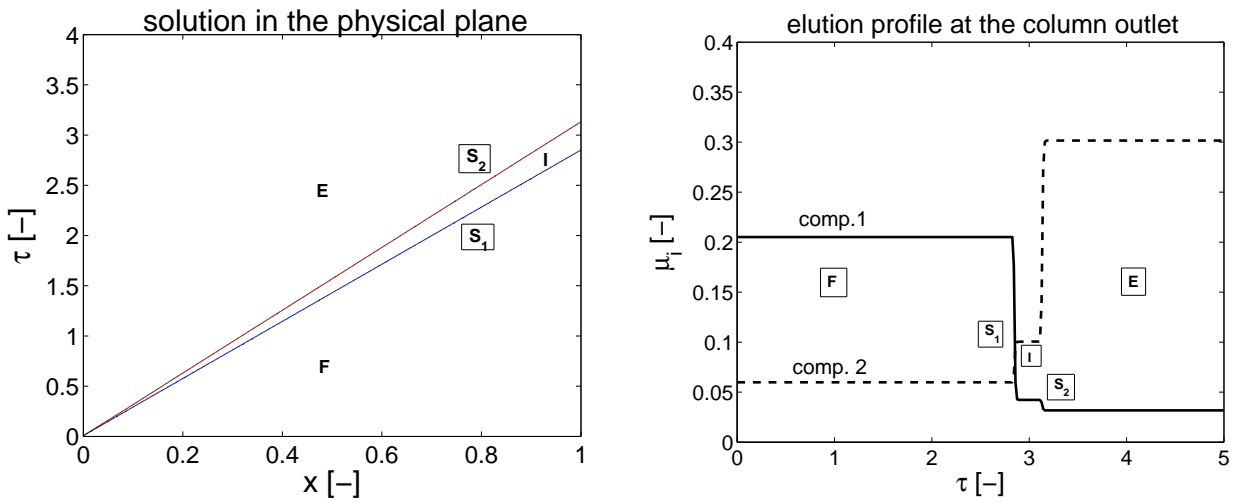


Figure 5.9: Section 5.1.2 (case 2d): Riemann problem leads to the  $C_2 - C_1$  solution,  $a_1 = 1.5, a_2 = 3.0$ , inlet state  $(\mu_1^E, \mu_2^E) = (0.0317, 0.3016)$ , initial state  $(\mu_1^F, \mu_2^F) = (0.2051, 0.0598)$ , and  $N_t = 5000$  (c.f. Eq. (4.4b)).

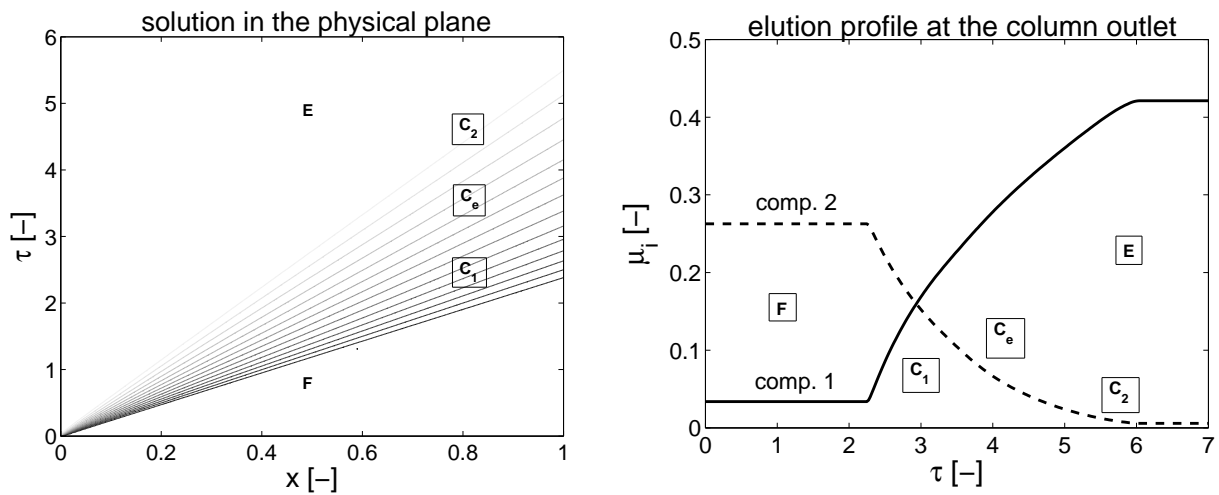


Figure 5.10: Section 5.1.2 (case 2e): Riemann problem leads to the  $S_2 - S_1$  solution,  $a_1 = 1.5, a_2 = 3.0$ , inlet state  $(\mu_1^A, \mu_2^A) = (0.4211, 0.0058)$ , initial state  $(\mu_1^B, \mu_2^B) = (0.0338, 0.2627)$ , and  $N_t = 5000$  (c.f. Eq. (4.4b)).

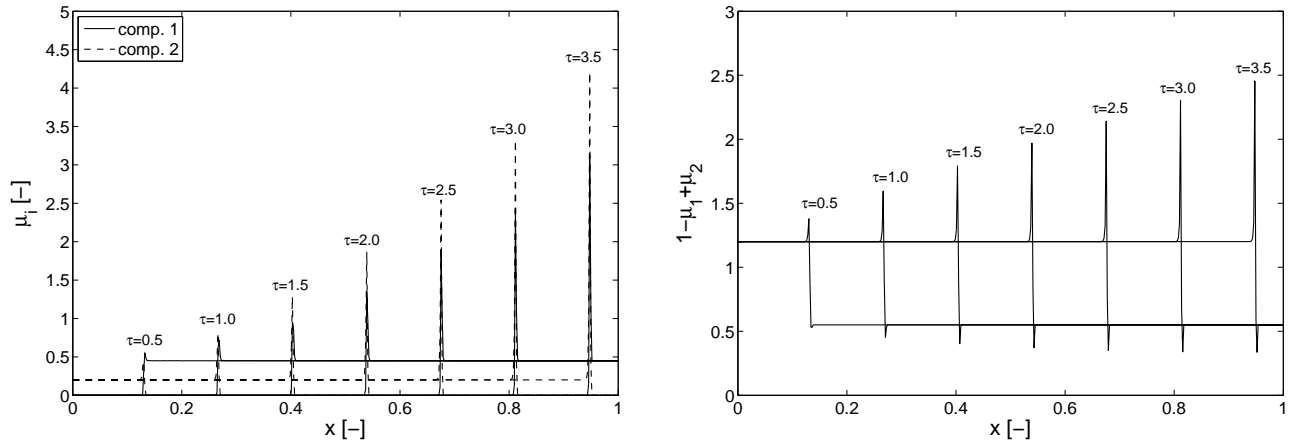


Figure 5.11: Section 5.1.2 (case 2f):  $\mu_i = b_i c_i$  and  $1 - \mu_1 + \mu_2$  profiles producing delta-shocks along the column,  $a_1 = 1.5, a_2 = 3.0$ , inlet state  $(\mu_1^E, \mu_2^E) = (0.0, 0.2)$ , initial state  $(\mu_1^F, \mu_2^F) = (0.45, 0.0)$ , and  $N_t = 5000$  (c.f. Eq. (4.4b)).

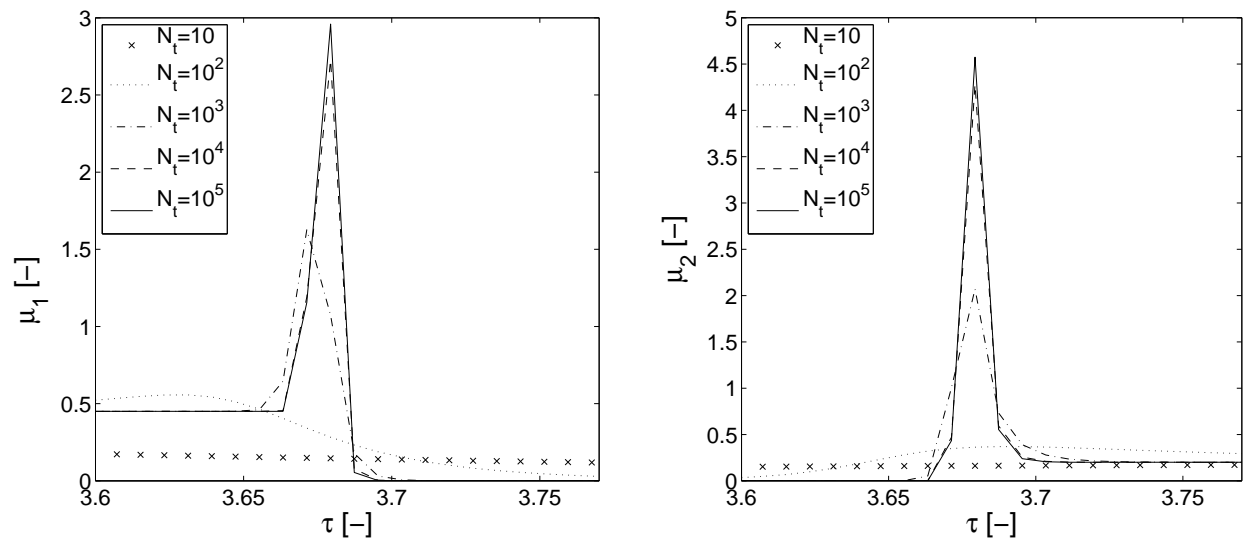


Figure 5.12: Section 5.1.2 (case 2f): Delta-shocks for different number of theoretical plates with  $a_1 = 1.5, a_2 = 3.0$ , inlet state  $(\mu_1^E, \mu_2^E) = (0.0, 0.2)$ , initial state  $(\mu_1^F, \mu_2^F) = (0.45, 0.0)$ .

### 5.1.3 Three-component elution

This section consists of three different case studies, such as a reaction  $C \rightleftharpoons A+B$  with linear isotherms, nonlinear displacement chromatography in a (fixed) bed, and displacement chromatography using a moving bed in counter-current direction.

#### Case 1: Reaction of the type $C \rightleftharpoons A+B$ with linear adsorption isotherm

In such a reaction, only reactant C is injected to the initially unloaded column, while components A and B are reaction products. Concentration profiles of A and B are detected at the column outlet. The FBCR model (2.23) with linear adsorption isotherms  $q_i^* = a_i c_i$  is considered. Based on conventional laws, the reaction rate can be written by the following equation [91]

$$Q_i(t, z, \mathbf{c}) = \nu_i r, \quad \text{where } r = k^{het} \left( q_C^* - \frac{q_A^* q_B^*}{K_{eq}^{het}} \right). \quad (5.12)$$

Here  $q_1^* := q_C^*$ ,  $q_2^* := q_A^*$ , and  $q_3^* := q_B^*$  represent the adsorption isotherms of each component, and the sign of the stoichiometric coefficient  $\nu_1 := \nu_C$  is negative, while the signs of  $\nu_2 := \nu_A$  and  $\nu_3 := \nu_B$  are positive. The heterogeneous equilibrium constant  $K_{eq}^{het}$  cannot be determined experimentally. For a linear adsorption isotherms, considered here, the chemical equilibrium constant of the heterogeneously catalyzed reaction  $K_{eq}^{het}$  can be written in terms of the solid-phase concentrations and the equilibrium constant of the homogeneous reaction  $K_{eq}^{hom}$  as

$$K_{eq}^{het} = K_{eq}^{hom} \frac{a_A a_B}{a_C}. \quad (5.13)$$

Substitution of Eq. (5.13) into Eq. (5.12) gives

$$r = k^{het} a_C \left( c_C - \frac{c_A c_B}{K_{eq}^{hom}} \right). \quad (5.14)$$

In this test problem, the parameters are taken from Tien [92]. Here we take the column length  $L = 0.25 \text{ m}$ , porosity  $\epsilon = 0.25$ ,  $N_t = 10^4$  (identical for all components),  $K_{eq}^{hom} = 0.5$ ,  $k^{het} = 5000 \text{ min}^{-1}$ ,  $a_C = 3$ ,  $a_A = 5$ , and  $a_B = 1$ . Moreover, concentration of reactant C, i.e.  $c_C^{\text{in}} = 0.5 \text{ mol/l}$ , is injected for 10 min with fluid velocity  $u = 1 \text{ m/min}$ . The corresponding



concentration profiles of  $c_C$ ,  $c_A$  and  $c_B$  are shown in Figure 5.13 (left) at 100 mesh cells. It can be seen that the DG-scheme resolves the discontinuous profiles better with their correct position compared to the Koren-scheme. These results are in good agreement with experimental observations of [92]. Outlet concentration profiles can be conveniently represented in the so-called hodograph space, see Figure 5.13 (right). Hodograph plots are very useful especially for illustrating problems of FBCR dynamics [30]. The hodograph plot often reflects the dynamics of process more clearly than the concentration trajectories. The following important geometrical condition for total conversion and total separation can be extracted, “total conversion and total separation in a fixed-bed chromatographic reactor with pulse injection of the reactant is possible, if the relevant wave solutions through the origin of the corresponding hodograph plot lie on the pure component axes of the products” [91]. In this plot the concentrations as dependent variables are plotted against each other. The vertical thick line  $P_0 - P_1$  shows the fraction of pure component B, obtained from the front of the elution profile, whereas the horizontal thick line  $P_0 - P_3$  represents pure A, collected from the rear of the elution profile. The other two straight lines  $P_0 - P_4$  and  $P_0 - P_5$  refer to Section 5.1.2 (case 1) with linear isotherms. The lines which are located for the case considered exclusively on the pure component axes (thick lines) prove the capability to obtain pure components A and B from the rear and front of the elution profiles, respectively.

### **Case 2: Non-reactive displacement chromatography with Langmuir isotherm**

This case study corresponds to an alternative attractive mode of chromatography, namely displacement chromatography. Displacement chromatography is a powerful method used to separate and purify compounds. It can be used to purify metal cations, small organic molecules, antibiotics, sugars, peptides, proteins, and nucleic acids [23]. This process follows the idea that one strong component, the displacer, has enough capability to displace the other components from the stationary phase. In this process a column packed with a solid material is initially equilibrated with the mobile liquid phase that has no or less affinity to the solid phase. The sample mixture is then injected into the column occupying part of the column inlet. Afterwards, a development agent, the so called displacer, is

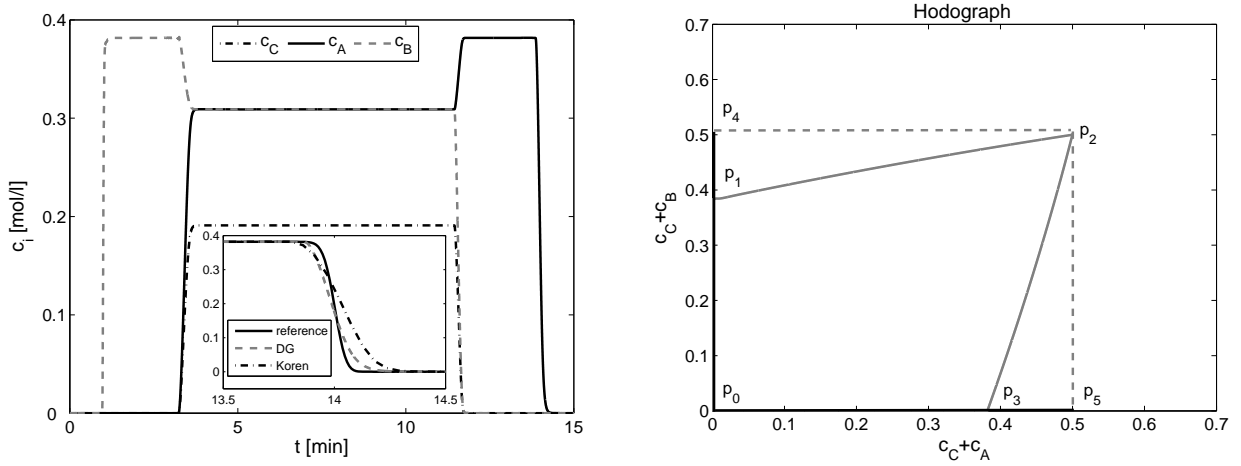


Figure 5.13: Section 5.1.3 (case 1): 3-component isothermal-reactive elution with linear isotherm. Parameters are given in text.

injected into the column. Note that, the displacer should have stronger affinity to the solid phase as compared to other components in the sample. For a sufficiently long column and favorably shaped isotherms, the sample components will ultimately transport along the column to build highly concentrated separated rectangular zones. The series of such zones is known as displacement train or an isotachic train [23]. The displacement effect reduces the tailing and simplifies the sample loading. Due to these characteristics, displacement chromatography could be eventually more attractive compared to elution in preparative scale chromatography.

For illustration, two solute samples with concentrations  $c_A$  and  $c_B$  and a displacer with concentration  $c_d$  are considered. The FBCR model (2.23) is used to simulate the process by taking the source terms  $Q_i(t, z, \mathbf{c})$  equal to zero. The Langmuir isotherm, c.f. Eq. (2.18),

$$q_i^* = \frac{a_i c_i}{1 + \sum_{i=1}^3 b_i c_i}, \quad i = 1, 2, 3 \quad (5.15)$$

were used. In simulation, the following parameters were considered: column diameter  $d = 0.357 \text{ cm}$ ,  $L = 100 \text{ cm}$ , porosity  $\epsilon = 0.5$ ,  $a_A = a_1 = 4$ ,  $a_B = a_2 = 5$ ,  $a_d = a_3 = 6$ ,  $b_1 = 4 \text{ l/g}$ ,  $b_2 = 5 \text{ l/g}$ , and  $b_d = 1 \text{ l/g}$ . Moreover,  $N_t = 10^4$  (identical for all components), and the volumetric flow rate at the column inlet was  $\dot{V} = 1 \text{ ml/min}$  ( $u = 19.98 \text{ cm/min}$ ). In the

first simulation study, a pulse of a mixture containing  $c_A^{\text{in}} = c_1^{\text{in}} = 1 \text{ g/l}$  and  $c_B^{\text{in}} = c_2^{\text{in}} = 1 \text{ g/l}$  is injected for an injection time  $t^{\text{in}} = 0.1 \text{ min}$ . Then, a displacer with a concentration  $c_d^{\text{in}} = 1 \text{ g/l}$  is fed continuously into the column for the rest of the simulation time. As the displacer pushes the mixture, both components start separating. For a sufficiently long column in the present study, the sample components will fully separate and build highly concentrated rectangular zones of individual concentrations. It is to be noted that component 1 is less retained than component 2 and the displacer is characterized by the highest adsorbability. The numerical results are shown in Figure 5.15 using 200 mesh cells. The operating line in Figure 5.14, plotted under equilibrium conditions, verifies that both components have less affinity as compared to the displacer. Consequently, both components are resolved into consecutive rectangular zones of pure substances after  $50 \text{ cm}$  and at simulation time  $t = 13 \text{ min}$ , see Figure 5.15. For the numerical approximation of displacement chromatographic process, both suggested schemes, namely the DG and Koren methods produce reliable results. Moreover, Figure 5.16 shows that the DG-scheme gives a better resolution of the rectangular profiles at the discontinuity compared to the Koren scheme. Therefore, the DG-scheme will be used to simulate the processes in the next case studies of this part.

In the second simulation study, the injection concentrations of both components are  $c_1^{\text{in}} = c_2^{\text{in}} = 1 \text{ g/l}$  and the displacer has a concentration  $c_d^{\text{in}} = 0.5 \text{ g/l}$ . Figure 5.17 shows the numerical results at 200 mesh points. Figure 5.14 shows that a line drawn from the origin intersects the isotherm of the component 2 but not the isotherm of the component 1. Hence, the component 2 forms an equilibrated rectangular pulse, while the component 1, which is now moving at higher speed fails to do so. This is depicted in Figure 5.17.

In the third simulation study, we consider  $c_d^{\text{in}} = 0.1 \text{ g/l}$ . For this value of displacer concentration the isotherm plots of both components are not intersected by the operating line. As a result, both components do not form a rectangular isotachic train as shown in Figure 5.18. The results presented in this section are found in good qualitative agreement with concentration profiles typically attained in experimental studies of displacement chromatography.

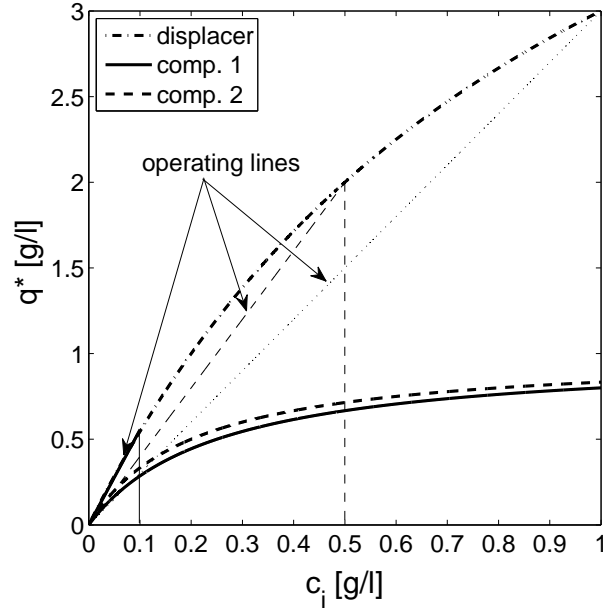


Figure 5.14: Section 5.1.3 (case 2): Representation of the operating line.

### Case 3: Displacement chromatography on movable (counter-current) beds

Moving bed chromatography is a mode in which two phases of the chromatographic system, the fluid and the solid phases, flow through the column in opposite directions. It is known to be a versatile technique for separating binary mixtures since the 1960s [5]. This simulated moving bed concept is now employed in a wide range of applications in the pharmaceutical, medical as well as cosmetic industries. In this case Eq. (2.21) is replaced by the following equation

$$\frac{\partial c_i}{\partial t} + \frac{1 - \epsilon}{\epsilon} \frac{\partial q_i^*}{\partial t} + u \frac{\partial c_i}{\partial z} - v_s F \frac{\partial q_i^*}{\partial z} = D_{\text{app},i} \frac{\partial^2 c_i}{\partial z^2}, \quad i = 1, 2, 3. \quad (5.16)$$

Here,  $v_s$  represents the speed of solid particles forming the diffusion free moving bed. Under steady state conditions, the solid and liquid concentrations at the column outlet are related as, c.f. Figure 5.19,

$$(q_{i,L}^* - q_{i,0}^*) \frac{1 - \epsilon}{\epsilon} = \frac{u}{v_s} (c_{i,L} - c_{i,0}) \quad (5.17)$$

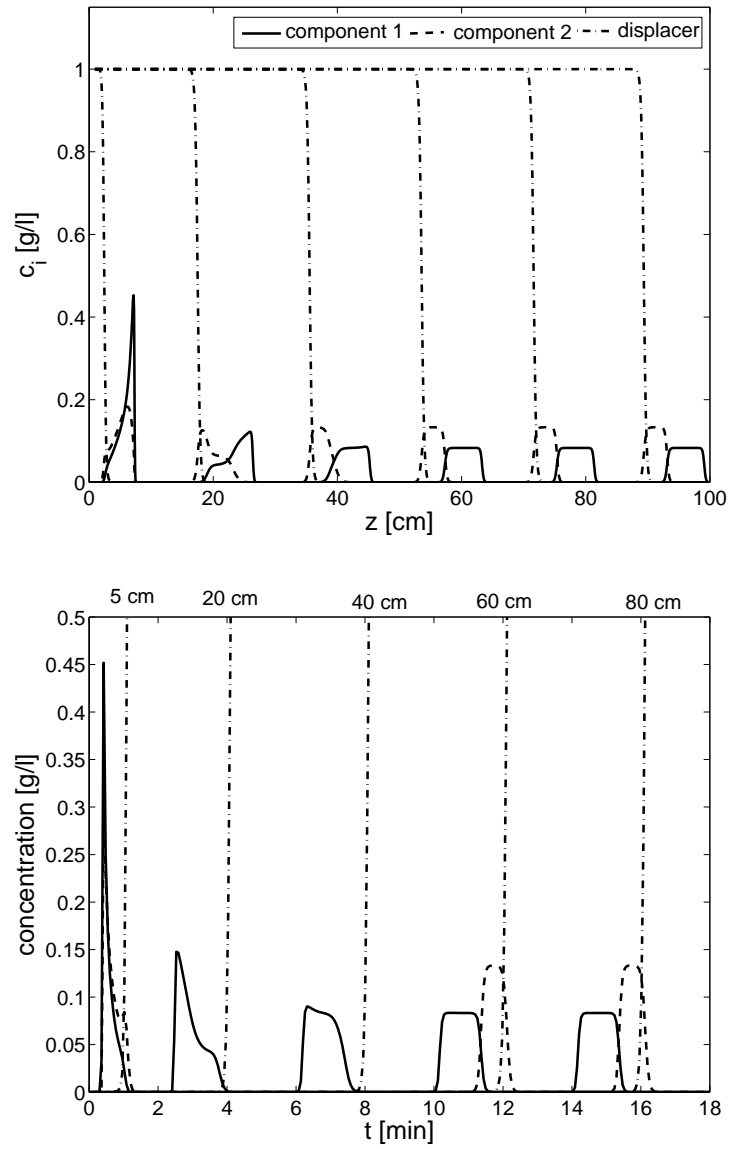


Figure 5.15: Section 5.1.3 (case 2): Formation of displacement train,  $\epsilon = 0.5$ ,  $N_t = 10^4$  (c.f. Eq. (4.4b)),  $a_1 = 4$ ,  $a_2 = 5$ ,  $a_d = 6$ ,  $b_1 = 4\text{ l/g}$ ,  $b_2 = 5\text{ l/g}$ , and  $b_d = 1\text{ l/g}$  with  $c_1^{\text{in}} = c_2^{\text{in}} = c_d^{\text{in}} = 1\text{ g/l}$  and  $t^{\text{in}} = 0.1\text{ min}$ .

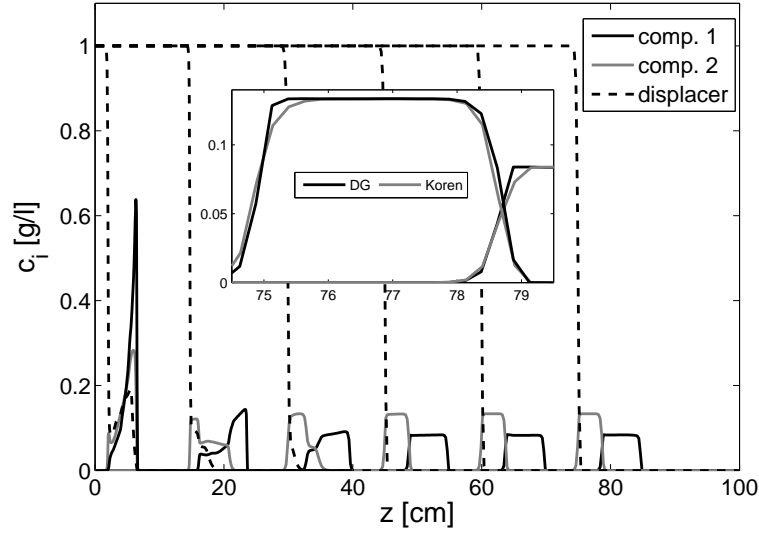


Figure 5.16: Section 5.1.3 (case 2): A comparison of the DG and Koren schemes. Formation of displacement train,  $\epsilon = 0.5$ ,  $N_t = 10^4$  (c.f. Eq. (4.4b)),  $a_1 = 4$ ,  $a_2 = 5$ ,  $a_d = 6$ ,  $b_1 = 4 l/g$ ,  $b_2 = 5 l/g$ , and  $b_d = 1 l/g$  with  $c_1^{\text{in}} = c_2^{\text{in}} = c_d^{\text{in}} = 1 g/l$  and  $t^{\text{in}} = 0.1 \text{ min}$ .

with boundary conditions

$$c_{i,0} = c_i^{\text{in}}, \quad q_{i,L}^* = q_i^{\text{in}}, \quad \left. \frac{dc_i}{dz} \right|_{z=L} = 0, \quad \left. \frac{dq_i^*}{dz} \right|_{z=0} = 0. \quad (5.18)$$

Here,  $c_i^{\text{in}}$  represents the injection concentration of component  $i$  at the left boundary  $z = 0$  and  $q_i^{\text{in}}$  denotes the corresponding injected solid concentration at  $z = L$ . The initial data are the same as used in the first simulation of fixed-bed displacement chromatography in the previous part, i.e. the concentrations of both components are  $c_1^{\text{in}} = c_2^{\text{in}} = 1 g/l$  with the displacer concentration  $c_d^{\text{in}} = 1 g/l$ . The numerical results were obtained by using the DG-scheme using 200 mesh points.

At the start of the process, the solid phase was fixed  $v_s = 0$  and a mixture was injected followed by the displacer. The components along with the displacer started moving in the column and approached the right end of the column after approximately 5 minutes, see top plot in Figure 5.20. The isotachic train is not reached yet. This would require more time and a longer bed. In order to reach this attractive pattern with the given bed length, a new concept is considered. At time  $t = 5 \text{ min}$ , a movement of the solid bed particles was

activated directed in the opposite direction while the fluid velocity  $u$  was set to zero keeping  $D_{\text{app}}$  unchanged. Consequently, all concentration fronts started moving back. It took about 4 minutes to approach the left end of the column, see the middle plot in Figure 5.20. Finally, the movement of the solid bed was stopped and the fluid velocity was re-activated. As a result, the pulses started moving in the forward direction for 4 more minutes, see bottom plot in Figure 5.20. These back and forth movements ultimately separated the mixture to build concentrated rectangular zones and form the isotachic train in the total simulation time of 13 minutes for the given column length. Note that, simulation times are the same for both fixed-bed and moving-bed processes. However, the moving-bed process allows to separate the same feed mixture with a relatively shorter column as compared to the fixed-bed process shown in Figure 5.15. In the bottom plot of Figure 5.20, we have also plotted the equilibrium profiles of the fixed-bed over the equilibrium profiles of the counter-current bed in order to verify that both processes give the same results. In that figure symbols are used for the fixed-bed profiles of Figure 5.15 and lines represent the counter-current bed profiles of Figure 5.20. Thus, the described moving-bed process can be very useful to separate mixtures which are difficult to separate and require long chromatographic columns. Currently, no experimental data or computational results are available for validation of the simulation results of this case study. However, the results of our numerical study appear to be useful for further investigation of such processes.

#### 5.1.4 Four-component reactive elution

This part contains two reactive chromatographic case studies with linear and nonlinear isotherms, respectively.

##### Case 1: Isothermal reaction with linear isotherms

In this final test problem, a reaction of type  $A+B \rightleftharpoons C+D$  along with the temperature influence on the process is investigated. The feed composition and the flow rate of mobile phase are assumed to be constant. The ester hydrolysis, experimentally studied by Tien [92] and Mai [56] is considered as a practical example. The general reaction mechanism is  $\text{ester} + \text{water} \rightleftharpoons \text{alcohol} + \text{acid}$ . In such a reaction, only the reactant A (ester) is injected into

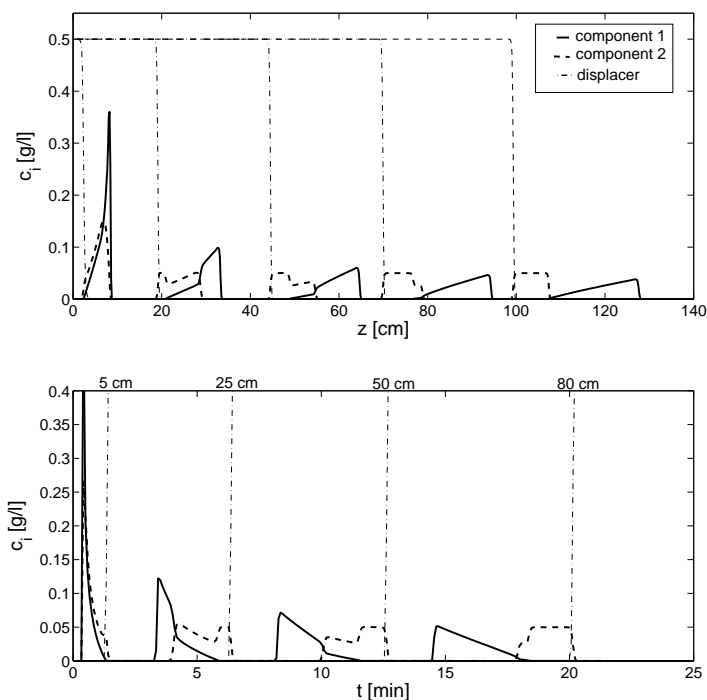


Figure 5.17: Section 5.1.3 (case 2): Displacement chromatography,  $\epsilon = 0.5$ ,  $N_t = 10^4$  (c.f. Eq. (4.4b)),  $a_1 = 4$ ,  $a_2 = 5$ ,  $a_d = 6$ ,  $b_1 = 4l/g$ ,  $b_2 = 5l/g$ , and  $b_d = 1l/g$  with  $c_1^{\text{in}} = c_2^{\text{in}} = 1g/l$  and  $c_d^{\text{in}} = 0.5g/l$ .

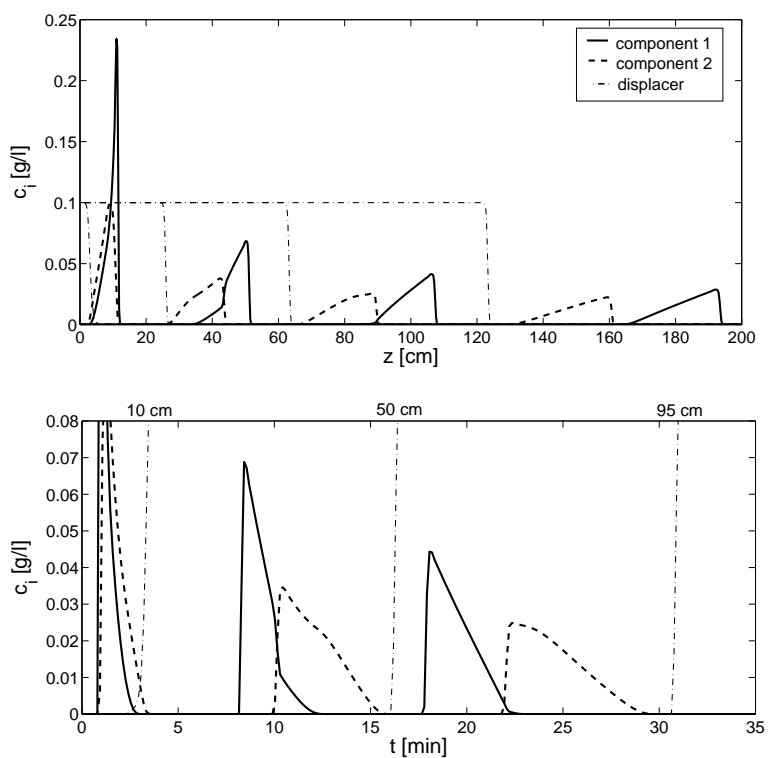


Figure 5.18: Section 5.1.3 (case 2): Displacement chromatography,  $\epsilon = 0.5$ ,  $N_t = 10^4$  (c.f. Eq. (4.4b)),  $a_1 = 4$ ,  $a_2 = 5$ ,  $a_d = 6$ ,  $b_1 = 4l/g$ ,  $b_2 = 5l/g$ , and  $b_d = 1l/g$  with  $c_1^{\text{in}} = c_2^{\text{in}} = 1g/l$ ,  $c_d^{\text{in}} = 0.1g/l$ .



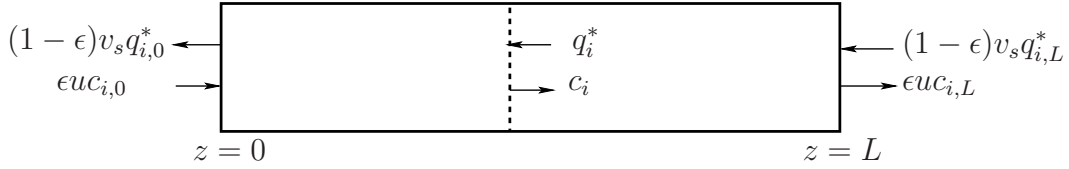


Figure 5.19: A schematic diagram of counter-current adsorption process.

the column initially loaded only with component B (water), while component C (alcohol) and component D (acid) are reaction products. Concentration profiles of C and D are detected at the column outlet. The parameters of reaction equilibrium, reaction kinetics, and adsorption isotherms are given in Table 5.8. The flow rate is  $0.75 \text{ ml/min}$ ,  $c_A^{\text{in}} = 0.5 \text{ mol/l}$ ,  $c_B^{\text{in}} = 0 = c_C^{\text{in}} = c_D^{\text{in}}$ ,  $u = 0.0622 \text{ m/min}$ ,  $\epsilon = 0.24$ ,  $L = 0.25 \text{ m}$ . The injection volume is  $100 \mu\text{l}$ . Initially, the column is equilibrated with water only, i.e.  $c_B^{\text{init}} = 55.525 \text{ mol/l}$  and  $c_A^{\text{init}} = c_C^{\text{init}} = c_D^{\text{init}} = 0$ . The FBCR model (2.23) with linear adsorption isotherms,  $q_i^* = a_i c_i$ , is considered. The reaction rate of the heterogeneously catalyzed ester hydrolysis reactions is described by

$$Q_i(t, z, c) = \nu_i r, \quad \text{where } r = k_{\text{for}}^{\text{het}} \left( q_A^* q_B^* - \frac{q_C^* q_D^*}{K_{\text{eq}}^{\text{het}}} \right). \quad (5.19)$$

Here, the signs of the stoichiometric coefficients  $\nu_A$  and  $\nu_B$  are negative, while the signs of  $\nu_C$  and  $\nu_D$  are positive. For linear adsorption isotherms, the chemical equilibrium constant  $K_{\text{eq}}^{\text{het}}$  can be written in terms of the solid-phase concentrations constant  $K_{\text{eq}}^{\text{hom}}$  as

$$K_{\text{eq}}^{\text{het}} = K_{\text{eq}}^{\text{hom}} \frac{a_C a_D}{a_A a_B}. \quad (5.20)$$

Substituting of equation (5.20) in (5.19), we get

$$r = k_{\text{for}}^{\text{het}} a_A a_B \left( c_A c_B - \frac{c_C c_D}{K_{\text{eq}}^{\text{hom}}} \right). \quad (5.21)$$

The eluted concentrations of the reaction products C and D are shown in Figure 5.21 using 200 mesh cells. To further analyze the performance of the chromatographic reactors, the

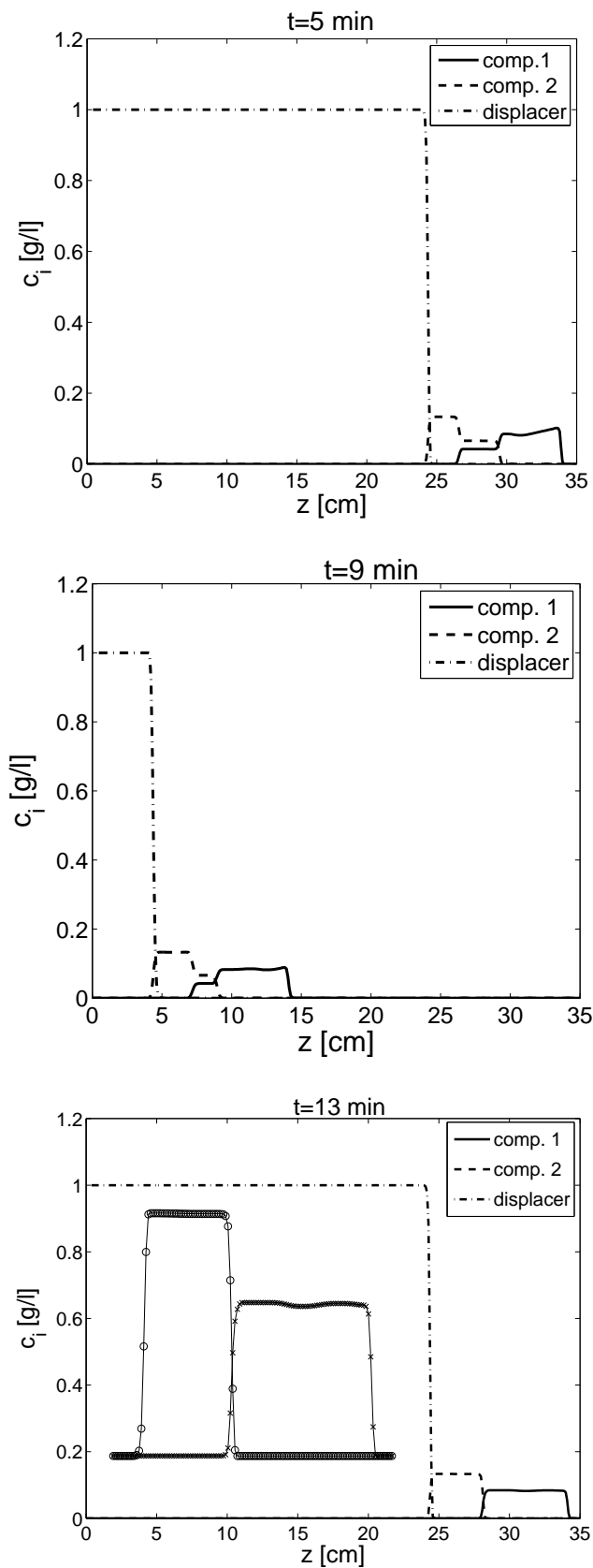


Figure 5.20: Section 5.1.3 (case 3): Displacement chromatography on counter-current bed,  $\epsilon = 0.5$ ,  $N_t = 10^4$  (c.f. Eq. (4.4b)),  $a_1 = 4$ ,  $a_2 = 5$ ,  $a_d = 6$ ,  $b_1 = 4$  l/g,  $b_2 = 5$  l/g, and  $b_d = 1$  l/g,  $c_1^{\text{in}} = c_2^{\text{in}} = c_d^{\text{in}} = 1$  g/l and  $t^{\text{in}} = 0.1$  min.

Table 5.8: Section 5.4: Temperature dependent reaction and adsorption parameters.

Temperature	$a_i$				$N_t$	$k_{\text{for}}^{\text{het}}$ [1/min]	$K_{\text{eq}}^{\text{hom}}$
	A	B	C	D			
298K	1.110	1	0.723	0.458	783	$5.88 \times 10^{-3}$	0.38
308K	1.082	1	0.750	0.452	886	$23.5 \times 10^{-3}$	0.48
318K	1.038	1	0.768	0.445	996.5	$41.6 \times 10^{-3}$	0.44
328K	0.993	1	0.782	0.425	$10^4$	$10^3$	0.45

reaction is considered at four different temperatures. The numerical results of the DG-scheme are also compared with the experimental data of [92]. Except for the porosity, other model parameters heavily depend on the temperature of the column as given in Table 5.8. The plots of Figure 5.21 show that component A was converted completely in all cases, but the separation of products C and D was significantly improved at higher temperatures. The peak widths are also reduced significantly at higher temperatures. In agreement with the course of the Henry constants, Table 5.8, the retention times of the product D have a tendency to decrease with temperature increase, whereas the retention times of the product C have the opposite tendency. The numerical results were found in relative good agreement with experimental data from [92].

### Case 2: Isothermal reaction with nonlinear isotherm

To extend the previous case study to the nonlinear isotherms of Eq. (2.18), we considered  $L = 0.25 \text{ m}$ ,  $u = 0.1322 \text{ m/min}$ . The remaining data are given in Table 5.8 at a temperature of  $318 \text{ K}$ . As Langmuir isotherm parameters were considered as  $b_A = 3 \text{ l/mol}$ ,  $b_B = 0$ ,  $b_C = 2 \text{ l/mol}$ ,  $b_D = 1 \text{ l/mol}$ , while the  $a_i$  are the same as in the linear case. No experimental data or analytical results are available for this setup. The numerical results of the DG-scheme shown in Figure 5.22. The typical behavior caused by nonlinear Langmuir isotherms is observed.

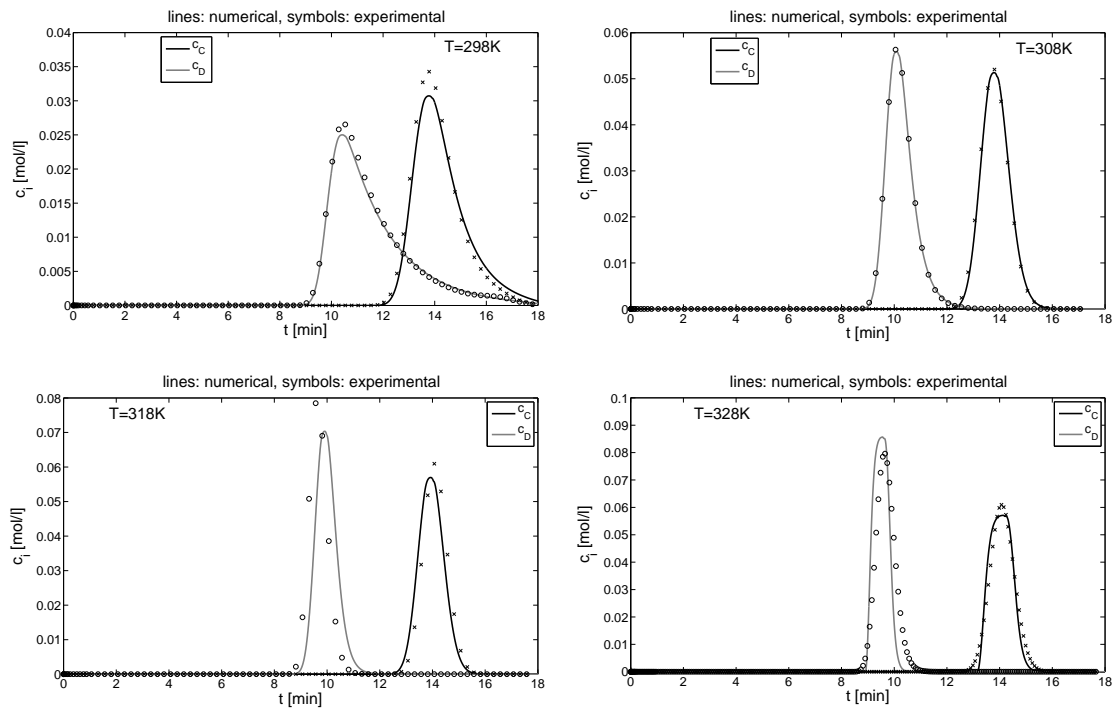


Figure 5.21: Section 5.1.4 (case 1): 4-component isothermal-reactive elution at different temperatures with linear isotherms.

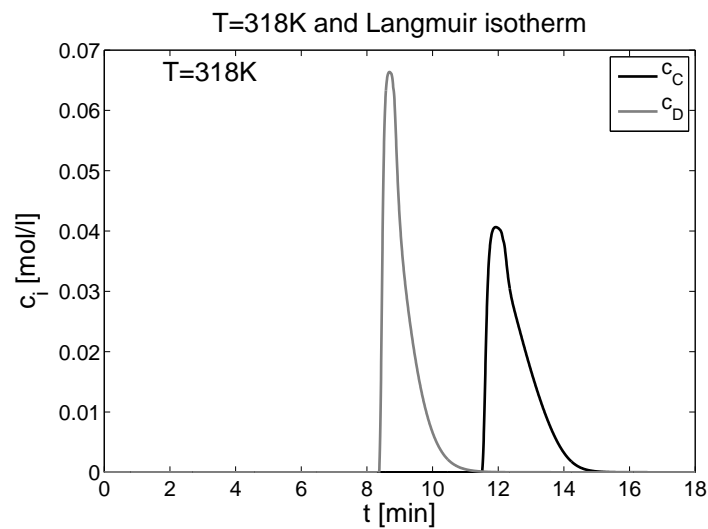


Figure 5.22: Section 5.1.4 (case 2): 4-component isothermal-reactive elution at temperature  $T = 318$  with nonlinear isotherm.

## 5.2 Conclusion

In this chapter, the discontinuous Galerkin finite element method and the Koren scheme were implemented for solving isothermal non-reactive and reactive chromatographic models. The second to third order accuracy of the Koren scheme in axial-coordinate was verified analytically and numerically. The scheme is a flux-limiting scheme in which fluxes are limited by using a nonlinear minmod limiter. This limiting procedure guarantees the positivity of the scheme and suppresses the numerical oscillations. The DG-scheme presented satisfies the TVB property and gives second order accuracy. The scheme can be easily extended to higher orders by using high order basis functions and by employing better slope limiters, for example reconstruction with the WENO limiters [69]. This method incorporates the ideas of numerical fluxes and slope limiters in a very natural way to capture the physically relevant discontinuities without producing spurious oscillations in their vicinity. In contrast to finite volume schemes, the DG-scheme is well suited to handle complicated geometries and avoids the extension of the mesh stencil that allows the incorporation of boundary conditions uniformly. The accuracy of the proposed schemes were validated against other flux-limiting finite volume schemes available in the literature. The numerical test problems verify that the suggested DG-scheme gives more resolved solutions than the high resolution scheme of Koren, especially at sharp discontinuities. However, desirable results can also be obtained by using the Koren scheme and we conclude that both the DG and Koren schemes are optimal methods for the numerical approximation of linear and nonlinear chromatographic models. The focus of this chapter was to simulate the dynamic behavior of isothermal chromatographic processes. In the subsequent chapter, the numerical scheme is extended to solve the non-isothermal reactive liquid chromatographic model.

## Chapter 6

# Thermal Effects in Reactive Liquid Chromatography

This chapter is focused on modeling and simulation of non-isothermal reactive liquid chromatography. The purpose of this study is to quantify how temperature gradients can influence conversion and separation in reactive liquid chromatography. Additionally, the coupling of concentration and thermal fronts are illustrated and key parameters influencing the reactor performance are identified.

Thermal effects are discussed widely in case of gas phase reactions in solid packings [21, 27, 40, 104, 105]. In reactive liquid chromatography, thermal effects are typically not considered and modeling of the process assumes that effects of heats of sorption and reaction are negligible. Only very few contributions considering thermal effects can be found in the literature [77, 78, 79, 90].

Non-isothermal reactive chromatography can be described by a convection dominated system of non-linear convection-diffusion-reaction type partial differential equations and algebraic equations describing thermodynamic and kinetic phenomena. The corresponding systems have to be solved numerically because analytical solutions cannot be obtained. The simulation of non-isothermal reactive chromatography is a challenging task for a numerical scheme due to the nonlinearity of the convection-dominated mass and energy balance equations and because of stiffness of the reactive source terms. These stiff terms may produce rapid variations in the solution and can render the numerical methods unstable, unless the

time step size is sufficiently small. Thus, an efficient and accurate numerical technique is needed to avoid excessive dissipation, incorrect phase speeds, spurious oscillations, and to capture sharp discontinuities of the elution profiles. In order to solve the current problem, a high resolution finite volume scheme, already developed for isothermal chromatography in this thesis, c.f. Chapter 3, is extended to solve the non-isothermal processes. Finite volume schemes were already applied in the chromatographic field [16, 34, 51, 60, 103], but were never implemented for the complex non-isothermal reactive chromatographic model considered in this work.

In this study, a flux-limiting semi-discrete high resolution finite volume scheme of Koren [39] is proposed for the numerical approximation of non-isothermal reactive chromatographic models. The scheme discretizes the model in axial-coordinate only, while keeps the time variable continuous. The suggested scheme was found to be second to third order accurate analytically and numerically in the previous chapter on equilibrium dispersive chromatographic models. The scheme gives high order accuracy on coarse grids, resolves sharp discontinuities, and avoids numerical dispersion [49]. Several challenging case studies are carried out which elucidate the effect of several sources for non-isothermal behavior. The numerical results were evaluated critically by performing consistency tests evaluating both mass and energy balances including considerations of limiting cases, which can be theoretically predicted. The results prove the accuracy of the numerical scheme and quantify the relevant thermal effects.

## 6.1 The non-isothermal chromatographic reactor model

This section focuses on mathematical modeling of non-isothermal chromatographic reactors. Mathematically, the non-isothermal single column chromatographic reactor is similar to a more frequently studied non-isothermal unsteady-state fixed bed reactor [72, 78]. The model is based on the following basic assumptions:

1. A permanent equilibrium is assumed between stationary and mobile phases at all positions of the column.

2. A single reaction takes place exclusively in the solid phase.
3. There are no radial concentration and temperature gradients in the column and a one dimensional description is used.
4. Only axial dispersion causes band broadening described by  $D_{\text{app}}$  and  $\lambda_{\text{ax}}$  in the mass and energy balances, respectively.
5. Compressibility of the mobile phase is negligible.
6. There are no interactions between the solvent (carrier) and the solid phase.
7. There is no heat added or removed from the system except via the inlet and outlet streams, i.e. adiabatic operation.

The classical mass balance equations of the equilibrium dispersive model for a fixed bed chromatographic column are given as

$$\left(1 + F \frac{\partial q_i^*}{\partial c_i}\right) \frac{\partial c_i}{\partial t} + u \frac{\partial c_i}{\partial z} = D_{\text{app},i} \frac{\partial^2 c_i}{\partial z^2} + F \nu_i r, \quad i = 1, 2, \dots, N_c, \quad (6.1)$$

where  $F$  is the phase ratio based on the porosity  $\epsilon \in ]0, 1[$  and  $F = \frac{1-\epsilon}{\epsilon}$ ,  $c_i$  is the concentration of the  $i$ -th component in the fluid phase,  $q_i^*$  is the solid phase equilibrium concentration of the  $i$ -th component,  $u$  represents the constant interstitial velocity of the mobile phase,  $D_{\text{app},i}$  represents the axial dispersion coefficient of the  $i$ -th component,  $t$  is the time, and  $z$  is the axial-coordinate along the column. Moreover,  $r$  is the rate of the reaction in the solid phases, the  $\nu_i$  are the corresponding stoichiometric coefficients of components and  $N_c$  represents the total number of components. Note that, the stoichiometric coefficients  $\nu_i$  are negative for reactants and positive for products.

If the enthalpy of mixing is neglected, the energy balance for a differential volume element in an adiabatic chromatographic reactor becomes

$$(\rho^L C_p^L + F \rho^S C_p^S) \frac{\partial T}{\partial t} + u \rho^L C_p^L \frac{\partial T}{\partial z} = \lambda_{\text{ax}} \frac{\partial^2 T}{\partial z^2} + F \sum_{i=1}^{N_c} (-\Delta H_{A,i}) \frac{\partial q_i^*}{\partial t} + F(-\Delta H_R)r. \quad (6.2)$$



Here  $\rho$  represents the density per unit volume,  $C_p$  is the heat capacity, and the superscripts L and S stands for the liquid and solid phases, respectively. The considered density and heat capacity are not depending on temperature and composition. Moreover,  $\Delta H_{A,i}$  denotes the enthalpy of adsorption for the  $i$ -th component and  $\Delta H_R$  represents the enthalpy of reaction. By using the assumptions of non-dispersive and non-reactive chromatography, the propagation velocities of concentration fronts  $u_c^i$  and of the thermal front  $u_T$  can be estimated from Eqs. (6.1) and (6.2) as:

$$u_c^i \cong \frac{u}{1 + F \frac{\partial q_i^*}{\partial c_i}}, \quad u_T \cong \frac{u}{1 + F \frac{\rho^S C_p^S}{\rho^L C_p^L}}, \quad i = 1, 2, \dots, N_c. \quad (6.3)$$

The Eq. (6.3) reveals that the propagation velocities  $u_c^i$  depend on the corresponding local slopes of the adsorption isotherms and that the propagation velocity  $u_T$  is influenced by the ratio of the volumetric density times heat capacities of solid and liquid phases. For weakly adsorbed components or small slopes of isotherm  $\frac{\partial q_i^*}{\partial c_i}$  and for significantly higher ratio of  $\frac{\rho^S C_p^S}{\rho^L C_p^L}$ , the velocities of concentration fronts  $u_c^i$  are higher than the thermal velocity  $u_T$ .

For non-reactive chromatography under non-isothermal conditions, it was shown that the energy balance can be formulated as the  $N_c + 1$ -th equation, analogously to the  $N_c$  mass balance equations [72]. This idea can be extended easily to reactive systems if the heat of reaction is assumed to be an analogue to the  $N_c + 1$  stoichiometric coefficient, i.e.  $\nu_{N_c+1} = -\Delta H_R$ . Hereby, the energy balance is formulated in a convenient way with respect to a reference temperature  $T^{\text{ref}}$ .

Generally, the computer implementation of dimensionless equations is more convenient to reduce rounding error. The current system can be transformed into a dimensionless form by introducing the following dimensionless time and axial coordinates

$$\tau = tu/L, \quad x = z/L \quad (6.4)$$

and the new variables

$$\nu_{N_c+1} = -\Delta H_R, \quad (6.5a)$$

$$c_{N_c+1} = \rho^L C_p^L (T - T^{\text{ref}}), \quad (6.5b)$$

$$q_{N_c+1}^* = \rho^S C_p^S (T - T^{\text{ref}}) + \sum_{i=1}^{N_c} \Delta H_{A,i} q_i^*. \quad (6.5c)$$

By using the chain rule and Eqs. (6.4) and (6.5), the Eqs. (6.1) and (6.2) can be lumped together as a single system of  $N_c + 1$  equations:

$$\left(1 + F \frac{\partial q_m^*}{\partial c_m}\right) \frac{\partial c_m}{\partial \tau} + F \sum_{\substack{l=1 \\ l \neq m}}^{N_c+1} \frac{\partial q_m^*}{\partial c_l} \frac{\partial c_l}{\partial \tau} + \frac{\partial c_m}{\partial x} = \frac{1}{Pe} \frac{\partial^2 c_m}{\partial x^2} + \frac{L \nu_m}{u} Fr, \quad (6.6)$$

where  $m = 1, 2, \dots, N_c + 1$ . The dimensionless Peclet number  $Pe$  is given as

$$Pe_m = \begin{cases} Pe_M = \frac{Lu}{D_{\text{app}}} & \text{if } m = 1, 2, \dots, N_c, \\ Pe_E = \frac{Lu \rho^L C_p^L}{\lambda_{\text{ax}}} & \text{if } m = N_c + 1, \end{cases} \quad (6.7)$$

where  $L$  is the column length and  $Pe_M$  is equal to two times of the frequently used number of theoretical plates  $N_t$  and assumed to be the same for all components.

Now it is required to define  $N_c + 1$  initial and  $2(N_c + 1)$  boundary conditions to close the model (6.6). For an initially uniformly equilibrated column, the initial and boundary conditions for the  $N_c$  dimensionless mass balance equations of Eq. (6.6) are given as:

$$c_m(0, x) = c_m^{\text{init}}, \quad c_m(\tau, 0) = c_m^{\text{in}}(t) + \frac{L}{Pe} \frac{\partial c_m}{\partial x} \Big|_{x=0}, \quad \frac{\partial c_m}{\partial x} \Big|_{x=1} = 0, \quad m = 1, 2, \dots, N_c, \quad (6.8a)$$

and the conditions for the  $N_c + 1$ -th dimensionless energy balance equation are given as

$$c_{N_c+1}(0, x) = 0, \quad c_{N_c+1}(\tau, 0) = T^{\text{in}} + \frac{L}{Pe} \frac{\partial c_{N_c+1}}{\partial x} \Big|_{x=0}, \quad \frac{\partial c_{N_c+1}}{\partial x} \Big|_{x=1} = 0, \quad (6.8b)$$

where  $c_j^{\text{in}}$ ,  $T^{\text{init}}$  and  $T^{\text{in}}$  represent the inlet concentrations, initial temperature and temperature at the column inlet, respectively. In this work,  $T^{\text{in}}$ ,  $T^{\text{init}}$  and the reference temperature  $T^{\text{ref}}$  are taken to be identical.

In this study, for illustration a simple reversible reaction  $A \rightleftharpoons B+C$  is considered and linear adsorption isotherms are assumed. An inert carrier (solvent), present in excess is

transporting the three components through the column. The amount of solute adsorbed depends on temperature as described by a van't Hoff type relation using the enthalpy of adsorption. In the case of a linear adsorption isotherms, the phase equilibrium relations for components can be written as

$$q_i^* = a_i c_i, \quad i = 1, 2, 3, \quad (6.9a)$$

$$\text{with } a_i = a_i^{\text{ref}} \exp\left(\frac{-\Delta H_{A,i}}{R} \left(\frac{1}{T} - \frac{1}{T^{\text{ref}}}\right)\right), \quad i = 1, 2, 3. \quad (6.9b)$$

To describe the reaction rate the standard expression for a reversible reaction is applied using the solid phase concentrations to define the driving force

$$r = k_{\text{for}}(T) \left( q_A^* - \frac{q_B^* q_C^*}{K_{\text{eq}}^*(T)} \right). \quad (6.10a)$$

The effect of temperature on the chemical reaction rate  $k_{\text{for}}(T)$  is an exponential function of the absolute temperature as described by the Arrhenius equation using the activation energy  $E_A$

$$k_{\text{for}}(T) = k_{\text{for}}(T^{\text{ref}}) \exp\left(\frac{-E_A}{R} \left(\frac{1}{T} - \frac{1}{T^{\text{ref}}}\right)\right). \quad (6.10b)$$

Chemical equilibrium constants  $K_{\text{eq}}^*(T)$  depend on the temperature as given below

$$\frac{d \ln K_{\text{eq}}^*}{dT} = \frac{\Delta H_R}{RT^2}. \quad (6.11a)$$

After integrating the above equation from  $T^{\text{ref}}$  to  $T$ , we obtain another von't Hoff expression

$$K_{\text{eq}}^*(T) = K_{\text{eq}}^*(T^{\text{ref}}) \exp\left(\frac{-\Delta H_R}{R} \left(\frac{1}{T} - \frac{1}{T^{\text{ref}}}\right)\right). \quad (6.11b)$$

This completes the derivation of the model for the non-isothermal chromatographic reactor. In the next section the flux-limiting finite volume scheme used to solve the model equations is presented.

## 6.2 Formulation of numerical scheme

In this section, the high resolution scheme of Koren [39] is described with respect to this particular problem. It should be noted that  $N_c = 4$  refers to three species A, B and C and

the fourth pseudo-component which captures the specifics of the energy equation, cf., Eq. (6.5b). The Eq. (6.6) can be re-written as

$$\mathbf{J} \frac{\partial \mathbf{c}}{\partial \tau} + u \frac{\partial \mathbf{c}}{\partial x} = \mathbf{P} \frac{\partial^2 \mathbf{c}}{\partial x^2} + \mathbf{Q}, \quad (6.12a)$$

where,  $\mathbf{J}$ ,  $\mathbf{c}$ ,  $\mathbf{P}$  and  $\mathbf{Q}$  are given as

$$\mathbf{J} = \begin{pmatrix} 1 + F \frac{\partial q_1^*}{\partial c_1} & F \frac{\partial q_1^*}{\partial c_2} & F \frac{\partial q_1^*}{\partial c_3} & F \frac{\partial q_1^*}{\partial c_4} \\ F \frac{\partial q_2^*}{\partial c_1} & 1 + F \frac{\partial q_2^*}{\partial c_2} & F \frac{\partial q_2^*}{\partial c_3} & F \frac{\partial q_2^*}{\partial c_4} \\ F \frac{\partial q_3^*}{\partial c_1} & F \frac{\partial q_3^*}{\partial c_2} & 1 + F \frac{\partial q_3^*}{\partial c_3} & F \frac{\partial q_3^*}{\partial c_4} \\ F \frac{\partial q_4^*}{\partial c_1} & F \frac{\partial q_4^*}{\partial c_2} & F \frac{\partial q_4^*}{\partial c_3} & 1 + F \frac{\partial q_4^*}{\partial c_4} \end{pmatrix}, \quad \mathbf{c} = \begin{pmatrix} c_1 \\ c_2 \\ c_3 \\ c_4 \end{pmatrix}, \quad (6.12b)$$

$$\mathbf{P} = \begin{pmatrix} \frac{1}{Pe_M} & 0 & 0 & 0 \\ 0 & \frac{1}{Pe_M} & 0 & 0 \\ 0 & 0 & \frac{1}{Pe_M} & 0 \\ 0 & 0 & 0 & \frac{1}{Pe_E} \end{pmatrix}, \quad \mathbf{Q} = Fr \begin{pmatrix} \frac{Lv_1}{u} \\ \frac{Lv_2}{u} \\ \frac{Lv_3}{u} \\ \frac{Lv_4}{u} \end{pmatrix}. \quad (6.12c)$$

Before applying the proposed numerical scheme to Eq. (6.12), it is required to discretize the computational domain. Let  $N$  represents the number of discretization points and the points  $(x_{j-\frac{1}{2}}), j \in \{1, \dots, N+1\}$  be partitions of the interval  $[0, 1]$ . For each  $j = 1, 2, \dots, N$ ,  $\Delta x$  is a constant width of each mesh interval. The  $x_j$  denote the cell centers, and  $x_{j \pm \frac{1}{2}}$  refer to the cell boundaries. We assign

$$x_{1/2} = 0, \quad x_{N+1/2} = 1, \quad x_{j+1/2} = j \cdot \Delta x, \quad \text{for } j = 1, 2, \dots, N. \quad (6.13)$$

Moreover, we have

$$x_j = (x_{j-1/2} + x_{j+1/2})/2 \quad \text{and} \quad \Delta x = x_{j+1/2} - x_{j-1/2} = \frac{1}{N+1}. \quad (6.14)$$

Let  $\Omega_j := [x_{j-1/2}, x_{j+1/2}]$  for  $j \geq 1$ . The cell averaged initial data in each cell are given as

$$\mathbf{c}_j(0) = \frac{1}{\Delta x} \int_{\Omega_j} \mathbf{c}^{\text{init}}(x) dx, \quad \text{for } j = 1, 2, \dots, N. \quad (6.15)$$

By integrating Eq. (6.12a) over the interval  $\Omega_j = [x_{j-1/2}, x_{j+1/2}]$ , we obtain

$$\int_{\Omega_j} \mathbf{J} \frac{\partial \mathbf{c}}{\partial \tau} dx = -u \left( \mathbf{c}_{j+\frac{1}{2}} - \mathbf{c}_{j-\frac{1}{2}} \right) + \mathbf{P}_j \left[ \left( \frac{\partial \mathbf{c}}{\partial x} \right)_{j+1/2} - \left( \frac{\partial \mathbf{c}}{\partial x} \right)_{j-1/2} \right] + \int_{\Omega_j} \mathbf{Q} dx. \quad (6.16)$$

In each  $\Omega_j$ , the averaged values of the conservative variables  $\mathbf{c}(t)$  are given as

$$\mathbf{c}_j(t) = \frac{1}{\Delta x} \int_{\Omega_j} \mathbf{c}(t, x) dx. \quad (6.17)$$

In Eq. (6.17),  $\mathbf{c}_j$  are cell averaged vectors of concentration components, while in Eq. (6.16),  $\mathbf{c}_{j\pm\frac{1}{2}}$  are the vectors at the respective cell boundaries. Similarly, the cell-averaged value of source term  $\mathbf{Q}$  can be defined. Moreover, the Jacobian matrix  $\mathbf{J}$  is calculated at the cell centroid  $x_j$ . Therefore, by using Eq. (6.17) in Eq. (6.16), the following semi-discrete scheme is obtained, for each,  $j = 1, 2, \dots, N$ ,

$$\mathbf{J}_j \frac{d\mathbf{c}_j}{d\tau} = -u \left( \mathbf{c}_{j+\frac{1}{2}} - \mathbf{c}_{j-\frac{1}{2}} \right) + \mathbf{P}_j \left[ \left( \frac{\partial \mathbf{c}}{\partial x} \right)_{j+1/2} - \left( \frac{\partial \mathbf{c}}{\partial x} \right)_{j-1/2} \right] + \mathbf{Q}_j. \quad (6.18)$$

The differential terms of the diffusion part can be approximated as

$$\left( \frac{\partial \mathbf{c}}{\partial x} \right)_{j\pm\frac{1}{2}} = \pm \left( \frac{\mathbf{c}_{j\pm 1} - \mathbf{c}_j}{\Delta x} \right). \quad (6.19)$$

The next step is to approximate the values for the convective variables at the cell interfaces  $\mathbf{c}_{j\pm\frac{1}{2}}$ , in Eq. (6.18). Hereby, different approximations give different numerical schemes.

**First order scheme:** In this case, the fluxes are approximated as

$$\mathbf{c}_{j+\frac{1}{2}} = \mathbf{c}_j, \quad \mathbf{c}_{j-\frac{1}{2}} = \mathbf{c}_{j-1}. \quad (6.20)$$

This approximation gives a first order accurate scheme in the axial-direction.

**High resolution schemes:** To achieve higher order accuracy, a piecewise interpolation polynomial can be used, such as

$$\mathbf{c}_{j+\frac{1}{2}} = \mathbf{c}_j + \frac{1+\kappa}{4} (\mathbf{c}_{j+1} - \mathbf{c}_j) + \frac{1-\kappa}{4} (\mathbf{c}_j - \mathbf{c}_{j-1}), \quad \kappa \in [-1, 1]. \quad (6.21)$$

Similarly,  $\mathbf{c}_{j-\frac{1}{2}}$  can be written as

$$\mathbf{c}_{j-\frac{1}{2}} = \mathbf{c}_{j-1} + \frac{1+\kappa}{4} (\mathbf{c}_j - \mathbf{c}_{j-1}) + \frac{1-\kappa}{4} (\mathbf{c}_{j-1} - \mathbf{c}_{j-2}), \quad \kappa \in [-1, 1], \quad (6.22)$$

where the parameter  $\kappa$  is selected from the interval  $[-1, 1]$ . For  $\kappa = -1$ , one gets the second order accurate fully one-sided upwind scheme, and for  $\kappa = 1$ , the standard second order

accurate central scheme centered around  $\mathbf{c}_j$ . For all other values of  $\kappa \in (-1, 1)$ , a weighted blend is obtained between the central scheme and the fully one-sided upwind scheme.

**Koren scheme:** Here  $\kappa = \frac{1}{3}$  is chosen which is third order accurate when there is no flux-limiting. For this choice of  $\kappa$ , Eq. (6.21) becomes in componentwise form

$$(c_m)_{j+\frac{1}{2}} = (c_m)_j + \frac{1}{2} \left( \frac{1}{3} + \frac{2(c_m)_{j+1} - (c_m)_j}{3(c_m)_j - (c_m)_{j-1}} \right) ((c_m)_j - (c_m)_{j-1}), \quad m = 1, 2, 3, 4. \quad (6.23)$$

However such approximations of flux terms may give negative solutions due to oscillations in the regions of strong variations. To deal with such problems, the Sweby-type flux-limiter, e.g. in [88] is used and Eq. (6.23) takes the form

$$(c_m)_{j+\frac{1}{2}} = (c_m)_j + \frac{1}{2} \phi \left( (r_m)_{j+\frac{1}{2}} \right) ((c_m)_j - (c_m)_{j-1}). \quad (6.24)$$

where  $r_{j+\frac{1}{2}}$  is the ratio of consecutive flux gradients

$$(r_m)_{j+\frac{1}{2}} = \frac{(c_m)_{j+1} - (c_m)_j + \eta}{(c_m)_j - (c_m)_{j-1} + \eta}. \quad (6.25)$$

Here  $\eta \approx 10^{-10}$  is used to avoid division by zero and the limiting function  $\phi$  is given as

$$\phi((r_m)_{j+\frac{1}{2}}) = \max \left( 0, \min \left( 2(r_m)_{j+\frac{1}{2}}, \min \left( \frac{1}{3} + \frac{2}{3}(r_m)_{j+\frac{1}{2}}, 2 \right) \right) \right). \quad (6.26)$$

Due to flux-limiting, the above scheme is a second to third order accurate [34, 39].

The approximations (6.23) and (6.24) are not applicable to the boundary intervals. Let us specifically consider the left boundary related to the inflow boundary condition. The position of the interval face  $x_{\frac{1}{2}}$  and inflow boundary are identical. However,  $x_0$  is not known, therefore Eqs. (6.23) and (6.24) are not applicable at  $x_{\frac{3}{2}}$ . To overcome this problem, the first order approximation (6.20) can be used at the cell interfaces  $x_{\frac{3}{2}}$  and  $x_{N+\frac{1}{2}}$ . Let  $(c_m)^{\text{in}}$  represent the concentrations of  $m$ -th injected pulse, then

$$(c_m)_{\frac{1}{2}} = (c_m)^{\text{in}}, \quad (c_m)_{\frac{3}{2}} = (c_m)_1, \quad (c_m)_{N+\frac{1}{2}} = (c_m)_N, \quad m = 1, 2, 3, 4. \quad (6.27)$$

The above equation shows that outflow boundary conditions are used at the outlet of the column. The fluxes at other cell interfaces can be computed using Eqs. (6.23) and (6.24). However, the use of a first order scheme in the boundary intervals does not affect the

global accuracy of the method due to shrinking cell sizes with increasing node numbers. The efficiency and accuracy of the scheme were thoroughly analyzed in the previous chapter on isothermal dispersive liquid chromatography.

The above described semi-discrete scheme was programmed in Matlab 7.9.1 software and the resulting ODE-system was solved by using the built-in Matlab routine ode15s.

## 6.3 Consistency tests for validation

Currently, not many experimental results are available to quantify non-isothermal reactive chromatographic processes. Thus, integral consistency tests for mass and energy balance equations are useful tools to validate numerical results and also the correctness of the model formulation. Based on such tests, the accuracy of the numerical scheme and the conservativity of mass and energy balances were evaluated for the considered reversible chemical reaction  $A \rightleftharpoons B+C$ .

### 6.3.1 Identity of integrated extents of reaction

In a chemical reaction, the changes in mole numbers of the components  $n_i$  are connected by the stoichiometry of the reaction. For the considered reversible chemical reaction  $A \rightleftharpoons B+C$ , the integrated extent of reaction  $\xi$  should be independent on component and should follow the subsequent equation

$$\xi = n_A^{\text{in}} - n_A^{\text{out}} = n_B^{\text{out}} = n_C^{\text{out}}. \quad (6.28)$$

The single variable  $\xi$  describes all the changes in the mole numbers due to the chemical reaction and  $n_i^{\text{in}} = c_i^{\text{in}}V^{\text{in}}$  represents injected moles into the column. In this study, the inlet concentrations of the products i.e.,  $c_B^{\text{in}}$  and  $c_C^{\text{in}}$  were taken to be zero. The symbol  $V^{\text{in}}$  denotes the volume injected at the column inlet during the injection time  $t^{\text{in}}$ .

After solving the PDEs the mole numbers can be calculated at the outlet using the following equation

$$n_i^{\text{out}} = \dot{V} \int_0^{t^*} c_i(t, x = L) dt, \quad i = A, B, C, \quad (6.29)$$

where  $\dot{V}$  represents the volumetric flow rate related to  $u$ . The above integrals were evaluated for each component using the trapezoidal rule. The integration of the PDEs solution should be carried sufficiently long to return to the initial state (time  $t^*$ ).

A standard deviation is calculated for the three values of  $\xi_i$  as

$$\sigma_{\xi,i}[\%] = 100 \times \sqrt{\frac{\sum_{i=1}^{N_c} (\xi_i - \bar{\xi})^2}{3}}, \quad i = A, B, C. \quad (6.30)$$

Here  $\bar{\xi}$  is the average of  $\xi_A$ ,  $\xi_B$ ,  $\xi_C$ . This standard deviation should tend to zero if the mass balances respect stoichiometry.

### 6.3.2 Integrated energy balance considering the extent of reaction

An energetic evaluation of the process can be made by comparing the enthalpies entering,  $\Delta H^{\text{in}}$ , and leaving,  $\Delta H^{\text{out}}$ , the system. These enthalpies are

$$\Delta H^{\text{in}} = \rho^L c_p^L \dot{V} \int_0^{t^*} (T^{\text{in}} - T^{\text{ref}}) dt, \quad \Delta H^{\text{out}} = \rho^L c_p^L \dot{V} \int_0^{t^*} (T(t, x = L) - T^{\text{ref}}) dt. \quad (6.31)$$

For  $T^{\text{in}} = T^{\text{ref}}$  holds  $\Delta H^{\text{in}} = 0$ . In case of a complete adsorption and desorption cycle ( $t^*$  sufficiently long), there will be no overall sorption effect and the following balance equation can be derived using exclusively the effect of reaction quantified by  $\Delta H_{\text{R}}$  and  $\xi$ , e.g. Eq. (6.30)

$$\Delta H^{\text{out}} + (\Delta H_{\text{R}}) \bar{\xi} = 0. \quad (6.32)$$

The fulfillment of Eq. (6.32) is required as a proof of accurate numerical simulations. There are several sources of numerical errors, such as discretization errors, round off errors, and errors in the numerical integrations of the outlet profiles, etc. Due to these errors, the right hand side of Eq. (6.32), called here  $\Delta H_{\text{err}}$ , might not be exactly zero

$$\Delta H_{\text{err}} = \Delta H^{\text{out}} + (\Delta H_{\text{R}}) \bar{\xi}. \quad (6.33)$$

The smaller the  $\Delta H_{\text{err}}$  the better is the fulfillment of the joint integral mass and energy balances. One can expect larger errors in  $\Delta H_{\text{err}}$  compared to errors in  $\xi$  due to the accumulation of all possible errors in this more critical consistency check. A relative percentage



error in this energy can be given as

$$E_H[\%] = 100 \times \left| \frac{\Delta H_{\text{err}}}{\Delta H_{R\xi}} \right|. \quad (6.34)$$

## 6.4 Demonstrations of thermal effects

The purpose of this section is to evaluate effects of parameters that influence conversion and separation in non-isothermal reactive liquid chromatography. Numerical test problems will explain the coupling between the concentration and thermal fronts in the reactor. We consider, the reversible reaction  $A \rightleftharpoons B+C$ , and linear isotherm with Henry constants  $a_A^{\text{ref}} = 1.0$ ,  $a_B^{\text{ref}} = 0.7$  and  $a_C^{\text{ref}} = 1.3$  at reference temperature  $T^{\text{ref}} = 300 \text{ K}$ . This means that the feed component A elutes between the two products B and C. Moreover, a reaction rate constant  $k_{\text{for}}(T^{\text{ref}}) = 10^{-4} \text{ 1/s}$ , a reaction equilibrium constant  $K_{\text{eq}}^* = 2 \text{ mol/l}$ , an activation energy  $E_A = 60 \text{ kJ/mol}$  and density times heat capacities for liquid and solid phases  $\rho^L C_p^L = \rho^S C_p^S = 4.0 \text{ kJ/lK}$  are used for numerical simulations. Further, the column length is  $L = 27 \text{ cm}$ , the interstitial velocity is  $u = 0.6240 \text{ cm/min}$ , the volumetric flow rate is  $\dot{V} = 0.4980 \text{ cm}^3/\text{min}$ . The phase ratio  $F = 1.5$  corresponds to the external porosity  $\epsilon = 0.4$ . A pulse of height  $c_A^{\text{in}} = 3 \text{ mol/l}$  is injected into the column initially equilibrated with the solvent, i.e.  $c_i^{\text{init}} = 0$  for an injection time  $t^{\text{in}}$  of  $16.68 \text{ min}$  corresponding to a dimensionless injection time  $\tau^{\text{in}}$  of  $0.385$ . In most of the cases, based on preliminary calculations a final simulation time  $174 \text{ min}$  is taken into account to assure complete regeneration. In all test problems, the dimensionless model, Eq. (6.6), is used and the Koren scheme mostly with 400 mesh cells in axial direction is employed for numerical simulations. The values for the reaction enthalpy and the adsorption enthalpies were varied in typical ranges, i.e.  $\Delta H_R = [-50, 50] \text{ kJ/mol}$ , and  $\Delta H_{A,i} = [-20, 0] \text{ kJ/mol}$ .

### 6.4.1 Trivial limiting cases

At first, some trivial limiting studies are considered for validation.

**Case 1:** There is no reaction,  $k_{\text{for}} = 0$ , and enthalpies of adsorption are negligible,  $\Delta H_{A,i} = 0$ , in the model Eq. (6.6). Moreover, dispersion effects are ignored by considering both

Peclet numbers of mass  $Pe_M$  and energy  $Pe_E$  approach to  $\infty$ . As a result, reactants would be not able to convert into the products. The reactant is only transported through the column and the product components B and C are not formed. The correctly obtained solution for this particular case is shown in Figure 6.1.

If the enthalpy of reaction is taken to be zero, i.e.,  $\Delta H_R = 0$ , then  $\Delta H^{\text{out}} = 0$ , and no temperature change can occur as depicted in Figure 6.1 (right).

### Case 2: Adiabatic temperature rise

This part evaluates the adiabatic temperature rise. The reactant A is continuously fed with three different injection concentrations  $c_A^{\text{in}} = 3 \text{ mol/l}$ ,  $c_A^{\text{in}} = 6 \text{ mol/l}$  and  $c_A^{\text{in}} = 12 \text{ mol/l}$  for sufficiently long injection and residence times along with a set of parameters namely,  $\Delta H_{A,i} = 0$ ,  $\Delta H_R = -10 \text{ kJ/mol}$ , and  $Pe_M$  and  $Pe_E$  approach to  $\infty$ . The formula describing the adiabatic temperature rise based on Eqs. (6.1) and (6.2) is

$$\Delta T_{\text{adabatic}} = \frac{-\Delta H_R c_A^{\text{in}}}{\rho^L c_p^L}. \quad (6.35)$$

For the considered injection concentrations, this formula give the values of  $\Delta T_{\text{adabatic}}$  as 7.5 K, 15 K and 30 K, respectively. The corresponding temperature profiles together with selected concentration profiles are shown in Figure 6.2. The figure verifies, that after complete conversion of the reactant, the predicted temperature profiles indeed attain the steady maxima and the values of  $\Delta T_{\text{adabatic}}$  in the figure agree with those obtained from Eq. (6.35). The slight overshoots in Figure 6.2 are produced by the numerical scheme which have no physical reason. This completes the discussion of trivial cases.

## 6.4.2 Non-trivial test problems

### Problem 1: Isothermal case:

The purpose of this first study is to analyze the isothermal behavior as well as to quantitatively investigate the errors of extent of reaction  $\xi$  and conversion. To simulate the isothermal case, the enthalpies of adsorption,  $\Delta H_{A,i}$ , and the enthalpy of reaction,  $\Delta H_R$ , are set equal to zero. Additionally, dispersion effects are neglected by considering both  $Pe_M$  and  $Pe_E$  approaching  $\infty$ . In order to analyze the effect of the adsorption isotherms,

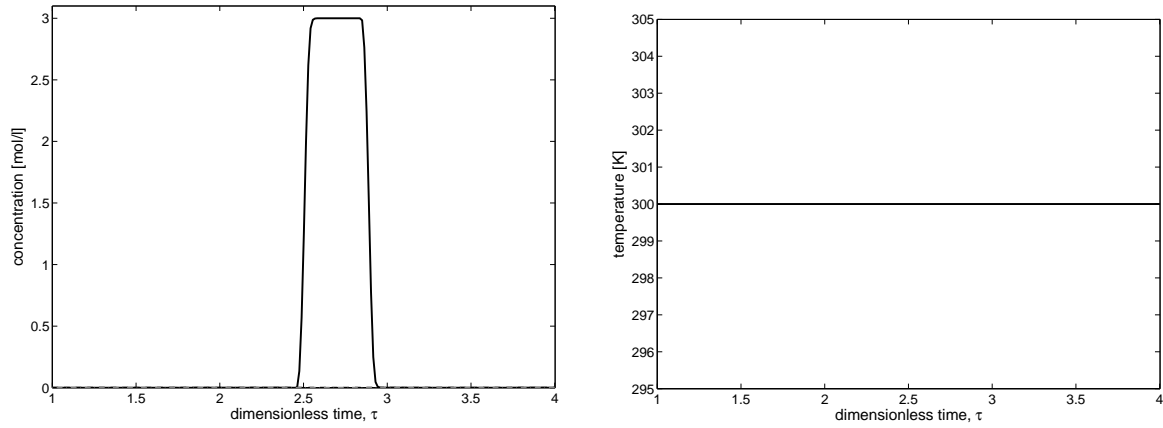


Figure 6.1: Trivial limiting cases: case 1:  $\Delta H_{A,i} = 0$  for  $i=A,B,C$ ,  $k_{\text{for}}(T^{\text{ref}}) = 0$ .

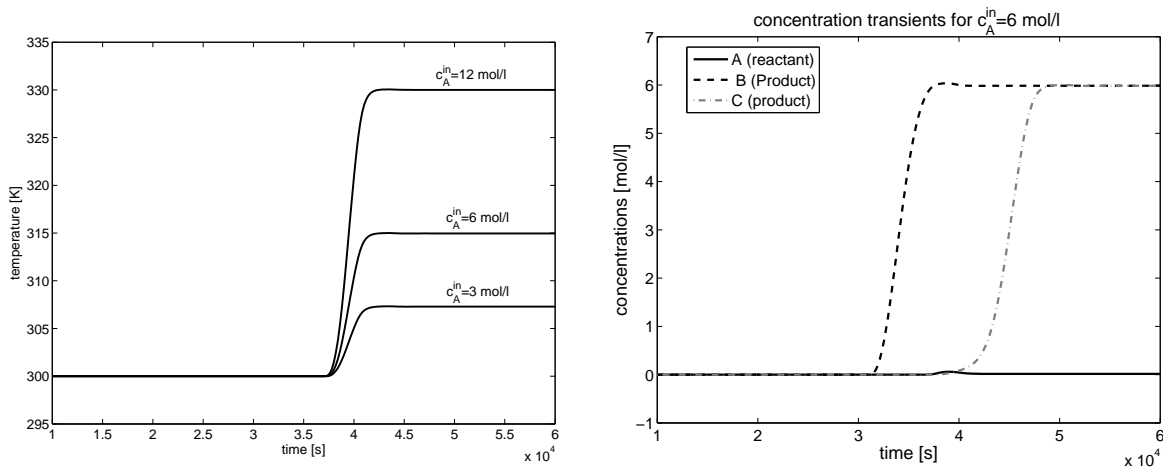


Figure 6.2: Trivial limiting cases: case 2:  $\Delta H_{A,i} = 0$  for  $i=A,B,C$ ,  $\Delta H_R = -10 \text{ kJ/mol}$ ,  $L = 1.62 \text{ m}$ ,  $k_{\text{for}}(T^{\text{ref}}) = 10^{-4} \text{ s}^{-1}$ , left: temperature transients at the column outlet for three inlet concentrations, right: the corresponding concentration transients for  $c_A^{\text{in}} = 6 \text{ mol/l}$ .

Table 6.1: Problem 1: Isothermal case. Here  $X_A[\%] = 100 \times \frac{n_A^{\text{in}} - n_A^{\text{out}}}{n_A^{\text{in}}}$ .

parameters	$\xi_A$	$\xi_B$	$\xi_C$	$\sigma_{\xi,i}$	$X_A$	$\Delta H^{\text{out}}$
	[mol]	[mol]	[mol]	[%]	[%]	[kJ]
$a_i = 0$	-0.0001	$-5.7e^{-27}$	$-1.0675e^{-10}$	$\approx 0$	-0.0040	0
$a_i^{\text{ref}} \neq 0$	0.0079	0.0080	0.0080	0.0058	31	0

at first the Henry constants  $a_i$  are put equal to zero for all components, i.e.  $a_A = 0$ ,  $a_B = 0$ , and  $a_C = 0$ . Due to Eq. (6.10a) the reaction rate would also be zero and the reactant A would not be converted into products and would be just transported along the column. This behavior can be seen in Figure 6.3 (top). Then we considered the reference Henry constants in Eq. (6.9) as  $a_A^{\text{ref}} = 1.0$ ,  $a_B^{\text{ref}} = 0.7$ , and  $a_C^{\text{ref}} = 1.3$ . The obtained concentration profiles on 400 mesh points are shown in the Figure 6.3 (middle). They reveal the appearance of components B and C. Furthermore, as expected there is no change in temperature. Table 6.1, shows the parameters required for the consistency tests described in the previous section. As required the extents of reactions are independent of the components. The results for the reference Henry constants reveal significant but incomplete conversion and separation.

Figure 6.3 (bottom) shows the comparison of results at different mesh points for isothermal case study, while keeping the other parameters unchanged. The results obtained by considering 400 and 1000 mesh points are almost same, while the resolution of 100 mesh points is diffusive. For that reason, 400 mesh points are chosen in the numerical simulations of this chapter to achieve acceptable accuracy.

### Problem 2: Influence of the enthalpy of reaction

This part evaluates the role of the heat of reaction that can be released or consumed when the chemical reaction takes place. Firstly, an exothermal reaction,  $\Delta H_R = -10 \text{ kJ/mol}$ , together with zero adsorption enthalpies,  $\Delta H_{A,i} = 0$ , are taken into account. It was further assumed that both Peclet numbers,  $Pe_M$  and  $Pe_E$  are approaching to  $\infty$ . The numerical results using 400 grid cells are shown in Figure 6.4 (top). The results depict the expected rise in the temperature profile, that improved the conversion slightly to 32 % compared

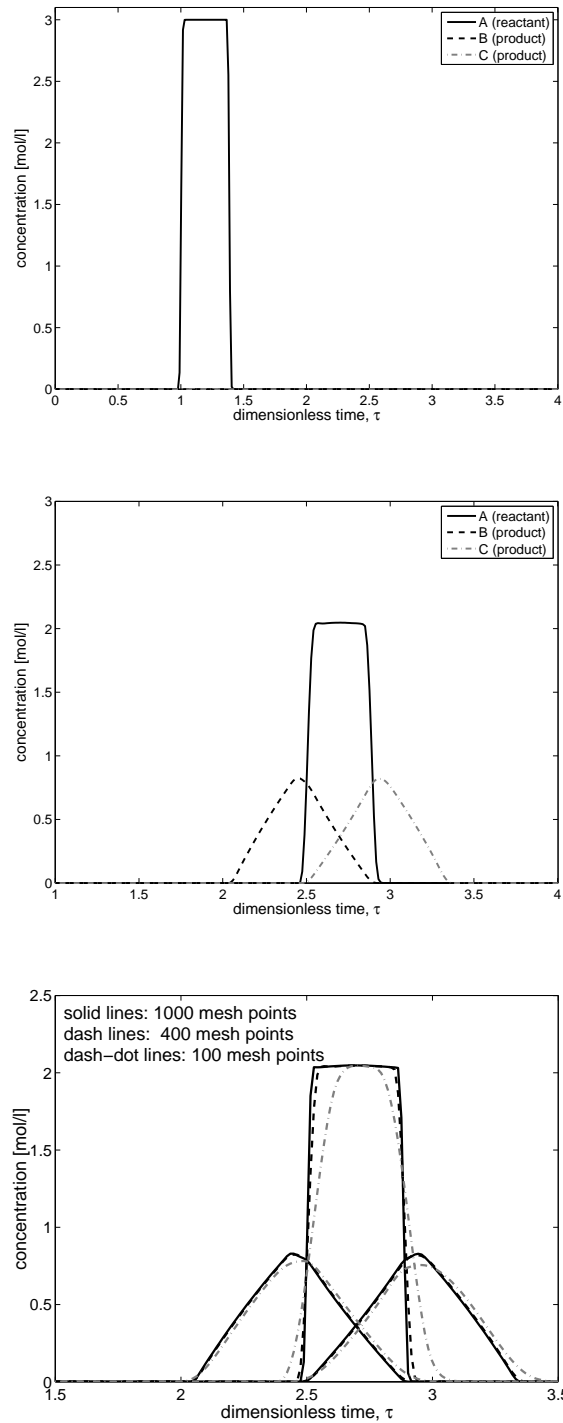


Figure 6.3: Problem 1: Isothermal case,  $\Delta H_{A,i} = 0$ ,  $\Delta H_R = 0$ , Henry constants top:  $a_i = 0$ , for  $i=A,B,C$ , middle:  $a_A^{\text{ref}} = 1.0$ ,  $a_B^{\text{ref}} = 0.7$ ,  $a_C^{\text{ref}} = 1.3$ , bottom: comparison of different mesh points.

Table 6.2: Problem 2:  $\Delta H_{A,i} = 0$ ,  $E_A = 60 \text{ kJ/mol}$ . Here  $X_A[\%] = 100 \times \frac{n_A^{\text{in}} - n_A^{\text{out}}}{n_A^{\text{in}}}$ .

parameters	$\xi_A$	$\xi_B$	$\xi_C$	$\sigma_{\xi,i}$	$X_A$	$\Delta H^{\text{out}}$	$\Delta H_{\text{err}}$	$E_H$
[kJ/mol]	[mol]	[mol]	[mol]	[%]	[%]	[kJ]	[kJ]	[%]
$\Delta H_R = -10$	0.0079	0.0080	0.0080	0.0058	32	0.0801	0.0004	0.49
$\Delta H_R = -40$	0.0119	0.0120	0.0120	0.0058	48	0.4790	0.0015	0.32
$\Delta H_R = +10$	0.0073	0.0074	0.0074	0.0058	29	-0.074	-0.0004	0.53

to the isothermal study 31 %, see Tables 6.1 and 6.2. For a larger enthalpy of reaction,  $\Delta H_R = -40 \text{ kJ/mol}$ , the simulated results are shown in Figure 6.4 (middle). Due to larger rise of the temperature profile, conversion of component A further increases to 48 % and more products B and C can be collected as shown in Figure 6.4 (middle). This trend can be seen also in Table 6.2. It is straightforward to conclude that increase in magnitude of the heat of reaction leads to the significant thermal effects. The rise in temperature also starts to influence the absorptivity of the components, but this is hard to see in Figure 6.4 (middle).

To analyze the influence of an endothermic reaction, the enthalpy of reaction  $\Delta H_R = 10 \text{ kJ/mol}$  is considered, while keeping other parameters unchanged. The simulated results are shown in Figure 6.4 (bottom). The corresponding quantitative results can be found in Table 6.2. The endothermic reaction absorbs heat causing a decline in temperature and reduction of conversion to 29 %. These calculations allowed to evaluate the consistency test describes in Section 6.3. The joint error of the integral mass and energy balances, expressed by the error  $E_H$  (Eq. (6.34)), is less than 1 %. This again demonstrates the high precision of the obtained numerical solutions.

### Problem 3: Influence of enthalpy of adsorption

This case study refers to the enthalpies of adsorption  $\Delta H_{A,i}$  for negligible enthalpies of reaction  $\Delta H_R$ . The chromatographic separation of the products is based on differences in adsorption strength, that depends on temperature through the enthalpies of adsorption,  $\Delta H_{A,i}$ . The adsorption equilibrium may change with temperature, depending on the relative magnitudes of the individual adsorption enthalpies. Note that, enthalpies of adsorption

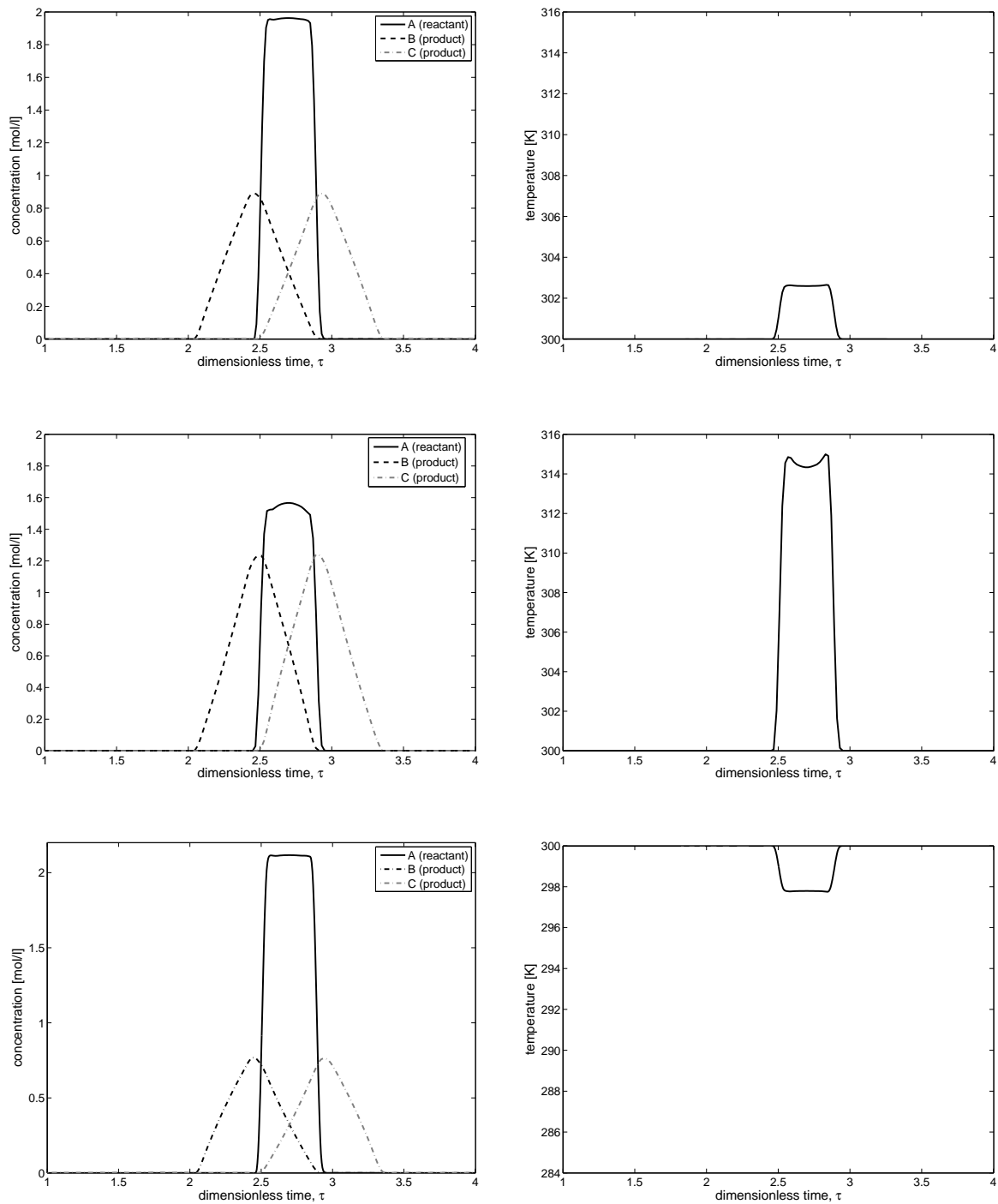


Figure 6.4: Problem 2: Influence of the enthalpy of reaction,  $\Delta H_{A,i} = 0$ , for  $i=A,B,C$ , top:  $\Delta H_R = -10 \text{ kJ/mol}$ , middle:  $\Delta H_R = -40 \text{ kJ/mol}$ , bottom:  $\Delta H_R = 10 \text{ kJ/mol}$ .

Table 6.3: Problem 3:  $\Delta H_R = 0$ . Here  $X_A[\%] = 100 \times \frac{n_A^{\text{in}} - n_A^{\text{out}}}{n_A^{\text{in}}}$ .

parameters	$\xi_A$	$\xi_B$	$\xi_C$	$\sigma_{\xi,i}$	$X_A$	$\Delta H^{\text{out}}$
[kJ/mol]	[mol]	[mol]	[mol]	[%]	[%]	[kJ]
$\Delta H_{A,i} = -20$	0.0098	0.0099	0.0099	0.0058	39	-0.0011
$\Delta H_{A,i} = -40$	0.0091	0.0092	0.0093	0.0082	37	-0.0015
$\Delta H_{A,i} = -60$	0.0079	0.0081	0.0079	0.0058	31	0.0011

are generally negative. We considered,  $\Delta H_{A,i} = -20 \text{ kJ/mol}$  for all components A, B and C,  $\Delta H_R = 0$  and, both  $Pe_M$  and  $Pe_E$  approach to  $\infty$ . The corresponding results are presented in Figure 6.5 (top). The behavior of concentration and temperature profiles are totally different from the isothermal and the other previously considered cases. The figures show the direct coupling of thermal and concentration waves and cause self-sharpening fronts although the adsorption isotherms are linear with respect to concentrations. It is worthwhile to mention that the adsorption and desorption “peaks” of temperature are identical in size because the enthalpy of reaction is zero. In order to extend the investigation of the effect of adsorption enthalpies, we considered also rather larger values of  $\Delta H_{A,i} = -40 \text{ kJ/mol}$  and  $\Delta H_{A,i} = -60 \text{ kJ/mol}$ , again with  $\Delta H_R = 0$ . The corresponding simulation results can be seen in Figure 6.5 (middle) and (bottom), respectively. The increase in the magnitude of  $\Delta H_{A,i}$ , strongly effects the adsorptivity of the components. The change in adsorptivity causes the differences in the retention times of the components that lead to significant reductions in conversion and separation, see Figure 6.5 and Table 6.3. The quantitative data presented in Table 6.3 demonstrate one more time the precision of the numerical calculations.

#### Problem 4a: Influence of both enthalpies of reaction and adsorption

For the complete description of the non-isothermal chromatographic processes, the effects of both enthalpies of adsorption and reaction are evaluated. For all three components, enthalpies of adsorption  $\Delta H_{A,i} = -20 \text{ kJ/mol}$  and the enthalpy of reaction  $\Delta H_R = -10 \text{ kJ/mol}$  are considered. Furthermore, it is assumed again that the Peclet numbers  $Pe_M$  and  $Pe_E$  both approach to  $\infty$ . The numerical calculations were made again



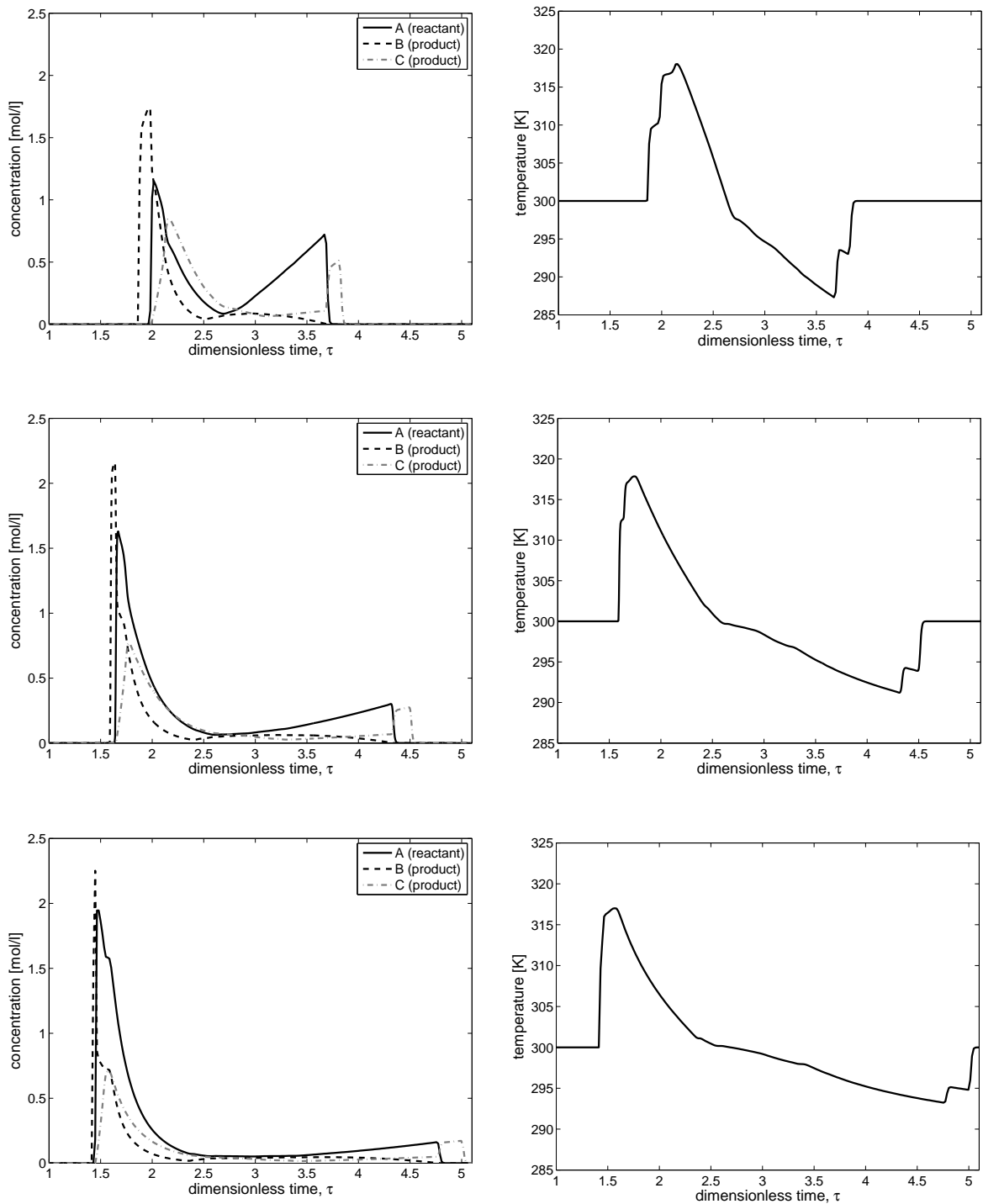


Figure 6.5: Problem 3: Influence of enthalpies of adsorption,  $\Delta H_R = 0$ , top:  $\Delta H_{A,i} = -20 \text{ kJ/mol}$ , middle:  $\Delta H_{A,i} = -40 \text{ kJ/mol}$ , bottom:  $\Delta H_{A,i} = -60 \text{ kJ/mol}$ ,  $i=A,B,C$ .

using 400 mesh points. The results are shown in Figure 6.6 (top). As an exothermic reaction is taken into account, in total heat is released. Consequently, conversion is improved as expected. Figure 6.6 (top), shows very different concentration profiles compared to the isothermal study (Figure 6.3 middle). The temperature profile in Figure 6.6 (top) has similar temperature excursions as observed in Figure 2 of [78]. Then we considered an endothermic reaction,  $\Delta H_R = 10 \text{ kJ/mol}$ , while keeping other parameters unchanged. The results can be seen in Figure 6.6 (bottom). Visibly, the concentration and thermal wave follow the same trends, but the conversion of reactant  $A$  is less for the endothermic reaction. Corresponding simulated results for an exothermic reaction with  $\Delta H_R = -50 \text{ kJ/mol}$  are presented in Figure 6.7 (top). The figure depicts again the typical non-linear behavior both in concentration and temperature profiles. The increase in magnitude of the exothermic reaction, leads to increase in maximum temperature. Thus, the forward reaction is enhanced and the reactant is further converted. The results for an endothermic reaction with  $\Delta H_R = 50 \text{ kJ/mol}$  are shown in Figure 6.7 (middle). An immense difference can be seen in the shape of the product peaks in comparison to the corresponding exothermic reaction of the same magnitude, see Figure 6.7.

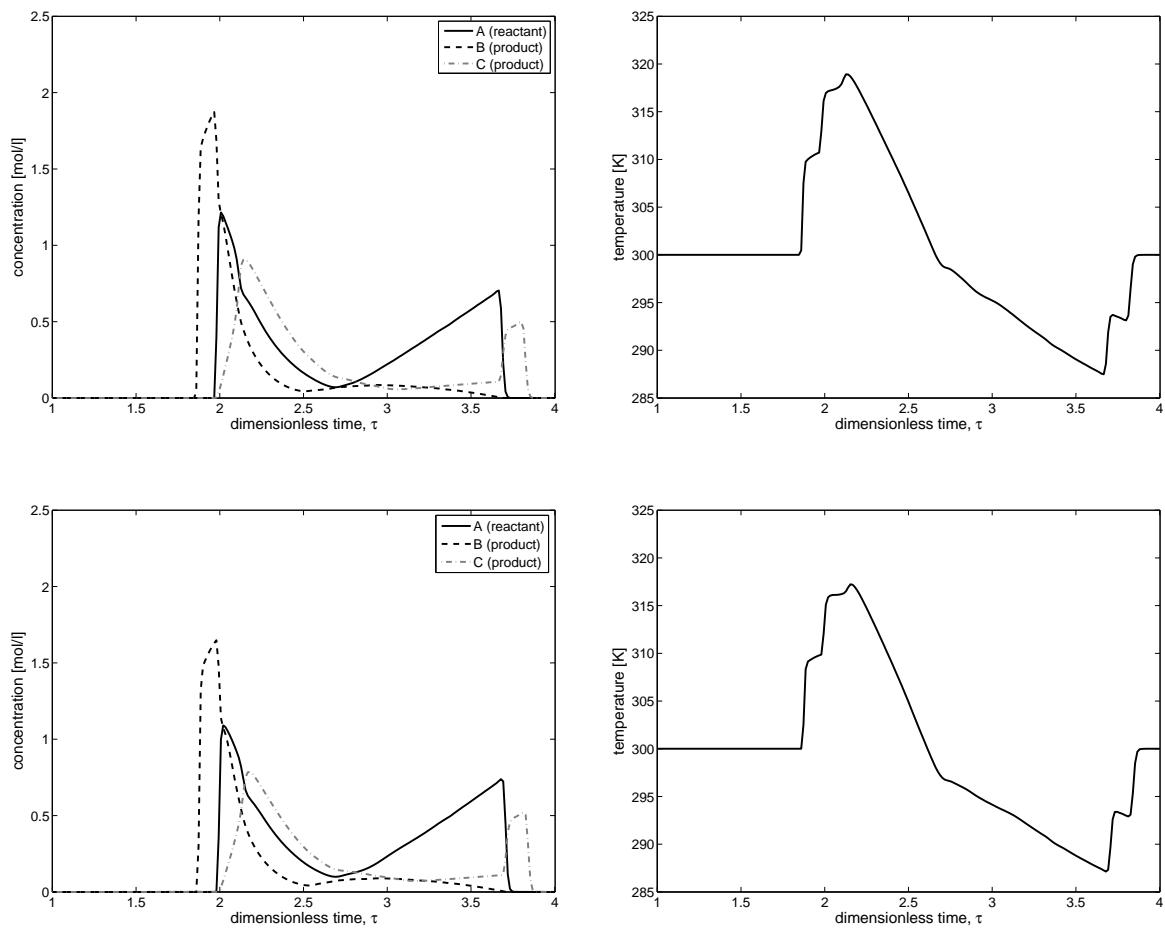
Another important parameter that can influence the performance of the chromatographic reactor is the activation energy,  $E_A$ . Above exclusively the reference value  $E_A = 60 \text{ kJ/mol}$  was applied. For illustration, we changed this reference value to  $E_A = 100 \text{ kJ/mol}$  with  $\Delta H_R = -10 \text{ kJ/mol}$  and plotted the eluted concentration profiles in Figure 6.7 (bottom) to compare with the results in Figure 6.6 (top). The simulated results show that more reactant is converted into products for the higher value of the activation energy and a higher maximum temperature is reached. The larger value of activation energy leads to a more pronounced enhancement of the reaction rate due to an increase of the temperature. The corresponding quantitative values in Table 6.4 elucidating the discussion above.

#### **Problem 4b: Influence of enthalpy of adsorption (componentwise)**

In above test problems, the same values of enthalpy of adsorption  $\Delta H_{A,i}$  were used for all components. In practice, the enthalpy of adsorption can vary with respect to the components. The following cases are investigated to analyze the impact of specific enthalpies of

Table 6.4: Problem 4a:  $\Delta H_{A,i} = -20 \text{ kJ/mol}$ . Here  $X_A[\%] = 100 \times \frac{n_A^{\text{in}} - n_A^{\text{out}}}{n_A^{\text{in}}}$ .

parameters	$\xi_A$	$\xi_B$	$\xi_C$	$\sigma_{\xi,i}$	$X_A$	$\Delta H^{\text{out}}$	$\Delta H_{\text{err}}$	$E_H$
[kJ/mol]	[mol]	[mol]	[mol]	[%]	[%]	[kJ]	[kJ]	[%]
$\Delta H_R = -10, E_A = 60$	0.0101	0.0102	0.0102	0.0058	40	0.1005	-0.0010	0.98
$\Delta H_R = +10, E_A = 60$	0.0096	0.0097	0.0097	0.0058	38	-0.0983	-0.0019	1.98
$\Delta H_R = -50, E_A = 60$	0.0112	0.0113	0.0113	0.0058	45	0.5643	6.51e-04	0.12
$\Delta H_R = +50, E_A = 60$	0.0086	0.0087	0.0088	0.0082	35	-0.4389	-0.0036	0.82
$\Delta H_R = -10, E_A = 100$	0.0124	0.0125	0.0125	0.0058	50	0.1234	-0.0010	0.80

Figure 6.6: Problem 4a: Influence of both enthalpies of reaction and adsorption,  $\Delta H_{A,i} = -20 \text{ kJ/mol}$ ,  $i=A,B,C$ , top:  $E_A = 60 \text{ kJ/mol}$ ,  $\Delta H_R = -10 \text{ kJ/mol}$ , bottom:  $E_A = 60 \text{ kJ/mol}$ ,  $\Delta H_R = +10 \text{ kJ/mol}$ .

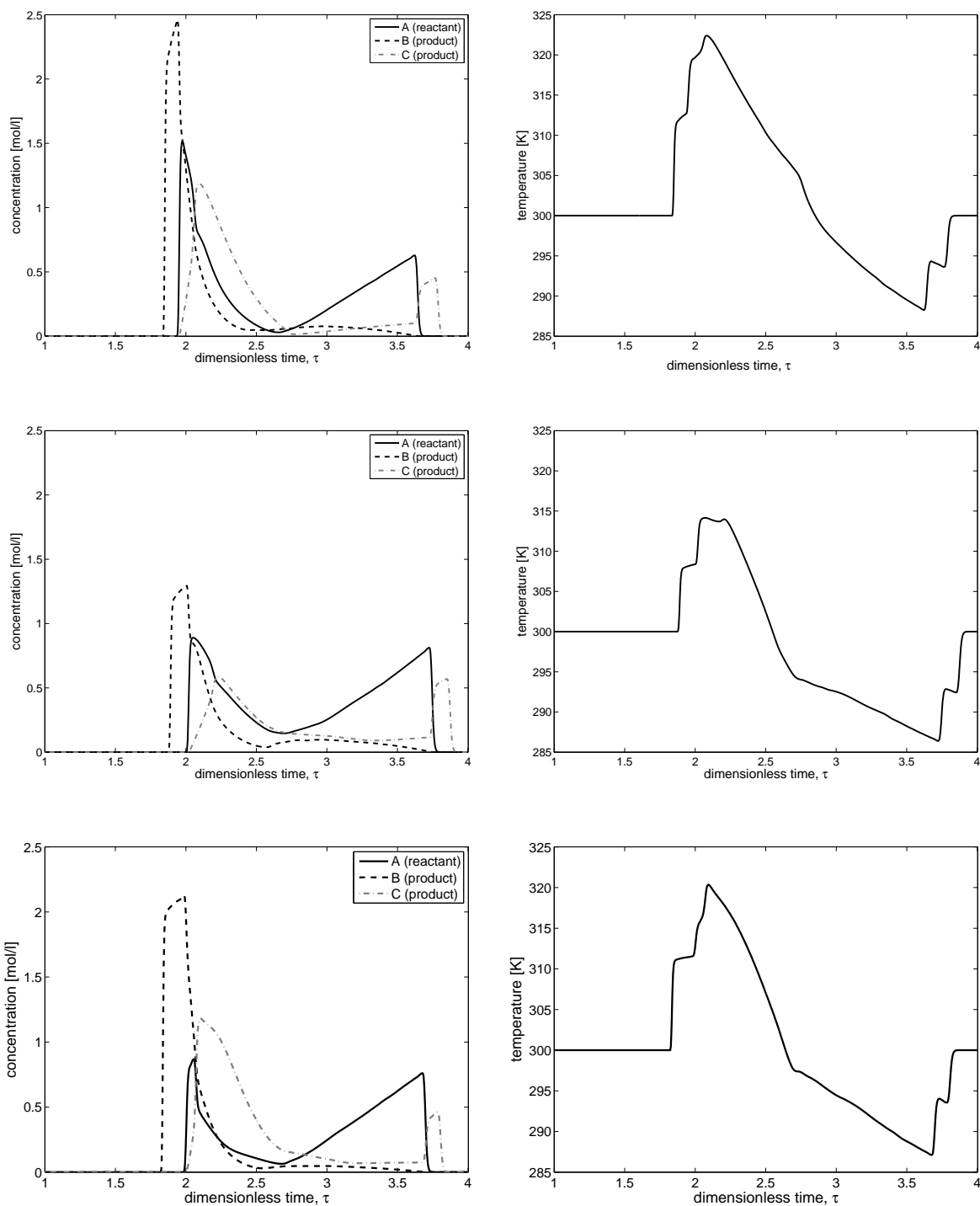


Figure 6.7: Problem 4a: Influence of both enthalpies of reaction and adsorption,  $\Delta H_{A,i} = -20 \text{ kJ/mol}$ ,  $i=A,B,C$ , top:  $E_A = 60 \text{ kJ/mol}$ ,  $\Delta H_R = -50 \text{ kJ/mol}$ , middle:  $E_A = 60 \text{ kJ/mol}$ ,  $\Delta H_R = +50 \text{ kJ/mol}$ , bottom:  $E_A = 100 \text{ kJ/mol}$ ,  $\Delta H_R = -10 \text{ kJ/mol}$ .

adsorption on the course of the effluent concentration and temperature profiles.

$$\text{case 1 : } \Delta H_{A,A} = 0, \Delta H_{A,B} = -20, \Delta H_{A,C} = -20, \quad (6.36a)$$

$$\text{case 2 : } \Delta H_{A,A} = -20, \Delta H_{A,B} = 0, \Delta H_{A,C} = -20, \quad (6.36b)$$

$$\text{case 3 : } \Delta H_{A,A} = -20, \Delta H_{A,B} = -20, \Delta H_{A,C} = 0, \quad (6.36c)$$

$$\text{case 4 : } \Delta H_{A,A} = -30, \Delta H_{A,B} = -20, \Delta H_{A,C} = -10. \quad (6.36d)$$

In all cases, the reaction enthalpies  $\Delta H_R = -10 \text{ kJ/mol}$  and the activation energy  $E_A = 60 \text{ kJ/mol}$  were considered. The results are shown in Figure 6.8 and are compared with the reference case where same value of  $\Delta H_{A,i} = 20 \text{ kJ/mol}$  was taken into account. The adsorption equilibrium constants are decreasing with increasing temperature, depending on the individual adsorption enthalpies. If  $\Delta H_{A,i} = 0$ , these equilibrium constant are not effected by temperature. The predicted profiles for all cases in Figure 6.8 together with Figure 6.6 (top), show the importance of knowing the correct adsorption enthalpies in order to predict properly concentration and temperature profiles.

#### **Problem 5: Influence of dispersion terms**

The last case refers to study the effects of dispersion terms in the model given by Eq. (6.6). For this, we took  $\Delta H_{A,i} = -20 \text{ kJ/mol}$  ( $i = A, B, C$ ),  $\Delta H_R = -10 \text{ kJ/mol}$ , and  $E_A = 60 \text{ kJ/mol}$ . We considered the following four cases for different values of Peclet numbers of  $Pe_M$  and  $Pe_E$  (c.f. Eq. (6.7))

$$\text{case 1 : } Pe_M = 10^4, Pe_E = 10^4, \quad (6.37a)$$

$$\text{case 2 : } Pe_M = 200, Pe_E = 0, \quad (6.37b)$$

$$\text{case 3 : } Pe_M = 0, Pe_E = 200, \quad (6.37c)$$

$$\text{case 4 : } Pe_M = 200, Pe_E = 200. \quad (6.37d)$$

For these particular scenarios, the corresponding results are shown in Figure 6.9. The larger the  $Pe_M$  numbers the steeper are the profiles. The difference between  $Pe_M = 10^4$  and  $Pe_E = 200$  are still almost negligible. A reduction of  $Pe_E$  appears to be faster causing band broadening compared to a reduction of  $Pe_M$ , but this effect can be hardly seen in Figure 6.9 for cases 2 and 3.

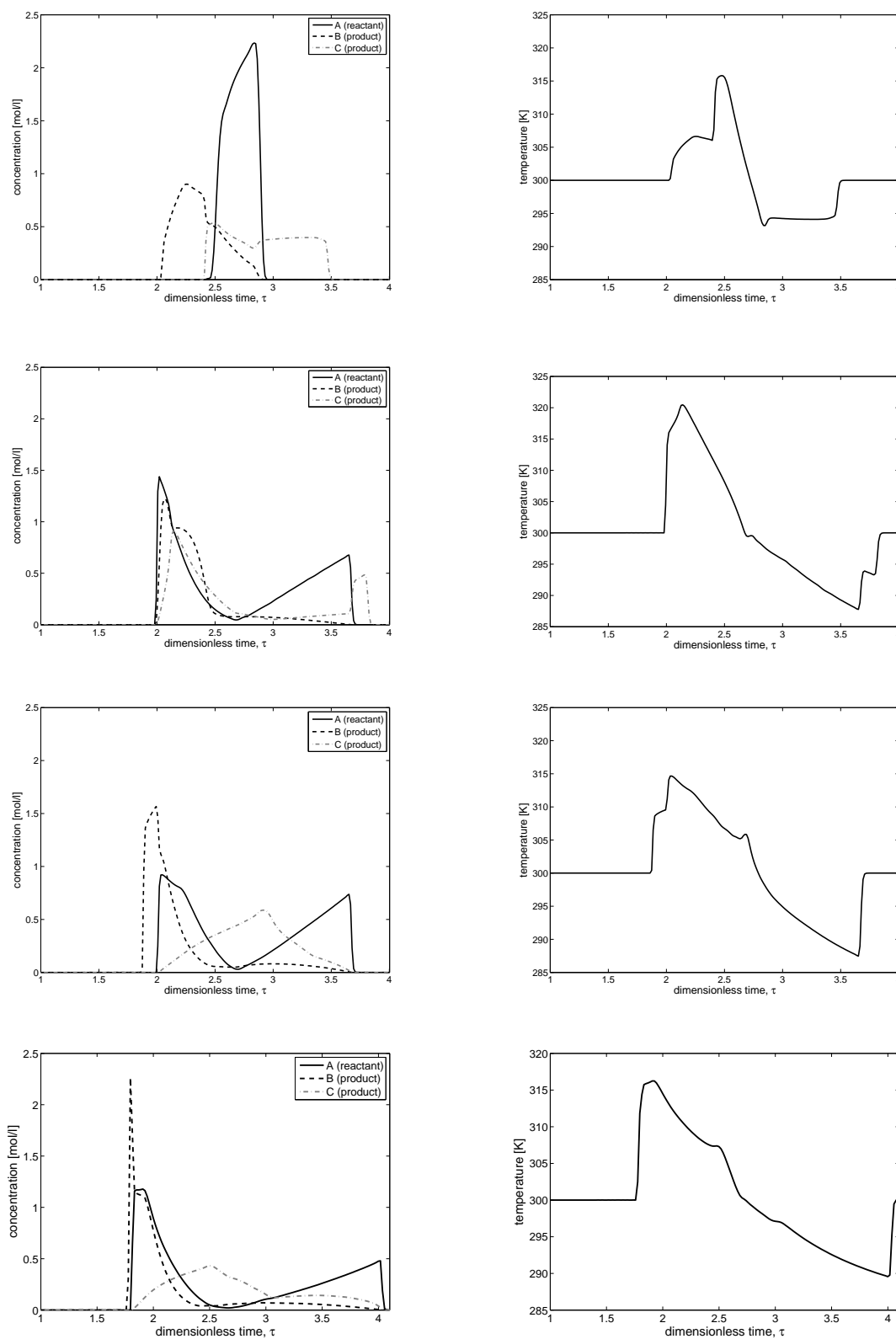


Figure 6.8: Problem 4b: Enthalpy of adsorption (componentwise):  $\Delta H_R = -10 \text{ kJ/mol}$ ,  $E_A = 60 \text{ kJ/mol}$ , row 1 (case 1):  $\Delta H_{A,A} = 0$ ,  $\Delta H_{A,B} = -20$ ,  $\Delta H_{A,C} = -20$ , row 2 (case 2):  $\Delta H_{A,A} = -20$ ,  $\Delta H_{A,B} = 0$ ,  $\Delta H_{A,C} = -20$ , row 3 (case 3):  $\Delta H_{A,A} = -20$ ,  $\Delta H_{A,B} = -20$ ,  $\Delta H_{A,C} = 0$ , row 4 (case 4):  $\Delta H_{A,A} = -30$ ,  $\Delta H_{A,B} = -20$ ,  $\Delta H_{A,C} = -10$ .

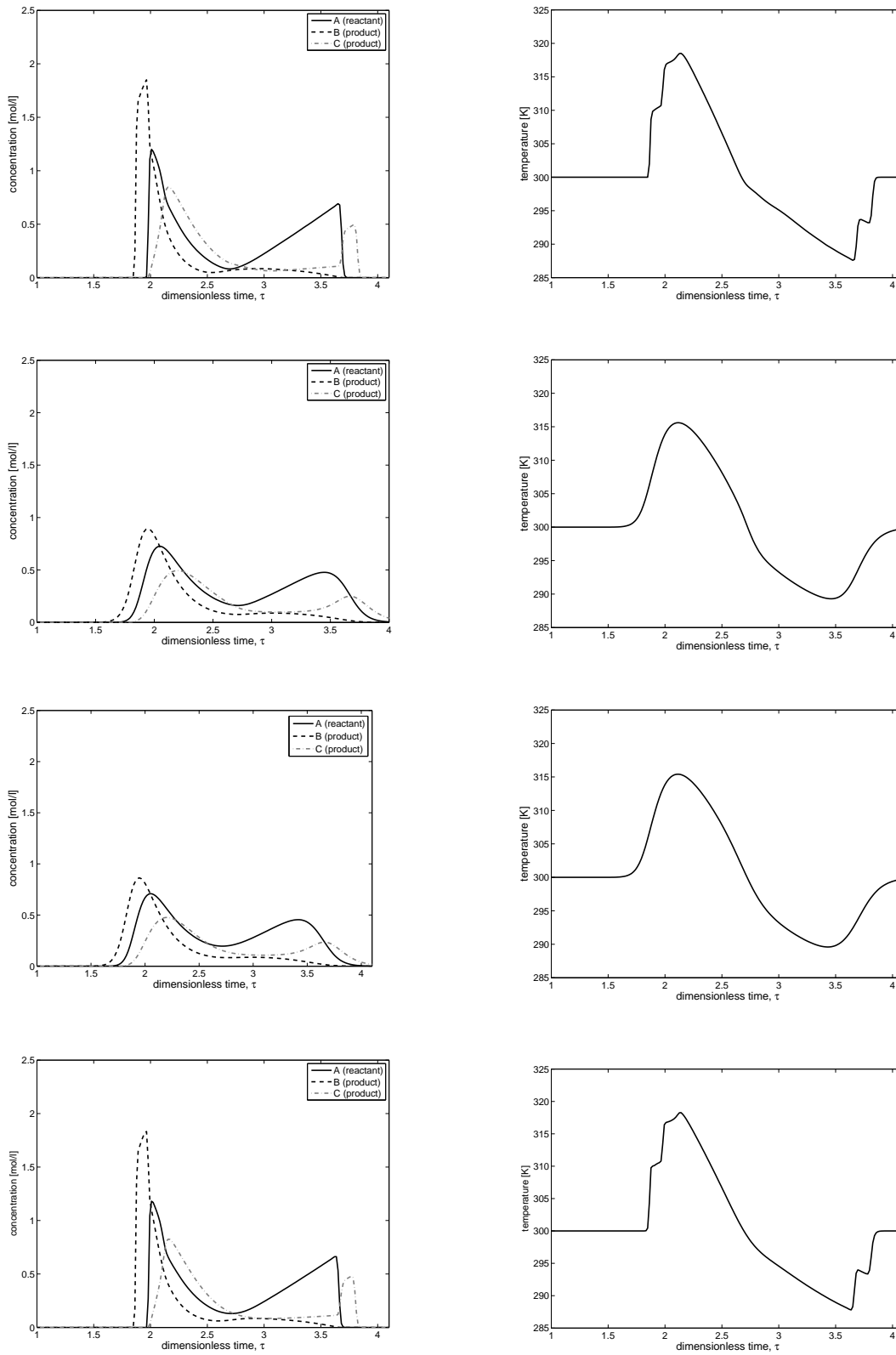


Figure 6.9: Problem 5: Influence of dispersion terms.  $\Delta H_{A,i} = -20 \text{ kJ/mol}$ ,  $i=A,B,C$ ,  $\Delta H_R = -10 \text{ kJ/mol}$ ,  $E_A = 60 \text{ kJ/mol}$ , row 1 (case 1):  $Pe_M = 10^4, Pe_E = 10^4$  row 2 (case 2):  $Pe_M = 200, Pe_E = 0$  row 3 (case 3):  $Pe_M = 0, Pe_E = 200$ , row 4 (case 4):  $Pe_M = 200, Pe_E = 200$ .

## 6.5 Conclusion

In this chapter, reactive liquid chromatography was investigated theoretically considering thermal effects that originate from heats of reaction and adsorption enthalpies. The systematic parametric studies carried out demonstrate that the related temperature gradients can significantly influence the achievable conversion and separation. A high resolution finite volume method was applied to numerically solve the mass and energy balances describing this non-isothermal process. The scheme is robust, gives high order accuracy on coarse grids and resolves sharp discontinuities. In order to verify the numerical results, several consistency tests related to the mass and energy conservations, and evaluations of trivial studies are carried out. The results prove the accuracy of the numerical scheme and agree well with theoretical predictions for limiting cases. The key parameters that influence the reactor performance were systematically investigated. It was found that the heats of reaction and the enthalpies are the reason for complex concentration and temperature profiles. It is important to mention, that higher conversion can be achieved under non-isothermal conditions as compared to isothermal chromatographic reactor operation. It was observed, that in particular an exothermic heat of reaction can be source for the development of a positive thermal waves leading to significant improvements in conversion and separation. The simulation results acquired in this study emphasize the necessity to account in more detail for thermal effects in reactive liquid chromatography. Further research is required, to further optimize internal temperature profiles.



# Chapter 7

## Summary and Conclusions

In this thesis models developed to describe, non-reactive and reactive liquid chromatographic processes under isothermal and non-isothermal conditions were theoretically studied. Both analytical and numerical investigations were the focus of this work. The equilibrium dispersive model and the lumped kinetic model were analyzed using Dirichlet and Robin boundary conditions. These models constitute of systems of convection-diffusion-reaction partial differential equations with dominating convective terms that are coupled with differential or algebraic equations.

For linear adsorption isotherms, the Laplace transformation was used to solve analytically the special case of single-component movements in chromatographic columns. The Laplace transformation technique has already been used to solve linear chromatographic models [42, 43]. In this work, statistical moments up to the third order were derived and calculated for both types of models and boundary conditions.

For nonlinear adsorption isotherms, numerical techniques are the only tool to obtain solutions of the models. However, the strong nonlinearities of realistic thermodynamic functions (isotherms) and the stiffness of reaction terms pose major difficulties for the numerical schemes. For this reason, computational efficiency and accuracy of numerical methods are of large relevance. They were a focus of this dissertation. The high resolution finite volume scheme of Koren [39] and the discontinuous Galerkin finite element method were implemented to solve isothermal non-reactive and reactive chromatographic models. The second to third order accurate Koren scheme is a flux-limiting finite volume scheme in which fluxes

are limited by using a nonlinear minmod limiter. This limiting procedure guarantees the positivity of the scheme by suppressing numerical oscillations, usually encountered in the numerical schemes of second and higher orders. The suggested DG-scheme satisfies the TVB property and gives second order accuracy. The scheme can be easily extended to higher orders by using high order basis functions and by employing better slope limiters, for example reconstruction with the WENO limiters [69]. This method incorporates the ideas of numerical fluxes and slope limiters in a very natural way to capture the physically relevant discontinuities without producing spurious oscillations in their vicinity. In contrast to the finite volume schemes, the DG-scheme is well suited to handle complicated geometries and avoids the extension of mesh stencil that allows the incorporation of boundary conditions uniformly.

Analytical solutions obtained in the Laplace domain were used to validate the numerical predictions generated by using proposed schemes. Analytical solutions were obtained for the single component linear equilibrium dispersive and lumped kinetic models using Dirichlet and Robin boundary conditions. Statistical moments of step responses were calculated and compared with numerical predictions for both types of models and boundary conditions. Good agreements up to the third moment were observed which assured the accuracy of suggested numerical solution techniques. A close connection between equilibrium dispersive and lumped kinetic models was pointed out and the strength of the simpler equilibrium dispersive model for linear isotherm was illustrated.

Available experimental results were also utilized to validate the numerical results. Due to unavailability of exact nonlinear models solutions, the accuracy of the proposed schemes were validated against some other flux-limiting finite volume schemes available in the literature. Both schemes were found to be robust, give a high order accuracy on coarse grids, and resolve sharp discontinuities. The numerical test problems showed that the suggested DG-scheme produced slightly more resolved solutions than the high resolution scheme of Koren, especially at sharp discontinuities. However, desirable results can also be achieved by using the Koren scheme. On the basis of these results, one can conclude that both DG and Koren schemes are highly recommendable methods for the numerical approximation

of linear and nonlinear chromatographic models. The suggested methods are efficient, accurate, and suited to carry out simulations of dynamic of chromatographic processes in packed columns.

Another important focus of this dissertation was to analyze thermal effects on reactive liquid chromatographic process that originate from reaction and adsorption enthalpies. Through systematic parametric studies, it was shown that temperature gradients can significantly influence the achievable conversion and separation. A high resolution finite volume method was implemented to numerically approximate the coupled mass and energy balances describing the non-isothermal process. In order to verify the numerical results, several consistency tests related to mass and energy conservations, and evaluations of trivial studies were carried out. The results proved the accuracy of applied numerical scheme, the correctness of the model formulation and agreed well with theoretical predictions for limiting cases. The key parameters that influence the reactor performance were systematically investigated. It was found that the heats of reaction and the adsorption enthalpies are the reason for complex concentration and temperature profiles. It is important to mention, that higher conversion can be achieved in certain cases under non-isothermal conditions as compared to isothermal chromatographic reactor operation. The simulation results acquired in this study emphasize the necessity to account in more detail for thermal effects in reactive liquid chromatography. Further work is required, to optimize the reactor by controlling internal temperature profiles.

The present contribution was based on the numerical approximation of chromatographic processes occurring in a single column. However, the suggested numerical schemes can also be used to deal with the non-linearity of more complicated processes, such as multi-column moving-bed processes and periodic operations. Especially, to develop an efficient and accurate numerical scheme for the simulated moving bed chromatography process will be the main focus of our future research work. Being a continuous purification process, simulated moving bed chromatography has higher outputs and requires less solvent than conventional batch chromatography.

In this dissertation, the equilibrium dispersive and lumped kinetic models were studied.

Future research tasks include the extension of our work to more complicated models, such as the general rate model. The simulation of such more detailed models are quite complicated. Therefore, further work is required to investigate the model and to search for efficient and accurate numerical schemes. In addition, the operating conditions for preparative chromatography, as for any industrial process, must be optimized. Such optimization is based on thorough understanding of process variables and economics. We will optimize the non-isothermal process to improve yield, productivity and, ultimately, to reduce the operational cost. Optimization of this complex process is a challenging task due to the nonlinearity of chromatographic models and the large number of operating variables. It is therefore, necessary to use effective mathematical tools as developed in this work to solve the nonlinear problems.

Finally, it can be concluded that accurate numerical tools are essential to understand and illustrate complex front propagation phenomena taking place in chromatographic columns.

# Appendix A

## Mathematical Derivations

Here, we present the complete derivations of the first three moments for both equilibrium dispersive and lumped kinetic models with Dirichlet and Danckwerts boundary conditions.

### Equilibrium dispersive model with Dirichlet boundary conditions

In this part, the moments of equilibrium dispersive model with Dirichlet boundary conditions are derived. By taking  $x = 1$  and  $c_0 = 1$ , the Eq. (4.13) can be written as

$$C(x = 1, s) = \frac{1}{s} \exp \left( \frac{Pe}{2} - \frac{1}{2} \sqrt{Pe^2 + 4Pe \frac{L}{u} (1 + aF)s} \right). \quad (\text{A.1})$$

With

$$Pe = \frac{Lu}{D_{\text{app}}}. \quad (\text{A.2})$$

We further define

$$b_1 = Pe(1 + aF) \frac{L}{u}. \quad (\text{A.3})$$

The moment generating property of the Laplace transform is used exploiting (e.g. [99])

$$\mu_n = (-1)^n \lim_{s \rightarrow 0} \frac{d^n(sC)}{ds^n}, \quad n = 0, 1, 2, 3, \dots \quad (\text{A.4})$$

Thus, the zeroth moment is given as

$$\mu_0 = \lim_{s \rightarrow 0} sC(x = 1, s) = \lim_{s \rightarrow 0} \exp \left( \frac{Pe}{2} - \frac{1}{2} \sqrt{Pe^2 + 4b_1 s} \right) = 1. \quad (\text{A.5})$$

The first initial moment can be obtained from Eq. (A.4) as

$$\mu_1 = (-1) \lim_{s \rightarrow 0} \frac{d(sC)}{ds} = \lim_{s \rightarrow 0} \frac{\exp \left( \frac{Pe}{2} - \frac{1}{2} \sqrt{Pe^2 + 4b_1 s} \right)}{\sqrt{Pe^2 + 4b_1 s}}. \quad (\text{A.6})$$

Thus,

$$\mu_1 = \frac{b_1}{Pe} = \frac{L}{u}(1 + aF). \quad (\text{A.7})$$

The second initial moment can be derived from the relation given in Eq. (A.4) as

$$\mu_2 = (-1)^2 \lim_{s \rightarrow 0} \frac{d^2(sC)}{ds^2}, \quad (\text{A.8})$$

where

$$\frac{d^2(sC)}{ds^2} = \frac{2b_1^2 \exp\left(\frac{Pe}{2} - \frac{1}{2}\sqrt{Pe^2 + 4b_1s}\right)}{(Pe^2 + 4a_1s)^{3/2}} + \frac{b_1^2 \exp\left(\frac{Pe}{2} - \frac{1}{2}\sqrt{Pe^2 + 4b_1s}\right)}{Pe^2 + 4a_1s}. \quad (\text{A.9})$$

Thus, the second initial moment is given as

$$\mu_2 = \frac{b_1^2(2 + Pe)}{Pe^3} = \frac{2L}{u^3}D_{\text{app}}(1 + aF)^2 + \frac{L^2}{u^2}(1 + aF)^2. \quad (\text{A.10})$$

The second central moment or the variance is given by the following expression

$$\mu_2' = \mu_2 - \mu_1^2 = \frac{b_1^2}{Pe^3} = \frac{2L}{u^3}D_{\text{app}}(1 + aF)^2. \quad (\text{A.11})$$

Finally, the third initial moment is again obtained using Eq. (A.4)

$$\mu_3 = (-1)^3 \lim_{s \rightarrow 0} \frac{d^3(sC)}{ds^3} = \frac{b_1^3}{Pe^5}(6Pe + 12 + Pe^2), \quad (\text{A.12})$$

or

$$\mu_3 = \frac{L^3}{u^3}(1 + aF)^3 \left( \frac{6D_{\text{app}}}{Lu} + \frac{12D_{\text{app}}^2}{L^2u^2} + 1 \right). \quad (\text{A.13})$$

The third central moment can be calculated from the moments given above using the subsequent formula

$$\mu_3' = \mu_3 - 3\mu_1\mu_2 + 2\mu_1^3. \quad (\text{A.14})$$

Thus

$$\mu_3' = \frac{12LD_{\text{app}}^2}{u^5}(1 + aF)^3. \quad (\text{A.15})$$

### Equilibrium dispersive model with Danckwerts boundary conditions

Here, the moments of the equilibrium dispersive model with Danckwerts boundary conditions are presented.

The zeroth moment is given as

$$\mu_0 = \lim_{s \rightarrow 0} A \exp(\lambda_1 x) + B \exp(\lambda_2 x) = 1. \quad (\text{A.16})$$

The first initial moment is obtained as

$$\mu_1 = \frac{b_1}{Pe} = \frac{L}{u}(1 + aF). \quad (\text{A.17})$$

The second initial moment is calculated as

$$\mu_2 = \frac{2b_1^2}{Pe^4} \left( -1 + Pe + \frac{Pe^2}{2} + e^{-Pe} \right), \quad (\text{A.18})$$

or

$$\mu_2 = \frac{2D_{\text{app}}^2(1 + Fa)^2}{u^4} \left( -1 + \frac{Lu}{D_{\text{app}}} + \frac{L^2u^2}{2D_{\text{app}}^2} + e^{-Lu/D_{\text{app}}} \right). \quad (\text{A.19})$$

The second central moment is given as

$$\begin{aligned} \mu_2' &= \frac{2b_1^2 e^{-Pe}}{Pe^4} (-e^{Pe} + e^{Pe}Pe + 1) \\ &= \frac{2L}{u^3} D_{\text{app}}(1 + aF)^2 \left( 1 + \frac{D_{\text{app}}}{Lu} (e^{-Lu/D_{\text{app}}} - 1) \right). \end{aligned} \quad (\text{A.20})$$

Lastly, the third initial moment is provided as

$$\mu_3 = \frac{b_1^3}{Pe^6} (-24 + 6Pe + 6Pe^2 + Pe^3 + 24e^{-Pe} + 18e^{-Pe}Pe). \quad (\text{A.21})$$

The third central moment formula based on (A.14) is given below

$$\mu_3' = \frac{12LD_{\text{app}}^2(1 + aF)^3}{u^5} \left[ \left( 1 + \frac{2D_{\text{app}}}{Lu} \right) e^{-Lu/D_{\text{app}}} + \left( 1 - \frac{2D_{\text{app}}}{Lu} \right) \right]. \quad (\text{A.22})$$

### Lumped kinetic model with Dirichlet boundary conditions:

This part presents the moments for the lumped kinetic model with Dirichlet boundary conditions. For  $x = 1$  and  $c_0 = 1$ , Eq. (4.25) can be rewritten as

$$C(x = 1, s) = \frac{1}{s} \exp \left( \frac{b}{2} - \frac{1}{2} \sqrt{b^2 + 4a_1s - \frac{4a_2}{s + a_3} + 4a_4} \right). \quad (\text{A.23})$$

With

$$b = Pe = \frac{Lu}{D}, \quad a_1 = Pe \frac{L}{u}, \quad a_2 = \frac{L^2}{\epsilon D} \frac{k^2 a}{(1-\epsilon)}, \quad a_3 = \frac{k}{(1-\epsilon)}, \quad a_4 = \frac{L^2 ak}{\epsilon D}. \quad (\text{A.24})$$

The zeroth moment is given as

$$\mu_0 = \lim_{s \rightarrow 0} \exp \left( \frac{b}{2} - \frac{1}{2} \sqrt{b^2 + 4a_1 s - \frac{4a_2}{s+a_3} + 4a_4} \right) = 1. \quad (\text{A.25})$$

The first initial moment is calculated as

$$\mu_1 = \lim_{s \rightarrow 0} \frac{4 \left( a_1 + \frac{a_2}{(s+a_3)^2} \right) \exp \left( \frac{b}{2} - \frac{1}{2} \sqrt{b^2 + 4a_1 s - \frac{4a_2}{s+a_3} + 4a_4} \right)}{4 \sqrt{b^2 + 4a_1 s - \frac{4a_2}{s+a_3} + 4a_4}}, \quad (\text{A.26})$$

or

$$\mu_1 = \frac{a_1 a_3^2 + a_2}{a_3^2 b} = \frac{L}{u} (1 + aF). \quad (\text{A.27})$$

The second initial moment is again derived using Eq. (A.8) with

$$\begin{aligned} \frac{d^2(sC)}{ds^2} &= \frac{4 \left( a_1 + \frac{a_2}{(s+a_3)^2} \right) \exp \left( \frac{b}{2} - \frac{1}{2} \sqrt{b^2 + 4a_1 s - \frac{4a_2}{s+a_3} + 4a_4} \right)}{8 \left( b^2 + 4a_1 s - \frac{4a_2}{s+a_3} + 4a_4 \right)^{3/2}} \\ &\quad + \frac{2 a_2 \exp \left( \frac{b}{2} - \frac{1}{2} \sqrt{b^2 + 4a_1 s - \frac{4a_2}{s+a_3} + 4a_4} \right)}{\left( b^2 + 4a_1 s - \frac{4a_2}{s+a_3} + 4a_4 \right)^{1/2} (s+a_3)^3} \\ &\quad + \frac{4 \left( a_1 + \frac{a_2}{(s+a_3)^2} \right) \exp \left( \frac{b}{2} - \frac{1}{2} \sqrt{b^2 + 4a_1 s - \frac{4a_2}{s+a_3} + 4a_4} \right)}{16 \left( b^2 + 4a_1 s - \frac{4a_2}{s+a_3} + 4a_4 \right)}. \end{aligned} \quad (\text{A.28})$$

Then

$$\mu_2 = \frac{1}{a_3^4 b^3} (2a_1^2 a_3^4 + 4a_1 a_3^2 a_2 + 2a_2^2 + 2a_2 a_3 b^2 + ba_1^2 a_3^4 + 2ba_1 a_3^2 a_2 + ba_2^2), \quad (\text{A.29})$$

or

$$\mu_2 = \frac{2LD(1+aF)^2}{u^3} + \frac{1}{k} \left( \frac{2LaF(1-\epsilon)}{u} \right) + \frac{L^2}{u^2} (1+aF)^2. \quad (\text{A.30})$$



Exploiting Eq. (A.11), the second central moment is defined as

$$\mu_2' = \frac{2}{a_3^4 b^3} (a_1^2 a_3^4 + 2a_1 a_3^2 a_2 + a_2^2 + a_2 a_3 b^2) = \frac{2LD(1 + a\frac{1-\epsilon}{\epsilon})^2}{u^3} + \frac{1}{k} \left( \frac{2La\frac{(1-\epsilon)^2}{\epsilon}}{u} \right), \quad (\text{A.31})$$

or

$$\mu_2' = \frac{2LD(1 + aF)^2}{u^3} + \frac{1}{k} \left( \frac{2LaF(1 - \epsilon)}{u} \right). \quad (\text{A.32})$$

The third initial moment is obtained using again Eq. (A.12) with

$$\begin{aligned} -\frac{d^3(sC)}{ds^3} = & \frac{3 \left( 4a_1 + \frac{4a_2}{(s+a_3)^2} \right)^3 \exp \left( \frac{b}{2} - \frac{1}{2} \sqrt{b^2 + 4a_1 s - \frac{4a_2}{s+a_3} + 4a_4} \right)}{16 \left( b^2 + 4a_1 s - \frac{4a_2}{s+a_3} + 4a_4 \right)^{5/2}} \\ & + \frac{3a_2 \left( 4a_1 + \frac{4a_2}{(s+a_3)^2} \right) \exp \left( \frac{b}{2} - \frac{1}{2} \sqrt{b^2 + 4a_1 s - \frac{4a_2}{s+a_3} + 4a_4} \right)}{\left( b^2 + 4a_1 s - \frac{4a_2}{s+a_3} + 4a_4 \right)^{3/2} (s+a_3)^3} \\ & + \frac{3 \left( 4a_1 + \frac{4a_2}{(s+a_3)^2} \right)^3 \exp \left( \frac{b}{2} - \frac{1}{2} \sqrt{b^2 + 4a_1 s - \frac{4a_2}{s+a_3} + 4a_4} \right)}{32 \left( b^2 + 4a_1 s - \frac{4a_2}{s+a_3} + 4a_4 \right)^2} \\ & + \frac{6a_2 \exp \left( \frac{b}{2} - \frac{1}{2} \sqrt{b^2 + 4a_1 s - \frac{4a_2}{s+a_3} + 4a_4} \right)}{\left( b^2 + 4a_1 s - \frac{4a_2}{s+a_3} + 4a_4 \right)^{1/2} (s+a_3)^4} \\ & + \frac{3a_2 \left( 4a_1 + \frac{4a_2}{(s+a_3)^2} \right) \exp \left( \frac{b}{2} - \frac{1}{2} \sqrt{b^2 + 4a_1 s - \frac{4a_2}{s+a_3} + 4a_4} \right)}{2 \left( b^2 + 4a_1 s - \frac{4a_2}{s+a_3} + 4a_4 \right)^{3/2} (s+a_3)^3} \\ & + \frac{\left( 4a_1 + \frac{4a_2}{(s+a_3)^2} \right)^3 \exp \left( \frac{b}{2} - \frac{1}{2} \sqrt{b^2 + 4a_1 s - \frac{4a_2}{s+a_3} + 4a_4} \right)}{64 \left( b^2 + 4a_1 s - \frac{4a_2}{s+a_3} + 4a_4 \right)^{3/2}}. \end{aligned} \quad (\text{A.33})$$

Then

$$\begin{aligned} \mu_3 = & \frac{1}{a_3^6 b^5} (12a_1^3 a_3^6 + 36a_1^2 a_3^4 a_2 + 36a_1 a_3^2 a_2^2 + 12a_2^3 + 12a_2 a_3^3 b^2 a_1 \\ & + 12a_2^2 a_3 b^2 + 6ba_1^3 a_3^6 + 18ba_1^2 a_3^4 a_2 + 18ba_1 a_3^2 a_2^2 + 6ba_2^3 + 6a_2 a_3^2 b^4 \\ & + 6a_2 a_3^3 b^3 a_1 + 6a_2^2 a_3 b^3 + b^2 a_1^3 a_3^6 + 3b^2 a_1^2 a_3^4 a_2 + 3b^2 a_1 a_3^2 a_2^2 + b^2 a_2^3), \end{aligned} \quad (\text{A.34})$$

or

$$\mu_3 = \frac{L^3}{u^3}(1 + aF)^3 \left( \frac{6D}{Lu} + \frac{12D^2}{L^2u^2} + 1 \right) + \frac{6L^2(1 + aF)a(1 - \epsilon)}{u^3k} \left( \frac{2D}{L} + \frac{(1 - \epsilon)u^2}{Lk(1 + aF)} + u \right). \quad (\text{A.35})$$

Using (A.14), the third central moment is given as

$$\mu_3' = \frac{12LD^2}{u^5}(1 + aF)^3 + \frac{6L^2(1 + aF)aF(1 - \epsilon)}{ku^3} \left( \frac{2D}{L} + \frac{(1 - \epsilon)u^2}{Lk(1 + aF)} \right). \quad (\text{A.36})$$

or

$$\mu_3' = \frac{12LD^2}{u^5}(1 + aF)^3 + \frac{1}{k} \left( \frac{12LD(1 + aF)aF(1 - \epsilon)}{u^3} \right) + \frac{1}{k^2} \left( \frac{6LaF(1 - \epsilon)^2}{u} \right). \quad (\text{A.37})$$

### Lumped kinetic model with Danckwerts boundary conditions

This part discusses the derivation of moments for lumped kinetic model with Danckwerts boundary conditions.

The zeroth moment is again given as

$$\mu_0 = 1. \quad (\text{A.38})$$

The first initial moment corresponding again to Eq. (A.7)

$$\mu_1 = \frac{a_1a_3^2 + a_2}{a_3^2b} = \frac{L}{u}(1 + aF). \quad (\text{A.39})$$

The second initial moment is given as

$$\begin{aligned} \mu_2 = & \frac{e^{-b}}{a_3^4b^4} (4a_1a_3^2a_2 - 2e^ba_1^2a_3^4 + 2e^bba_2^2 + e^bb^2a_2^2 \\ & - 4e^ba_1a_3^2a_2 + 2e^bba_1^2a_3^4 + e^bb^2a_1^2a_3^4 + 2a_2e^ba_3b^3 + 4e^bba_1a_3^2a_2 \\ & + 2e^bb^2a_1^2a_3^2a_2 + 2a_1^2a_3^4 + 2a_2^2 - 2be^ba_2^2). \end{aligned} \quad (\text{A.40})$$

The second central moment is defined as, c.f. (A.11),

$$\mu_2' = \frac{2L}{u^3}D(1 + aF)^2 \left( 1 + \frac{D}{Lu} (e^{-Lu/D} - 1) \right) + \frac{1}{k} \left( \frac{2LaF\epsilon}{u} \right). \quad (\text{A.41})$$

The third initial moment is given as

$$\begin{aligned}
\mu_3 = \frac{e^{-b}}{a_3^6 b^6} & \left( 24a_1^3 a_3^6 + 24a_2^3 + 72a_1^2 a_3^4 a_2 + 72a_1 a_3^2 a_2^2 + 12a_2^2 a_3 b^2 + 18ba_1^3 a_3^6 \right. \\
& + 54ba_1^2 a_3^4 a_2 + 54ba_1 a_3^2 a_2^2 + 6a_2 e^b a_3^2 b^5 + 6a_1^3 a_3^6 e^b b^2 - 12a_2^2 e^b a_3 b^2 + 12a_2^2 e^b a_3 b^3 \\
& + 6e^b b a_1^3 a_3^6 + 6a_2^2 a_3 b^4 + e^b b^3 a_1^3 a_3^6 + 18ba_2^3 + 6e^b b a_2^3 + e^b b^3 a_2^3 - 24e^b a_1^3 a_3^6 \\
& + 6e^b b^2 a_2^3 - 24e^b a_2^3 + 18e^b b a_1^2 a_3^4 a_2 - 12a_2 e^b a_3^3 b^2 a_1 + 12a_2 e^b a_3^3 b^3 a_1 + 18e^b b a_1 a_3^2 a_2^2 \\
& + 6e^b a_2 a_3^3 b^4 a_1 + 3e^b b^3 a_1^2 a_3^4 a_2 + 3e^b b^3 a_1 a_3^2 a_2^2 + 18a_1^2 a_3^4 e^b b^2 a_2 + 18a_1 a_3^2 e^b b^2 a_2^2 \\
& \left. - 72e^b a_1^2 a_3^4 a_2 - 72e^b a_1 a_3^2 a_2^2 + 12a_2 a_3^3 b^2 a_1 \right) . \tag{A.42}
\end{aligned}$$

The third central moment is using again (A.14) as

$$\begin{aligned}
\mu_3' = \frac{12LD^2(1+aF)^3}{u^5} & \left[ \left( 1 + \frac{2D}{Lu} \right) e^{-Lu/D} + \left( 1 - \frac{2D}{Lu} \right) \right] \\
& + \frac{1}{k} \left[ \frac{12DLaF^2\epsilon(1+aF)}{u^3} \left( \frac{D}{Lu} e^{-Lu/D} + 1 - \frac{D}{Lu} \right) \right] + \frac{1}{k^2} \left( \frac{6LaF^3\epsilon^2}{u} \right) . \tag{A.43}
\end{aligned}$$

# Appendix B

## Nomenclature

$a_i$	Henry constants of component $i$ , [-]
$b$	nonlinearity parameter in Eq. (2.18), [ $l/mol$ ]
$c_i$	liquid phase concentration of component $i$ , [ $mol/l$ ]
$c_p$	concentration in the pores of particles $i$ , [ $mol/l$ ]
$C_p$	heat capacity, [ $kJ/gK$ ]
$d$	column diameter, [ $m$ ]
$D_{app}$	apparent dispersion coefficient in EDM [ $m^2/s$ ]
$D$	dispersion coefficient in LKM [ $m^2/s$ ]
$E_A$	activation energy, [ $kJ/mol$ ]
$E_H$	a relative percentage error in energy balance, [-]
$E_\xi$	a relative percentage error in molar concentration $\xi$ , [-]
$F$	phase ratio, [-]
$\Delta H_A$	enthalpy of adsorption, [ $kJ/mol$ ]
$\Delta H_R$	enthalpy of reaction, [ $kJ/mol$ ]
$\Delta H^{out}$	temperature at the column outlet, [ $kJ$ ]
$I_j$	$j$ th mesh interval, [-]
$k$	mass transfer coefficient, [ $1/s$ ]
$k_{for}$	forward reaction rate constant, [ $1/s$ ]
$K_{eq}$	reaction equilibrium constant, [-]
$K_{eq}^*$	reaction equilibrium constant, [ $mol/l$ ]
$L$	column length, [ $m$ ]
$n_i$	molar amount of component $i$ , [ $mol$ ]
$N_c$	number of components, [-]
$N_t$	number of theoretical plates, [-]
$N$	number of grid cells, [-]
$P_l$	Legendre polynomial of order $l$ (-)
$Pe_M$	Peclet number of mass balance, [-]
$Pe_E$	Peclet number of energy balance, [-]
$q_i^*$	solid phase concentration of component $i$ , [ $mol/l$ ]
$r$	rate of chemical reaction, [ $mol/l_s$ ]
$R$	gas constant, $8.314 \times 10^{-3}$ , [ $kJ/molK$ ]
$t$	time, [ $s$ ]

**Nomenclature (continued)**

T	pure thermal wave
$u$	interstitial velocity, $[m/s]$
$V$	volume, $[l]$
$\dot{V}$	volumetric flow rate, $[l/s]$
$X_A$	conversion of reactant A, $[-]$
$z$	spatial coordinate, $[m]$
<i>Greek symbols</i>	
$\nu_i$	stoichiometric coefficient of component $i$
$\lambda$	conductivity coefficient, $[m^2kJ/slK]$
$\eta$	very small number
$\Delta x_j$	width of mesh interval $I_j$
$\Delta t$	time step
$\epsilon$	external porosity
$\xi$	extent of reaction, $[mol]$
$x$	dimensionless distance, $x = \frac{z}{L}$
$\tau$	dimensionless time, $\tau = \frac{tu}{L}$
$\rho$	density, $[g/l]$
$\phi_l$	local basis function of order $l$
$\mu_n$	$n$ -th initial normalized moment
$\mu'_n$	$n$ -th central moment
<i>Superscripts</i>	
in	inlet value
init	initial value
out	outlet profile
L	liquid phase
p*	p* is order of numerical scheme
S	solid phase
<i>Subscripts</i>	
E	energy
i	$i$ is the number of $N_c$ components
j	$j$ is the number of discretized cells
m	$m$ is the number of $N_c + 1$ pseudo-components
M	mass
<i>Abbreviations</i>	
BCs	boundary conditions
DG	discontinuous Galerkin
EDM	equilibrium dispersive model
FBCR	fixed-bed chromatographic reactor
FDMs	finite difference methods
FEMs	finite element methods
FVMs	finite volume methods
LKM	lumped kinetic model
ODEs	ordinary differential equations
PDEs	partial differential equations
TVB	total variation boundedness

# Bibliography

- [1] Aizinger, V., Dawson, C., Cockburn, B., Castillo, P., 2000. Local discontinuous Galerkin method for contaminant transport. *Advances in Water Resources* 24, 73-87.
- [2] Bahhar, A., Baranger, J., Sandri, D., 1998. Galerkin discontinuous approximation of the transport equation and viscoelastic fluid flow on quadrilaterals. *Numerical Methods of Partial Differential Equations* 14, 97-114.
- [3] Bassi, F., Rebay, S., 1997. A high-order accurate discontinuous finite element method for the numerical solution of the compressible Navier-Stokes equations. *Journal of Computational Physics* 131, 267-279.
- [4] Borren, T., Fricke, J.: Schmidt-Traub, H., (Ed.), 2005. *Chromatographic reactors in preparative chromatography of fine chemicals and pharmaceutical agents*, Wiley-VCH Verlag, Weinheim, 371-395.
- [5] Broughton, D.B., 1961. Continuous sorption process employing fixed bed of sorbent and moving inlets and outlet. US Patent 2, 985, 589.
- [6] Carey, G.F., Finlayson, B.A., 1975. Orthogonal collocation on finite elements. *Chemical Engineering Science* 30, 587-596.
- [7] Chen, Z., Cockburn, B., Jerome, J., Shu, C.-W., 1995. Mixed-RKDG finite element methods for the 2-D hydrodynamic model for semiconductor device simulation. *VLSI Design* 3, 145-158.

- 
- [8] Clough, R.W., 1960. The finite element method in plane stress analysis. Proceedings of 2nd ASCE conference on Electronic computation, Pittsburgh, PA, September 8-9.
- [9] Cockburn, B., Shu, C.-W., 1989. TVB Runge-Kutta local projection discontinuous Galerkin finite element method for conservation laws II: General framework. *Mathematics of computation* 52, 411-435.
- [10] Cockburn, B., Lin, S.-Y., 1989. TVB Runge-Kutta local projection discontinuous Galerkin finite element method for conservation laws III: One-dimensional systems. *Journal of Computational Physics* 84, 90-113.
- [11] Cockburn, B., Hou, S., Shu, C.-W., 1990. TVB Runge-Kutta local projection discontinuous Galerkin finite element method for conservation laws IV: The multidimensional case. *Mathematics of computation* 54, 545-581.
- [12] Cockburn, B., Shu, C.-W., 1989. The Runge-Kutta discontinuous Galerkin finite element method for conservation laws V: Multidimensional systems. *Journal of Computational Physics* 141, 199-224.
- [13] Cockburn, B., Shu, C.-W., 2001. Runge Kutta discontinuous Galerkin methods for convection-dominated problems. *Journal of Scientific Computing* 16, 173-261.
- [14] Cockburn, B., Dawson, C., 2002. Approximation of the velocity by coupling discontinuous Galerkin and mixed finite element methods for flow problems. *Computational Geosciences* 6, 502-522.
- [15] Craig, L.C., 1944. Identification of Small Amounts of Organic Compounds by Distribution Studies. II. Separation By Counter-current Distribution. *Journal of Biology Chemistry* 155, 519-534.
- [16] Cruz, P., Santos, J.C., Magalhães, F.D., Mendes, A., 2005. Simulation of separation processes using finite volume method. *Computer & Chemical Engineering Journal* 30, 83-98.

- 
- [17] Danckwerts, P.V., 1953. Continuous flow systems. *Chemical Engineering Science* 2, 1-9.
- [18] Dinwinddie, J.A., Morgan, W.A., 1961. U.S. Patent 2, 976, 132, to Esso Research and Engineering Company.
- [19] Dondi, F., Remelli, M., 1986. The characteristic function-method in the stochastic-theory of chromatography. *Journal of Physical Chemistry* 90, 1885-1891.
- [20] Dreyer, W., Qamar, S., 2005. Second order accurate explicit finite volume schemes for the solution of Boltzmann-Peierls equation. *Journal of Applied Mathematics and Mechnaics* 85, 4-22.
- [21] Eigenberger, G., Kolios, G., NieKen, U., 2007. Efficient reheating of a reverse-flow reformer-An experimental study. *Chemical Engineering Science* 62, 4825-4841.
- [22] Felinger, A., Cavazzini, A., Dondi, F., 2004. Equivalence of the microscopic and macroscopic models of chromatography: stochastic-dispersive versus lumped kinetic model. *Journal of Chromatography A* 1043, 149-157.
- [23] Frenz, J., Horvath, C.S., and Horvath (Ed.), 1988. High-performance liquid chromatography *Advances and Perspectives*, vol. 5. Academic Press, New York.
- [24] Fricke, J., Schmidt-Traub, H., Kawase, M., 2005. Chromatographic reactor, *Ullmann's Encyclopedia of Industrial Chemistry*, Wiley-VCH Verlag, Weinheim.
- [25] Ganetsos, G., Barker, P.E., 1993. Preparative and production scale chromatography, vol. 61. Marcel Dekker, Inc., New York, 375-523.
- [26] Gaziev, G.A., Roginskii, S.Z., Yanovskii, M.J., 1962. U.S.S.R. Patent 149, 398.
- [27] Glöckler, B., Dieter, H., Eigenberger, G., NieKen, U., 2006. Efficient reheating of a reverse-flow reformer-An experimental study. *Chemical Engineering Science* 62, 5638-5643.



- 
- [28] Guiochon, G., 2002. Preparative liquid chromatography. *Journal of Chromatography A* 965, 129-161.
- [29] Guiochon, G., Lin, B., 2003. *Modeling for preparative chromatography*, Academic Press, Amsterdam.
- [30] Guiochon, G., Felinger, A., Shirazi, D.G., Katti, A.M., 2006. *Fundamentals of preparative and nonlinear chromatography*, 2nd ed., Academic Press imprint of Elsevier, Boston.
- [31] Holik, M., 2009. Application of discontinuous Galerkin method for the simulation of 3D inviscid compressible flows. *Proceedings of ALGORITMY* 304-312.
- [32] Hughes, T.J.R., Brooks, A.N., 1979. A multidimensional upwind scheme with no crosswind diffusion. In Hughes, T.J.R., (Ed.), *Finite Element Methods for Convection Dominated Flows*, ASME, New York, 19-35.
- [33] Hughes, T.J.R., 1995. Multiscale phenomena: Green's functions, the Dirichlet-to-Neumann formulation, subgrid scale models, bubbles and the origins of stabilized methods. *Computer Methods in Applied Mechanics and Engineering* 127, 387-401.
- [34] Javeed, S., Qamar, S., Seidel-Morgenstern, A., Warnecke, G., 2011. Efficient and accurate numerical simulation of nonlinear chromatographic processes. *Computer & Chemical Engineering* 35, 2294-2305.
- [35] Javeed, S., Qamar, S., Seidel-Morgenstern, A., Warnecke, G., 2011. A discontinuous Galerkin method to solve chromatographic models. *Journal of Chromatography A* 1218, 7137-7146.
- [36] Javeed, S., Qamar, S., Seidel-Morgenstern, A., Warnecke, G., 2012. Parametric study of thermal effects in reactive liquid chromatography. *Chemical Engineering Journal* 191, 426-440.

- 
- [37] Javeed, S., Qamar, S., Seidel-Morgenstern, A., Warnecke, G., 2013. Analysis and numerical investigation of two dynamic models for liquid chromatography. *Chemical Engineering Science* 90, 17-31.
- [38] Jeansonne, M.S., Foley, J.P., 1992. Improved equations for the calculation of chromatographic figures of merit for ideal and skewed chromatographic peaks. *Journal of Chromatography A* 594, 1-8.
- [39] Koren, B. 1993. A robust upwind discretization method for advection, diffusion and source terms. In Vreugdenhil, C.B., Koren, B., (Eds.), *Numerical Methods for Advection-Diffusion Problems*, Volume 45 of *Notes on Numerical Fluid Mechanics*, Braunschweig: Vieweg Verlag, 117-138.
- [40] Kruglov, A., 1994. Methanol synthesis in a simulated countercurrent moving-bed adsorptive catalytic reactor. *Chemical Engineering Science* 49, 4699-4716.
- [41] Kubin, M., 1965. Beitrag zur Theorie der Chromatographie. *Collection of Czechoslovak Chemical Communications* 30, 1104-1118.
- [42] Kubin, M., 1965. Beitrag zur Theorie der Chromatographie. 11. Einfluss der Diffusion Ausserhalb und der Adsorption Innerhalb des Sorbens- Kornes. *Collection of Czechoslovak Chemical Communications* 30, 2900-2907.
- [43] Kucera, E., 1965. Contribution to the theory of chromatography: Linear non-equilibrium elution chromatography. *Journal of Chromatography A* 19, 237-248.
- [44] Kuhn, R., Winterstein, A., Lederer, E., 1931. The xanthophylls, *Zeitschrift für Physiologische Chemie* 197, 141-160.
- [45] Kumar, A., Jaiswal, D.K., Kumar, N., 2009. Analytical solutions of one-dimensional advection-diffusion equation with variable coefficients in a finite domain. *Journal of Earth System Science* 118, 539-549.

- 
- [46] Kurganov, A., Tadmor, E., 2000. New High-Resolution Central Schemes for Nonlinear Conservation Laws and Convection-Diffusion Equations. *Journal of Computational Physics* 160, 241-282.
- [47] Langer, S.H., Patton, J.E., 1974. Chemical reactor applications of the gas chromatographic column. In Purnell, H., (Ed.), *New developments in gas chromatography*, Wiley, New York, 293-373.
- [48] Lapidus, L., Amundson, N.R., 1952. Mathematics of adsorption in beds, VI. The effect of longitudinal diffusion in ion exchange and chromatographic columns. *The Journal of Physical Chemistry* 56, 984-988.
- [49] LeVeque, R.J., 1992. *Numerical methods for conservation laws*. Birkhäuser Verlag, Basel, Germany.
- [50] LeVeque, R.J., 2003. *Finite Volume Methods for Hyperbolic Systems*. Cambridge University Press, Cambridge.
- [51] Lieres, E.V., Andersson, J., 2010. A fast and accurate solver for the general rate model of column liquid chromatography. *Computer & chemical Engineering* 34, 1180-1191.
- [52] Lim, Y.I., Jorgen, S.B., 2004. A fast and accurate numerical method for solving simulated moving bed (SMB) chromatographic separation problems. *Chemical Engineering Science* 59, 1931- 1947.
- [53] Lim, Y.I., Jorgen, S.B., 2009. Performance evaluation of the conservation element and solution element method in the SMB process simulation. *Chemical Engineering and Processing: Process Intensification* 59, 1931- 1947.
- [54] Ma, Z., Guiochon, G., 1991. Application of Orthogonal Collocation on Finite Elements in the Simulation of Non-Linear Chromatography. *Computer & chemical Engineering* 15, 415-426.
- [55] Magee, E.M., 1961. Canadian Patent 631, 882.

- [56] Mai, P., Tien, V.D., Mai, K.X., Seidel-Morgenstern, A., 2004. Analysis of heterogeneously catalyzed ester hydrolysis performed in a chromatographic reactor and in a reaction calorimeter. *Industrial & Engineering Chemistry Research* 43, 4691-4702.
- [57] Martin, A.J.P., Synge, R.L.M., 1941. A new form of chromatogram employing two liquid phases: A theory of chromatography. 2. Application to the micro-determination of the higher monoamino-acids in proteins. *Biochemical Journal* 35, 1358-1368.
- [58] Mazzotti, M., 2009. Nonclassical composition fronts in nonlinear chromatography: Delta-shock. *Industrial & Engineering Chemistry Research* 48, 7733-7752.
- [59] Mazzotti, M., Tarafderb, A., Cornela, J., Gritti, F., Guiochon, G., 2010. Experimental evidence of a delta-shock in nonlinear chromatography. *Journal of Chromatography A* 1217, 2002-2012.
- [60] Medi, B., and Amanullah, M., 2011. Application of a Finite-Volume Method in the Simulation of Chromatographic Systems: Effects of Flux Limiters. *Industrial & Engineering Chemistry Research* 50, 1739-1748.
- [61] Minceva, M., Pais, L., Rodrigues, A., 2003. Cyclic steady state of simulated moving bed processes for enantiomers separation. *Chemical Engineering and Processing: Process Intensification* 42, 93-104.
- [62] Miyabe, K., Guiochon, G., 2000. Influence of the modification conditions of alkyl bonded ligands on the characteristics of reversed-phase liquid chromatography. *Journal of Chromatography A* 903, 1-12.
- [63] Miyabe, K., Guiochon, G., 2003. Measurement of the parameters of the mass transfer kinetics in high performance liquid chromatography. *Journal of Separation Science* 26, 155-173.
- [64] Miyabe, K., 2007. Surface diffusion in reversed-phase liquid chromatography using silica gel stationary phases of different C1 and C18 ligand densities. *Journal of Chromatography A* 1167, 161-170.

- 
- [65] Miyabe, K., 2009. Moment analysis of chromatographic behavior in reversed-phase liquid chromatography. *Journal of Separation Science* 32, 757-770.
- [66] Qamar, S., Warnecke, G., 2005. A high order kinetic flux-splitting method for the special relativistic magnetohydrodynamics. *Journal of Computational Physics* 205, 182-204.
- [67] Qamar, S., Warnecke, G., 2006. A space-time conservative method for hyperbolic systems with stiff and non stiff source terms. *Communications in Computational Physics* 1, 451-480.
- [68] Qamar, S., 2008. Modeling and simulation of population balances for particulate processes, Habilitation thesis, Faculty of Mathematics, OVGU, Magdeburg, Germany.
- [69] Qiu, J.X., Shu, C.-W., 2004. Hermite WENO schemes and their application as limiters for Runge-Kutta discontinuous Galerkin method: One dimensional case. *Journal of Computational Physics* 193, 115-135.
- [70] Qiu, J.X., Khoo, B.C., Shu, C.-W., 2006. A numerical study for the performance of the Runge-Kutta discontinuous Galerkin method based on different numerical fluxes. *Journal of Computational Physics* 212, 540-565.
- [71] Reed, W.H., Hill, T.R., 1973. Triangular mesh methods for the neutron transport equation. Los Alamos Scientific Laboratory Report LA-UR, 73-79.
- [72] Rhee, H.-K., Aris, R., Amundson, N.R., 1989. First-order partial differential equations. Theory and Application of Hyperbolic Systems of Quasilinear Equations, Volume. II. Prentice-Hall, New Jersey.
- [73] Rice, R.G., Do, D.D., 1995. Applied Mathematics and Modeling for Chemical Engineers, New York, Wiley.
- [74] Roe, P.L., 1986. Characteristic-based schemes for the Euler equations. *Annual Review of Fluid Mechanics* 18, 337-365.

- [75] Rouchon, P., Schoenauer, M., Valentin, P., Vidal-Madjar, C., Guiochon, G., 1985. Theory of propagation of finite concentration bands in gas chromatography. A numerical solution of the ideal problem. *Journal of Physical Chemistry* 89, 2076-2082.
- [76] Ruthven, D. M., 1984. Principles of adsorption and adsorption processes. Wiley-Interscience.
- [77] Sainio, T., 2005. Ion-exchange resins as stationary phase in reactive chromatography. *Acta Universitatis Lappeenrantaensis* 218, PhD thesis, Lappeenranta University of Technology, 2005.
- [78] Sainio, T., Kaspereit, M., Kienle, A., Seidel-Morgenstern, A., 2007. Thermal effects in reactive liquid chromatography. *Chemical Engineering Science* 62, 5674-5681.
- [79] Sainio, T., Zhang, L., Seidel-Morgenstern, A., 2011. Adiabatic operation of chromatographic fixed-bed reactors. *Chemical Engineering Journal* 168, 861-871.
- [80] Sardin, M., Schweich, D., Villiermaux J., 1993. Preparative fixed-bed chromatographic reactor. In Ganetsos, G., Barker, P.E., (Eds.), *Preparative and Production Scale Chromatography*, Marcel Dekker Inc., New York, USA, 477-522.
- [81] Schmidt-Traub, H., Schulte, M., Seidel-Morgenstern, A., 2012. *Preparative Chromatography*, Weinheim, Germany: Wiley.
- [82] Schneider, P. and Smith, J. M., 1968. Adsorption rate constants from chromatography. *A.I.Ch.E. Journal* 14, 762-771.
- [83] Seidel-Morgenstern, A., 1991. Analysis of boundary conditions in the axial dispersion model by application of numerical Laplace inversion. *Chemical Engineering Science* 46, 2567-2571.
- [84] Shipilova, O., Sainio, T., Haario H., 2008. Particle transport method for simulation of multicomponent chromatography problems. *Journal of Chromatography A* 1204, 62-71.

- 
- [85] Sundmacher, K., Kienle, A., Seidel-Morgenstern, A., 2005. *Integrated Chemical Processes*, Weinheim, Germany, Wiley.
- [86] Suzuki, M., Smith, J.M., 1971. Kinetic studies by chromatography. *Chemical Engineering Science* 26, 221-235.
- [87] Suzuki, M., 1973. Notes on Determining the Moments of the Impulse Response of the Basic Transformed Equations. *Journal of Chemical Engineering of Japan* 6, 540-543.
- [88] Sweby, P.K., 1984. High resolution schemes using flux limiters for hyperbolic conservation laws. *SIAM Journal on Numerical Analysis* 30, 995-1011.
- [89] Thiele, A., Falk, T., Tobiska, L., Seidel-Morgenstern, A., 2001. Prediction of elution profiles in annular chromatography. *Journal of Computer & Chemical Engineering* 13, 1089-1101.
- [90] Tien, V.D., Seidel-Morgenstern, A., 2011. Quantifying Temperature and Flow Rate Effects on the Performance of a Fixed-bed Chromatographic Reactor. *Journal of Chromatography A* 1218, 8097-8109.
- [91] Tien, V.D., Seidel-Morgenstern, A., Gruner, S., Kienle, A., 2005. Analysis of ester hydrolysis reactions in a chromatographic reactor using equilibrium theory and a rate model. *Industrial & Engineering Chemistry Research* 44, 9565-9574.
- [92] Tien, V.D., 2007. Analysis of heterogeneously catalyzed ester hydrolysis reactions in a fixed-bed Chromatographic reactor. PhD thesis, Faculty of Process and System Engineering, OVGU, Magdeburg, Germany.
- [93] Tiselius, A., 1943. Displacement development in adsorption analysis, *Arkiv foer Kemi, Mineralogi och Geologi* 16A 194, 1-18.
- [94] Toro, E.F., 1999. *Riemann solvers and numerical method for fluid dynamics*, Second Edition, Springer-Verlag.

- 
- [95] Toumi, A., Engell, S., Diehl, M., Bock, H.G., Schlöder, J., 2007. Efficient optimization of simulated moving bed processes. *Chemical Engineering and Processing* 46, 1067-1084.
- [96] Tswett, M., 1906. Physikalisch-chemische Studienüber das Chlorophyll. Die Adsorptionen. *Berichte der Deutschen Botanischen Gesellschaft* 24, 316-323.
- [97] Tswett, M., 1906. Adsorptionsanalyse und chromatographische Methode. Anwendung auf die Chemie des Chlorophylls. *Berichte der Deutschen Botanischen Gesellschaft* 24, 384-393.
- [98] Van Deemter, J.J., Zuiderweg, F.J., A. Klinkenberg, A., 1956. Longitudinal diffusion and resistance to mass transfer as causes of nonideality in chromatography. *Chemical Engineering Science* 5, 271-289.
- [99] Van der Laan, Th., 1958. Letter to the Editors on Notes on the diffusion type model for the longitudinal mixing in flow. *Chemical Engineering Science* 7, 187-191.
- [100] Van Leer, B., 1977. Towards the ultimate conservative difference scheme, IV: a new approach to numerical convection. *Journal of Computational Physics* 12, 276-299.
- [101] Van Leer, B., Engquist, B.E., Osher, S., Somerville, R.C.J., 1985. Upwind-difference methods for aerodynamic problems governed by the Euler equations, large-scale computations in fluid mechanics. AMS series, American Mathematical Society, 327-336.
- [102] Villiermaux J., Rodrigues, A.E., Tondeur, D., (Eds.), 1981. The chromatographic reactor in precolation processes: Theory and applications, Sijthoffen Noordhoff, Alpena an den Rijn, The Netherlands, 539-588.
- [103] Webley, P.A., He, J., 2000. Fast solution-adaptive finite volume method for PSA/VSA cycle simulation; 1 single step simulation. *Computer & chemical Engineering* 23, 1701-1712.



- 
- [104] Xiu, G., Li, P., Rodrigues, A.E., 2002. Sorption-enhanced reaction process with reactive regeneration. *Chemical Engineering Science* 57, 3893-3908.
- [105] Yongsunthon, I., Alpay, E., 1999. Design of periodic adsorptive reactors for the optimal integration of reaction, Separation and Heat Exchange. *Chemical Engineering Science* 54, 2647-2657.
- [106] Zechmeister, L., Chohnoky, L.V., 1937. *Die chromatographische Adsorptionsmethode. Grundlagen, Methodik, Anwendungen*, Julius Springer, Wein.
- [107] Zhang, P., Liu, R.-X., 2005. Hyperbolic conservation laws with space-dependent fluxes: II. General study of numerical fluxes. *Journal of Computational and Applied Mathematics* 176, 105-129.
- [108] Zhang, X., Shu, C.-W., 2011. Positivity-preserving high order discontinuous Galerkin schemes for compressible Euler equations with source terms. *Journal of Computational Physics* 230, 1238-1248.
- [109] Zienkiewicz, O.C., Chung, O.C., 1967. *The finite element method in continuum and structural mechanics*, McGraw Hill.

# Curriculum Vitae

## Personal Information

Name Shumaila Javeed  
Date of Birth 29.01.1985  
Place of Birth Rawalpindi, Pakistan  
Nationality Pakistani  
Marital Status Single

## Education and Employment

2010-2013 PhD studies at the Otto-von-Guericke-University and the Max Planck Institute for Dynamics of Complex Technical Systems, Magdeburg, Germany

2008-2010 MS(Mathematics), COMSATS Institute of Information Technology, Islamabad, Pakistan

2002-2006 BS(Mathematics), COMSATS Institute of Information Technology, Islamabad, Pakistan

2000-2002 F.Sc or Intermediate studies, Rawalpindi, Pakistan

1990-2000 Schooling, Rawalpindi, Pakistan

2007-2010 Lecturer, COMSATS Institute of Information Technology, Islamabad, Pakistan

## Academic Honors

- Three months research scholarship from Max Planck Institute, Magdeburg, Germany
- Research productivity award from COMSATS, Islamabad, Pakistan
- Scholarship for BS(Mathematics) studies
- Acquired distinction at Matriculation and Intermediate level